Performance Evaluation of Fiber Optical Sensors for Health Monitoring of Civil Structures

A Thesis

Submitted in fulfilment of the requirement for the award of degree of

DOCTOR OF PHILOSOPHY

Submitted by

Gurpreet Kaur

Registration No. 901406009

Supervisor

Dr. R.S. Kaler
Senior Professor (ECED)

Dr. Naveen Kwatra
Professor (CED)

Department of Electronics & Communication Engineering,
Thapar Institute of Engineering and Technology (Deemed to be University), Patiala-147004, Punjab, India

October, 2019

Dedicated to

My

Family, Husband & Son

Certificate

I, Gurpreet Kaur hereby certify that the work which is being presented in this thesis entitled "**Performance Evaluation of Fiber Optical Sensors for Health Monitoring of Civil Structures**" in partial fulfillment of requirements for the award of degree of the Doctor of Philosophy in Electronics and Communication Engineering from Thapar Institute of Engineering and Technology (TIET), Patiala, Punjab, India is an authentic record of my own work carried out under the supervision of **Dr. R.S. Kaler and Dr. Naveen Kwatra.** I have also cited the reference about the text(s)/figure(s)/table(s) from where they have been taken.

The matter presented in this thesis has not been submitted in any other University/Institute for the award of any degree or diploma.

Date: 24|10|2019

(Gurpreet Kaur) 24|10|20

Signature of candidate

This is certified that the above statement made by the candidate is correct to the best of my knowledge.

Supervisors

Dr. R. S. Kaler

Senior Professor (ECED)

Date: 24|10|2019

Dr. Naveen Kwatra

Professor (CED)

Date: 24|10|19

Abstract

The presence of optical devices has made their deep place in our everyday life through various processes like sensing, communication, entertainment, fashion, security, medical diagnosis, industrial growth etc. In recent years, optical fiber has found major application in sensor technology due to inherent advantages such as immunity to electromagnetic interference, electrical isolation, chemical passivity, small size, low weight, long range operation, and ability to sense variety of measurands.

Nowadays, optical sensors are commercially available to monitor the health of civil structures in real time scenario but still it is required to enhance the sensitivity. Multiparameter sensing using single sensor is an open area of research, so on existing optical sensors many things can be investigated to further enhance the performance of optical sensors. With same motivation, in this thesis, several optical sensors are proposed to sense the important parameters i.e. strain, vibration, temperature, refractive index, portlandite etc. for civil structures with high sensitivity and speed.

To achieve the first objective, an optical refractive index (RI) fiber Bragg grating (FBG) sensor is proposed to monitor the chemical concentrations i.e. calcium hydroxide $Ca(OH)_2$ and calcium analogue of brucite $Mg(OH)_2$ which can introduce the corrosion and spalling in civil structures. The motivation to sense these parameters is that if the undesired level of these parameters can detect at early stage then structure against corrosion and spalling can be protected. At first stage, to sense $Ca(OH)_2$ and $Mg(OH)_2$, cladding etched sensor with uniform grating is used and it is observed that the sensitivity is required to enhance further. In second stage, to address this problem, on the same sensor a layer of indium tin oxide (ITO) is coated and observed the wavelength shift of 12 nm and 10 nm with respect to $Ca(OH)_2$ and $Mg(OH)_2$ On the other hand, with respect to same parameters, cladding etched FBG sensor induced wavelength shift of 8 nm and 6 nm only. The OptiFDTD software was used to perform these investigations with chemical concentrations.

For better clarity, several experiments have been performed on different civil structures using FBG sensor (having uniform grating). Concrete and steel beams with different dimensions are considered to perform these experiments. The load is applied and release by computer servo-controlled material testing machine and hanger, respectively. As

expected, the wavelength shifts are observed with respect to the change in strain values. The testing is stopped when the deformation (in term of cracks) is observed on structures. From the experiments on FBG sensor, maximum 7 nm of wavelength shift is observed which needs to be improved. These experiments have been performed by using FBG sensors, Interrogator, power supply, ENLIGHT sensing analysis software for PC and ethernet cables of Micron Optics Pvt. Ltd.

Further, the aim was to enhance the sensitivity and range of the FBG sensor. To achieve this aim, in first step, a genetic algorithm (GA) is used for multiparameter optimization. Three important parameters (i.e. Poisson's Ratio (PR), photo-elastic coefficient P_{11}, and photo-elastic coefficient P_{12}) of FBG sensor are selected which are processed by GA to get best combination yielding large wavelength shift. It is observed that the optimized FBG sensor provides enormous wavelength shift of 38.16 nm with respect to PR of 1.94, photoelastic coefficient P_{11} of 1.994, and photoelastic coefficient P_{12} of 1.8103. Apart from optimization, other possibilities such as grating shapes, grating length and core refractive indexes of FBG have been examined to enhance the sensitivity of FBG sensor. It is observed that the FBG sensor with uniform grating shape having 1.46 of refractive index and 50000 μm of grating length provides high sensitivity. These simulations and numerical calculations have been performed when 0.2145 (1/με) strain is applied on FBG sensor.

This study establishes the design, characterization and optimization of highly sensitive optical sensors for health monitoring of civil structures. Most of the research findings of this thesis have been published in various International referred Journals and International Conference as per the list at page (5).

List of Publications

SCI Journals

[1]. Gurpreet Kaur and R.S. Kaler, "Sensitivity Enhancement of FBG Sensor for Portlandite Monitoring", **Elsevier:** Optical Fiber Technology, vol. 46, pp. 83-87, 2018.

[2]. Gurpreet Kaur and R.S. Kaler, "Nano Hybrid Optical Sensor for Simultaneous Measurements of Strain, Temperature and Vibration," **IET**: Micro and Nano letters, vol. 13, no. 1, pp. 1–3, 2018.

[3]. Gurpreet Kaur and R.S. Kaler, "Design and Performance Evaluation of Hybrid Optical Sensor," **Elsevier**: International Journal of Light and Electron Optics, vol. 140, pp. 508–514, 2017.

[4]. Gurpreet Kaur, R. S. Kaler, Naveen Kwatra, "Investigations on Highly Sensitive Fiber Bragg Gratings with Different Grating Shapes for Far Field Applications," **Elsevier**: International Journal of Light and Electron Optics, vol. 131, pp. 483–489, 2016.

[5]. Gurpreet Kaur, R. S. Kaler, Naveen Kwatra, "On the Optimization of Fiber Bragg Grating Optical Sensor Using Genetic Algorithm to Monitor the Strain of Civil Structure with High Sensitivity," **SPIE**: Optical Engineering, vol. 55, no. 8, pp. 087103-1 to 087103-6, 2016.

[6]. Gurpreet Kaur, R. S. Kaler, Naveen Kwatra, "Experiment on Highly Sensitive Fiber Bragg Grating Optical Sensor to Monitor Strain and Corrosion in Civil Structures," **OSA**: Journal of Optical Technology, vol. 85, no. 1, pp. 36-41, 2018.

International Conference

[1]. Gurpreet Kaur, R. S. Kaler, "Photonic Based Refractive Index Sensor for Portlandite Monitoring in Civil Structure", IEEE: 6th International Conference on Wireless Networks & Embedded Systems, held at Chitkara University Rajpura, on Nov. 16-17, 2018, paper no. 35.

Communicated

[1]. Gurpreet Kaur and R. S. Kaler, "Experiment on FBG Sensor to Monitor Displacement and Vibration in Civil Structure", Micro and Nano Letters, manuscript ID MNL-2019-0244. (resubmitted after formatting)

Acknowledgement

I would like to offer my exuberant tribute to the omnipotent ***Dhan Dhan Sri Guru Granth Sahib Ji***, ***Baba Attar Singh Ji "Mastuana Sahib***", ***Baba Sadhu Ram Ji "Tibba Sahib"*** for giving me eminent soul and body and determination granted to me in all the adversities at every step and moment of life including the entire duration of my studies. I am also thankful to almighty for providing me with priceless treasures in the shape of my parents ***Sardar Sukhwinder Singh*** and ***Sardarni Baljinder Kaur*** who provided me with continuous strength, encouragement and love.

I am also thankful to the almighty for providing me with a marvelous mentor in the form of my guide ***Dr. R. S. Kaler.*** I extend my deepest gratitude and respect to my guide ***Dr. R. S. Kaler***, Senior Professor, Department of Electronics and Communication Engineering, Thapar Institute of Engineering and Technology (TIET), Patiala, Punjab, India, for the continuous support of my Ph.D study and research, for his patience, motivation, enthusiasm, and immense knowledge. His guidance helped me in all the time of research and writing of this thesis. I could not have imagined having a better advisor and mentor for my PhD study who spared his precious time for proper guidance. The experimental work in the thesis during my research work would not be possible without the necessary guidance of ***'Dr. Naveen Kwatra'*** Professor in Department of Civil Engineering, Thapar Institute of Engineering and Technology (TIET), Patiala, Punjab, India

I also express my sincere and hearty thanks to ***Dr. Rafat Siddique*** Dean (RSP), ***Dr. Alpana Aggarwal***, Head ECED and members of the esteemed **Doctorate Committee** for their continuous motivation, appreciation and support.

I would also like to thank, TIET (Deemed to be university) Patiala who gave me the best memorable years of my life

A special thanks to my lab mates, Mrs. Rajan Gupta, Mrs. Shivani, Ms. Jiwanpreet, Ms. Mukti, Ms. Madhavi, Ms. Rupinder and Ms. Ramanjeet Kaur ensured me to never feel bored and helped at each and every step of my research work. Together, we have undertaken many tasks and completed successfully with good team spirit.

My acknowledgment would be incomplete without thanking the biggest source of my strength my brother '***Dr. Simranjit Singh'***- the sole driving force behind me who

encouraged me to pursue higher studies and due to his motivation and support I am able to achieve this academic feat.

Finally, words are not adequate to express my gratitude to my sister **'*Ramandeep Kaur*',** my brother in law **'*Rajandeep Singh*',** my brother ***'Hardeepak Singh'***, my sister in law '***Sunaina***' and my sweet title nephews '***Anoopjot Singh'*** and '***Prithmjot Singh***' who never let things get dull or boring, have all make a tremendous contribution in helping me reach this stage in my life. Additionally, I would like to thank my mother-in-law Sdn, Paramjeet Kaur, father-in- law S. Pritpal Singh and sister-in-law Kushalpal Kaur for their role to finish this piece of work.

Last but not the least I would like to thank my dear husband, ***'Er. Tapanjot Singh (S.D.O)'***, for keeping the things going on very smoothly and for always showing me how proud he is of me. Without his co-operation and help I could not have completed my research. I express my deep love and affection to my dear son ***'Dilviraaj Singh'*** for his understanding and adjusting nature and his pleasant smile which gave me strength to finish my work.

Gurpreet Kaur

Table of Content

List of Figures

List of Tables

List of Acronyms

EMI	Electromagnetic Interference
WDM	Wavelength Division Multiplexing
IWDM	Intensity Wavelength Division Multiplexing
TDM	Time Division Multiplexing
OE	Optoelectronics
FBG	Fiber Bragg Grating
pH	Pouvoir Hydrogene
SHM	Structural Health Monitoring
LPFG	Long Period Fiber Grating
SMF	Single Mode Fiber
SOA	Semiconductor Optical Amplifier
EFPI	Extrinsic Fabry- Perot Interference
PM-PCF	Polarimetric Photonic Crystal Fiber
EDFA	Erbium Doped Fiber Amplifier
CMRW	Cladding Mode Resonance Wavelength
FMRW	Fundamental Mode Resonance Wavelength
WSFL	Wavelength Swept Fiber Laser
RH	Humidity
SLD	Super Luminescence Diode
CFRP	Carbon Fiber Reinforced Polymers
RC	Reinforced Concrete
FRP	Fiber Reinforced Plastic
AE	Acoustic Emission
PZT	Piezoelectric Sensors
MEMS	Micro electro Mechanical System
SPR	Surface Plasmon Resonance
ITO	Indium Tin Oxide
OSNR	Optical Signal to Noise Ratio
UFBG	Uniform Fiber Bragg Grating
RIU	Refractive Index Unit
HOS	Hybrid Optical Sensor
GA	Genetic Algorithm

NHOS	Nano-Hybrid Optical Sensor
PCW	Photonic Crystal Waveguide
TFBG	Tilted Fiber Bragg Grating
SFBG	Superstructure Fiber Bragg Grating
CFBG	Chirped Fiber Bragg Grating
FDTD	Finite Difference Time Domain
RI	Refractive Index
2D	Two Dimensional
3D	Three Dimensional
dB	Decibel
cm	Centimeter
Hz	Hertz
nm	Nano meter
µm	Micrometer
a.u.	Astronomical Unit
FRR	Fiber Ring Resonator
PBF	Photonic Bandgap Fiber
R-FOG	Resonator Fiber Optic Gyroscope
IM	Intensity Modulated
PM	Phase Modulated
SM	Spectrally Modulated
FFPIS	Fiber Fabry Perot Interferometer Sensor

Chapter 1

Motivation

1.1 Motivation of Research

Optical fiber has recently found extensive use in the telecommunication industry [1-3]. Fiber optic technology is ideal for this application when compared to their electronic equivalent because fiber optic system allows low noise, high bandwidth, high data transmission with low loss. It is also relatively simple to design systems which are immune to electromagnetic interference [4-6].

Apart from the telecommunication application, for the last few years extensive research and development has been done on an optical based fiber sensor in many sensing applications. Optical sensors are an attractive approach for making a chemical measurement, (i.e. Pouvoir Hydrogene (pH) detection, gas monitoring, case study for spectroscopic etc.), physical measurement (i.e. strain, temperature, corrosion, humidity, etc.) and biomedical measurement (i.e. Blood flow, glucose content, etc.). Recently optical sensors were also used for effective health monitoring and maintenance of civil structures with fast and cost-effective solutions [1-4].

Civil infrastructures (Towers, Dams, Tunnels, Bridges etc.) have always been a lifeline or an asset for us in our daily role. Malfunctioning of civil infrastructure may cause certain losses to lives as well as the economy. So, in the era of growing technology, it is necessary to have complete awareness about the health of persistent civil infrastructures [2]. To monitor the health of civil structure, we have to monitor several parameters e.g. vibration, cracks, pressure, strain, corrosion etc. [9-11]. To monitor these parameters different electronic devices have been introduced in literature, but these are limited to measure a specific parameter and also have certain limitations such as electromagnetic interference, weight and dimensions. An optical sensor can efficiently monitor the health of civil structures in real time scenario and with better precision. The Structure Health Monitoring (SHM) techniques using optical sensors in real time scenario can possibly detect the deformations at early stages so that appropriate remedial action can be taken.

The main motivations behind the use of optical based sensors are the inherent fact that the data is codified in the optical domain, so these types of sensors are useful in hostile environments where electrical currents of electronic devices might pose a hazard. The optical fiber sensors have a capability to multiplex large numbers of channels and each channel can monitor different parameter which makes a system cost effective [12-14].

With the same motivation, in this work, we have proposed different types of optical sensors to monitor the strain, temperature, vibration and corrosion induced different civil structures. The main aim is to identify new areas where optical sensors can be used in civil applications and how these sensors can be exploited to their maximum limits to determine when it will be better in place of existing sensors [15-17]. We also have performed several experiments on SHM using optical sensors and measured the strain, vibration and displacement applied on civil structures. It was observed that the commercially available optical sensors are limited to range and less sensitive. To increase the sensitivity, an optimization using GA has been done to improve the performance of the proposed optical sensor in terms of large wavelength shift.

1.2 Research Challenges

Civil structures are usually the most expensive resources for all countries, and these structures are deteriorating at an alarming rate. In addition, from these structures it is expected that these should have long life as comparison of other commercial products. To increase the life time of the structure it is necessary to monitor its health and maintain it as per the requirement. In the market, several techniques based on electronics and optical are available to monitor the health of civil structures. Many evidences are in the literature [3-5] presenting optical sensors as better solution than electronic sensors for SHM, see Table 1.

Table 1.1: Physical parameters of electronic versus optical sensor

Media	**Technology**	**Electrical Noise Immunity**	**Measurement Speed**	**Sensor Configuration**	**Mounting**
Electrical	Foil Gages	Low	Up to ~100kHz	Single-Point: One sensor/channel	Surface Mount
	Vibrating Wire	Moderate	~1Hz	Single-Point: One sensor/channel	Embeddable
Optical	FBG	Complete	Typically < 1kHz	Distributed: Multisensory/ Channel	Surface Mount and Embeddable

Following are the research challenges in the domain of optical sensors:

1. **Enhancement in Sensitivity:** The sensitivity shows how much the output of a sensor varies when the input quantity being measured. For instance, if the mercury in a thermometer moves 1 cm when the temperature changes by 1 °C, the sensitivity is 1 cm/°C (it is basically the slope dy/dx assuming a linear characteristic). Some sensors

can also affect what they measure; for instance, a room temperature thermometer inserted into a hot cup of liquid cools the liquid while the liquid heats the thermometer. Sensors are usually designed to have a small effect on what is measured; making the sensor smaller often improves this and may introduce other advantage. Now a day, increasing the sensitivity is the main issue to resolve in sensing application such as biomedical, chemical, structure health monitoring, biomedical application etc. In particular to the civil application, for example, the strain may be high or low, so to sense these large variations the sensor should have large range and sensitivity. So, there is a demand to increase the range and sensitivity of the optical sensor.

2. **Multiple Parameter Detection:** Compact size and multiparameter sensing capability might present an important evolution step in sensing systems for several reasons. These capabilities can be achieved, when the less uses of components and wires in sensing system setup. With the help of multiparameter detection technique it is possible to make a system cost effective. Multiple detection can be useful for sensing application where we can measure the different parameter at same time using single sensor. Using optical sensor (distributed sensor, sensor array or hybrid sensor) multiparameter can be detected and also analyze the performance of sensor under different type chemical and physical measurands. But the major challenge is the compact design of optical sensor. The main task is how multiple structures (which can filter out the desired measured) can be made in single substrate to sense multiple parameters at same time.
3. **Acquisition of Sensor Network Technique:** Sensor network technique is required for communication purchase where the data can have shared between multiple users, data can be stored in networking storage area and also used for data updating on time. Due to high security it is used the most for communication field as well as for sensing application. The topology of network such as ring, star and bus topology can be used for sensing application, because it is possible to cover the largest structure using suitable topology structure. Apart from the real-time sensing, real time communication is also the major requirement.
4. **Continuous Monitoring:** Cracking of concrete is a common phenomenon. There are various factors such as natural, physical, chemical and biological, which cause cracks in concrete. Other natural factors are weather, faults, land subsidence, earthquakes and human activities. Weathering induces increased porosity, structural weakening of surface layers, unattractive appearance and ultimately reduces the service life of the structures. Without immediate and proper treatments, cracks in concrete structures tend

to expand further and eventually require costly repair. Keeping all these points in consideration, we need such technique(s) which has the potential to contribute both better environmental sustainability as well as enhanced mechanical and durability concrete properties**.**

5. **Results accuracy:** Accuracy in results is very important factor in continue monitoring of civil structure because it refers to how closely the measured value of a quantity corresponds to its "true" value. Precision expresses the degree of reproducibility or agreement between repeated measurements. To get the accurate result, the sensor should design very carefully and before fabrication the proper investigation and analyzing should be done using various techniques.

1.3 Potential Impact

In the past few years, the FBG sensors offered a great potential for a wide range of applications in many fields. Many Bragg grating sensors such as FBG sensors, LPFBG sensors, TFBG sensors, chirped fiber Bragg gratings sensors have shown high sensitivity, stability, immunity to electromagnetic interference and environmental ruggedness. There is a noticeable contribution and potential of Bragg gratings-based components in different fields such as biomedical applications for brain pressure monitoring, military applications for guided missiles temperature measurement and civil applications for structural health monitoring. Table 1.2 describes the potential of FBGs in different applications.

Table 1. 2: Various applications of FBG sensor

S. No	Application	Reference
1.	FBG sensor for monitoring Bridges	[20-22]
2.	FBG sensor for monitoring Mines	[8], [23-25]
3.	FBG sensor for monitoring Aircraft	[11], [10]
4.	FBG sensors for monitoring electric power industry	[11]
5.	FBG sensors for monitoring of power transmission lines	[28-29]
6.	FBG sensors for monitoring winding temperature	[22-23]
7.	FBG sensors for underwater monitoring	[12]
8.	FBG sensors for chemicals	[31-33]
9.	FBG sensors for biomedical	[34-35]

1.4 Research Objectives

Based on the initial studies, literature survey and the understanding established the following objective are proposed.

1) To propose a model of optical sensor to increase sensitivity in terms of refractive index, wavelength shifting and signal to noise ratio.
2) To propose and optimize hybrid optical sensors to increase the sensitivity for measuring strain, temperature, vibration etc.
3) To investigate the optical sensors with different grating shapes to enhance the performance.
4) To investigate the optical sensors for monitoring the health of civil structures.

1.5 Organization of Thesis

The thesis has been unified into seven chapters. The goal of every section is characterized succinctly as follows:

- **Chapter-1** focused solely on the motivation of the work, research challenges and objectives with highlight of the thesis outline and its potential impact.
- **Chapter-2** Presents the background knowledge with basic detail of systems. It explains the classification of fiber optic sensor, SHM of civil structure, FBG with different types of grating shapes and also present the previous research contributions in the field focusing on types of methods used for SHM. Critical review for sensitivity, simultaneous monitoring and continuous monitoring in optical sensors has been made. It also reveals the research gaps from previous studies and the aims of research.
- **Chapter-3** deals with the first objective which is to increase the sensitivity of optical sensor. Refractive index optical sensor is proposed to monitor the portlandite for civil structure. Propagation of light through optical sensor is also investigated at different wavelength and at different incident of light to analyze diffraction of light, optical Signal to Noise Ratio (OSNR) and transmittance power.
- **Chapter-4** deals with optimization and simultaneous monitoring using optical sensor. The optical sensor has been optimized using genetic algorithm to enhance the sensitivity. This chapter is related to second objective of this thesis.
- **Chapter-5** deals with the third objective and in this chapter, we have enhanced the performance of optical sensor using different grating shapes for far field applications.
- **Chapter-6** is related to fourth objective of this research which is to investigate the optical sensor for structure health monitoring of civil structures.
- **Chapter-7** consolidates the results and concludes the work. Further, the scope for the future work is also discussed.

Chapter 2

Introduction and Literature Review of Thesis

2.1 Introduction

FBG sensor is most extensively studied subject in fiber optic technology on account of its interesting applications in biomedical, military, radar systems, drone missiles and SHM. The behaviour of FBG sensor makes it unique and appealing product in the market owing to its distinct features like sensitivity, stability, flexible to harsh conditions and immune to electromagnetic/ radiofrequency interferences. All these properties vary in accordance with surrounding temperature, grating length, core material and its dimensions. The conventional optical fiber sensors were not very stable, accurate and had low sensitivity. So, the researchers are focusing on developing a feasible, concise, stable, low cost, high sensitive sensor which could able to sense strain, vibration and temperature concurrently.

In this chapter, we have presented the evolution, basic introduction and extensive literature review of optical FBG sensor. Section 1 covers the sensitivity part of optical sensor, Section 2 is for multiparameter sensing using optical sensor and Section 3 elaborates the continuous monitoring using optical sensor. Literature survey starts with theoretical analysis and later on covers the sensing applications.

2.2 Evolution of Optical Sensor

The field of optical fiber sensors concerns a very dynamic community for over 35 years. The late 70s and the following years allowed pioneers to explore the potential of an innovative component: the optical fiber, whose intrinsic features have led some researchers to develop the very first OFS prototypes in the dark rooms of their labs, and others to initiate projects in telecommunications. The 80s gave the opportunity to explore possibilities offered by some OFS mock-ups, thanks to the very first single-mode fibers, some optical components (e.g. the famous "3-dB coupler") and to some equipment's then available (fusion splicers, multimode optical connectors). Many principles were explored at that time, particularly those implementing the interferometry (Sagnac, Mach-Zehnder) respectively for the development of Fiber Optic Gyroscopes (the "FOG"; Sagnac effect), current sensors (Faraday effect), and also hydrophones for the navy. In 1986, the concept of OFS Network (OFSN), distributed and quasi-distributed, was born, i.e. the possibility to multiplex sensors on a given fiber, to reduce cabling, sensor data management, and finally the cost-per-measurement-point. Then, by the end of the 80s, new products based on optical reflectometry, i.e. the OTDR (Optical

Time Domain Reflectometer; somehow a guided optics Radar) appeared, as the Raman DTS (Distributed Temperature Sensor) that provides a selective measurement of the fiber temperature profile. At the early beginning of the 90s (more accurately in Sept. 1989 at OFS-9, Paris, France [2]), a very important technology for SHM applications has been introduced: FBG. As a reminder, this transducer (a narrow spectral filter photo-written by laser in the fiber core) reflects a characteristic wavelength used to simultaneously provide its address in the sensor network, and the measurement (temperature, strain). During this decade, leaving the labs, only robust techniques survived: those based on FBG filters, and to a lesser extent on micro Fabry-Perot (both quasi-distributed sensors), and the reflectometry (distributed sensing) which implement backscattering phenomena, namely Rayleigh effects (OTDR), Raman (DTS) and Brillouin sensing, usually designated by the letters BOTDR (Brillouin Optical Time Domain Reflectometry) and BOTDA (the letter A being for Analysis). Both kind of Brillouin sensing techniques became commercially available towards the end of the 90s. In the same time, the first OFS applications devoted to materials and structures monitoring started to appear [3]. As an example, fibers were soon identified as quasi non-intrusive embeddable sensors, able to monitor composite curing (smart manufacturing), strain testing for qualification, and of course for SHM purposes. The end of the 90s and the first years of the millennium were that of the optical Telecommunications 'boom', followed in 2001 by the Internet bubble 'crack'. During several years, many SMEs disappeared but others emerged. Some of them were involved in sensors, optoelectronic systems, or applications increasingly SHM-oriented. The 2000s saw the advent of a new optical guides: the "Photonic Crystal Fibers". Indeed, after 30 years of traditional optical fibers manufacturing refinement (OVD, MCVD), studies concerning fiber design and development have had to adapt to requests from new scientific/industrial sectors (wideband optical sources, sensors, bio-photonic). We may anticipate that these new fibers are likely to offer new opportunities for the SHM in a near future.

2.2.1 Advancement of Optical Sensor

Almost four decades have passed since the research on optical fiber sensors began in earnest. Various approaches and technologies have been utilized for measuring a number of different physical parameters, but only some types of optical fiber sensors are commercially interesting. In particular, fiber Bragg grating (FBG), long period gratings (LPGs), evanescent field and hollow core optical fiber sensors are mentioned. Examples of recent optical fiber sensors for the measurement of strain, temperature, displacement, air

flow, pressure, liquid-level, magnetic field, and the determination of methadone and hydrocarbons are described in table below

Table 2.1: Optical sensor for different application

Sr. No.	Company	Product	Features	Parameters
1.	Micron Optics	Displacement sensor (OS5100)	• Measurement of displacement between two gage points • Continuous monitoring of construction joints and crack growth in rock, concrete, and structural member.	• Displacement: 0to 50 mm • Peak reflectivity: >70% • Accuracy: 0.03 mm in steady state environment
		Accelerometer(os7100)	• Measurement of acceleration on large structures from DC to low frequencies. • Continuous lifetime health monitoring of bridges, dams, buildings, tunnels, ships, aircraft, trains, and other complex structures	• Reference sensitivity ~16pm/g • Operating range: ~40 to 80 ^{o}C • Peak reflectivity >70%
		Non-metallic optical strain Gage (os3200)	• Core building block for fiber optic transducers for strain, temperature, displacement, pressure, and acceleration. • Measurement of strain on a structure's surface. • Experimental mechanics evaluations requiring many sensors.	• Strain sensitivity ~1.2pm/με • Peak reflectivity >70%
2.	New age instruments & Materials Pvt. Ltd.	FBG Temperature sensor (ALST-01)	Temperature sensor	• Temperature resolution: 0.1^{0}C • Temperature Accuracy: 1^{0}C • - Temperature Range: -40 ~+120 ^{0}C
		Displacement sensor (ALDS01)	• Continuous monitoring of construction joints and crack growth in rock, concrete, and structural member. • Measurement of displacement between two gage points	• Displacement Range: 80mm • Resolution: 0.5%FS • Displacement Accuracy: 1%FS

		Strain Sensor (ALEST01)	• Measurement of strain on a structure's surface. • Experimental mechanics evaluations requiring many sensors	• Strain Measurement Range: +/- 1000με • Strain Accuracy: 1‰
		Accelerometer (ALAL01)	• Continuous lifetime health monitoring of bridges, dams, buildings, tunnels, ships, aircraft, trains, and other complex structures	• Range: 0 ~ 3 ms-2 Accuracy: 1% F.S. • Sensitivity: 250 ~ 500 pm/ms-2
3.	Fox Tek	Corrosion monitoring with a FOX-TEK FT sensor system	• Faster access to corrosion data from difficult-to-access locations • More reliable data based on direct measurement of the pipe wall in areas of concern • Better record of inspections through maintaining a secure on-line database • Reduced inspection-related labor costs • Greater operating time through accurate end-of-life assessments • Greater reliability and lower risk	
4.	Smart Fibres	FBG Sensor in Acrylate Coated Fibre	• Optical strain and/or temperature sensor • Zero power, EMI immune • Intrinsically safe • Highly stable • Multiple km signal integrity • Available singly or in multiple FBG arrays • Suitable for composite embedment • Can be used to manufacture smart sensors and transducers • Suitable for long-term SHM	• Peak Reflectivity >70% • Strain sensitivity 12pm/micro-strain
		Smart Flow	• FBG vortex shedding flowmeter suitable for liquids and gases	• Maximum Operating Pressure 140bar • Turndown Ratio >15

			• Also measures density from which steam quality and thermal mass flow is derived • No electronics enables ultra-harsh environment use • Intrinsically safe operation with ATEX certified Smart Scan interrogator • Numerous meters can multiplex to a single, remote instrument • Surface, subsea or downhole application • Designs available for 1" to 12" lines	• Steam Quality Accuracy 10% to 20%
		Smart Patch	• FBG strain and/or temperature sensor • Sensor embedded within protective laminate • Zero power, EMI immune, intrinsically safe • Developed by Smart Fibres for surface bonding to metal, concrete, composite etc • Installations include wind turbine, ship hulls, yacht masts and concrete civil structures • Suitable for long-term SHM • Multiple km signal integrity	• Strain Range 5000 με • Strain sensitivity 12pm/ με
5.	Optromix	FBG Tiltmeter Sensor	• Tiltmeter can be used for monitoring of the constructions inclination (tower buildings, mine shafts). • The sensor is equipped with thermal compensation sensors and self-calibration system.	• Wavelength Range 1500-1600 nm • Reflectivity >65 %
		Load/ Weight Sensor	• Sensor can be used for measuring the load applied to various surfaces and structures. • It is located between two interacting surfaces. It is equipped with thermal compensation sensor	• Wavelength Range 1500-1600nm • Accuracy 0.35 %

6.	Precision Sensing	Optical CO_2 Sensors	• CO2 measurement in solutions Pre-calibrated sensors Contactless measurement of dissolved CO2 From µL to m3 scale 0.04 – 5 % CO2, 1- 25 % CO2 measurement range	• Temperature performance: • From 0 ^{0}C to +50 ^{0}C, • Accuracy +/- 1.0 ^{0}C
		Optical pH sensor and meter	• Minimally invasive or even contactless measurement Pre-calibrated µL up to m3 range Insertion in plant and animal tissue For microbial and cell culture	

2.3 Optical Fiber Sensor System

The simple optical sensor system is represented in Fig.2.1. Light is transmitted into the optical fiber from an input source and moved through the measurand region and finally received by the photodetector. During propagation through the area of measurement, the fiber light parameters changes (in terms of amplitude, phase, wavelength or polarization state) with respect to the physical, chemical or biological phenomena.

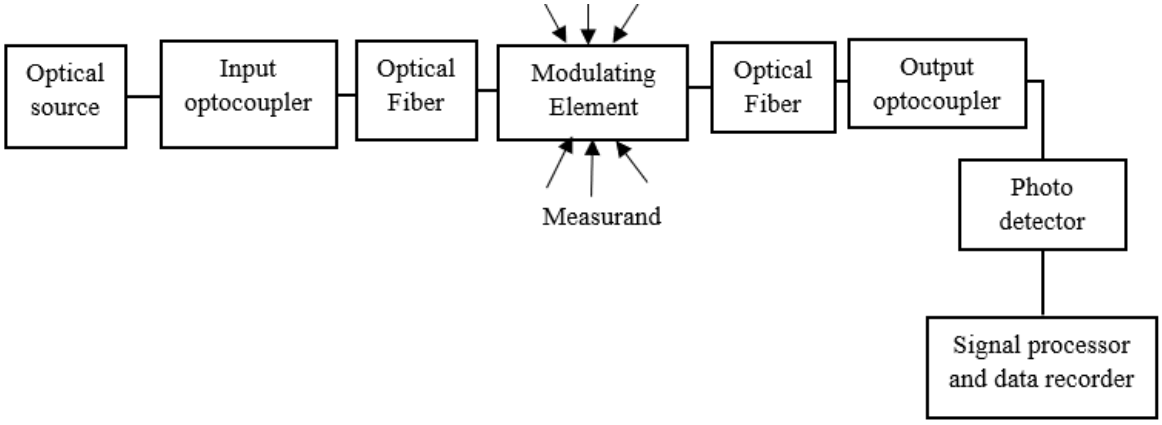

Figure 2.1: Schematic view of a simple fiber optical sensor system.

The overall power of the modulated light of the sensor is dependent on several discrete parameters which are given by the product of power of light source, efficiency of input and/or output optocouplers, transmission efficiency, modulation function response and responsivity of photodetector.

2.4 Classification of Optical Fiber Sensor

The optical fiber sensor is classified into various categories based on sensing site, operating principle and application. The detail of these categories is described below.

2.4.1 Sensing Site or Location: In general, fiber sensor is grouped into two basic classes, namely extrinsic and intrinsic.

2.4.1.1 Extrinsic Sensors

When light beam leaves the fiber cable and get changed due to object before it reaches to the optical detector end then it is known as extrinsic optical sensor, which is described in Fig. 2.2.

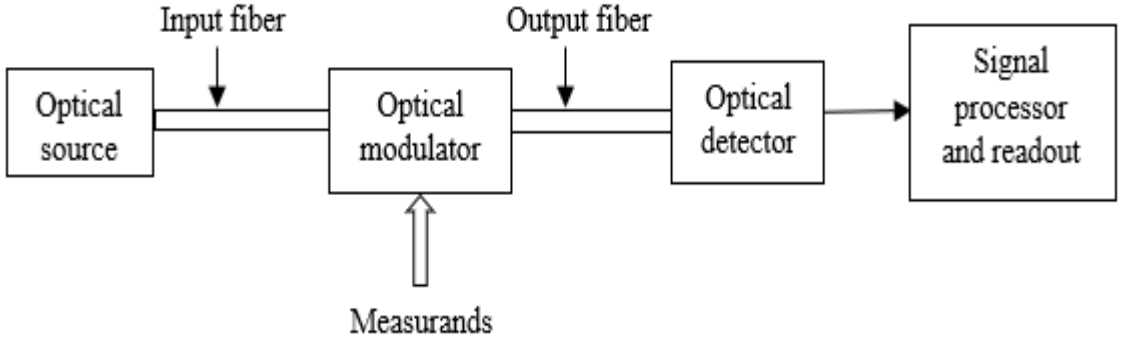

Figure 2.2: Extrinsic optical fiber sensor.

2.4.1.2 Intrinsic Sensor

In this type of sensors, the detection of measurands are performed within the fiber before forwarding it to the optical detector and it is shown in Fig.2.3. The measurands can be monitored by observing the changes in the intensity, wavelength, reflection and transmittance power.

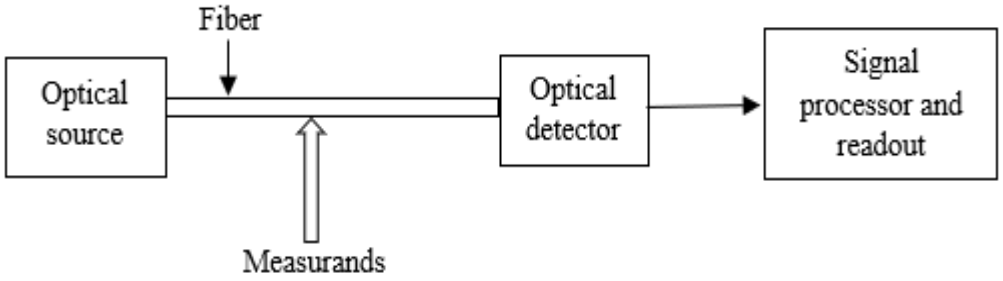

Figure 2.3: Intrinsic optical fiber sensor.

2.4.2 Modulation: Optical sensors can be classified according to the modulation scheme as follow.

2.4.2.1 Intensity Modulated (IM) Sensor

IM sensor is an easiest and inexpensive technique to measure the various parameters. In this technique, the physical or chemical parameters modulates the amplitude of input light along the fiber and these modulations in amplitude can be observed using photo-detector at the output side. The IM sensor can be sensed with change in light due to the mismatch between two fibers. Different ways of mismatch are shown in Fig.2.4. The lateral mismatch fiber sensor is highly sensitive than other mismatch sensors. In this technique, the performance of fiber sensor can be improved by cutting and refining the two ends diagonally and placing the inclined faces of both fibers adjacent to each other.

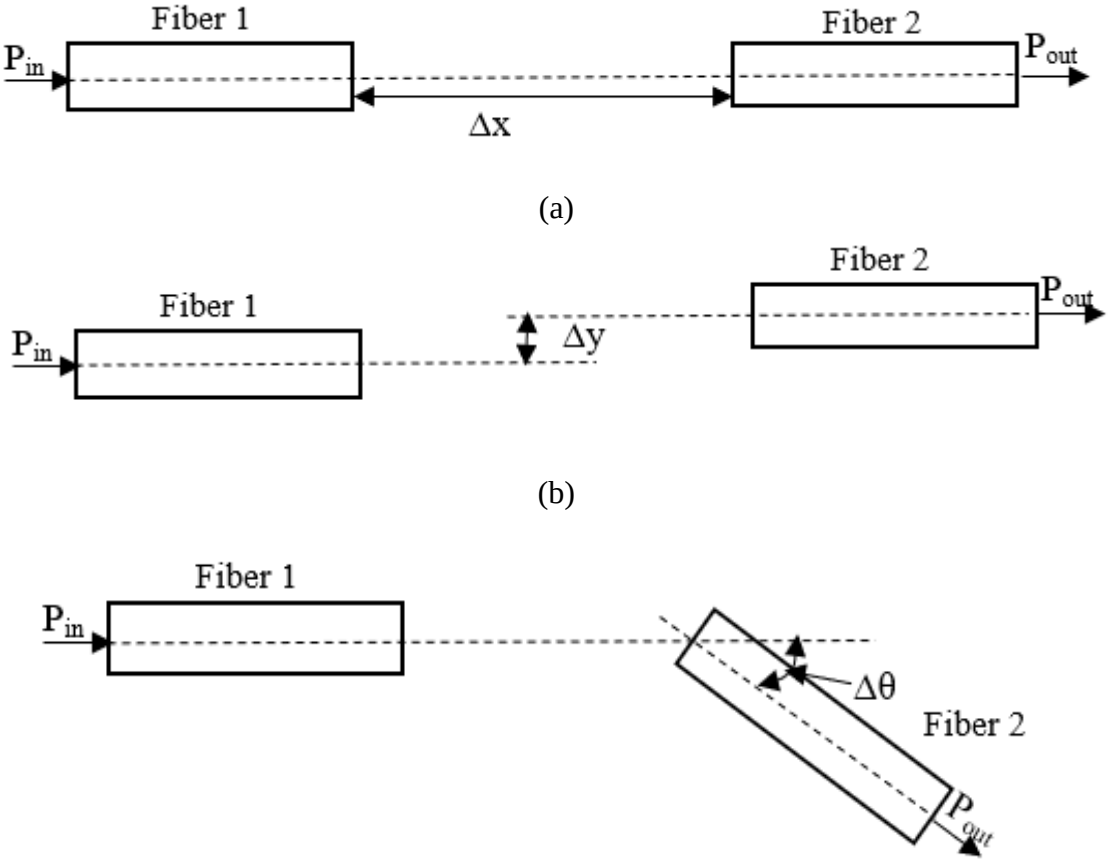

Figure 2.4: Types of misalignments between two fibers (a) Longitudinal Misalignment (b) Lateral Misalignment (c) Angular Misalignment.

Due to mismatching, the total internal reflection light is forwarded from the first fiber into the other fiber through inclined face.

2.4.2.2 Phase Modulated (PM) Sensors

The numerous sensing methods with high sensitivity are based upon optical phase modulation and the phase depends on various factors such as fiber length, direction of light and RI profile of the sensor. The length of fiber may be changed by strain, pressure and thermal expansion and these changes can be monitored through observing the variation in refractive index values. The variation in refractive index values is occurring through photoelastic effect. The diagram for PM sensor is shown in Fig. 2.5. These changes are detected via fiber interferometric method.

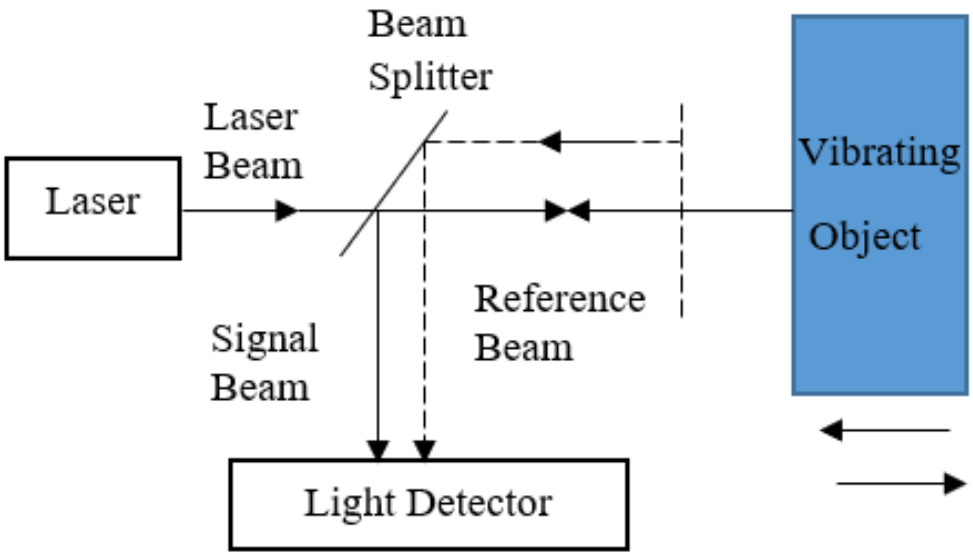

Figure 2.5: Optical phase modulated sensor for vibrating object.

2.4.2.3 Spectrally Modulated (SM) Sensors

This type of sensor is based on the light beam which changes its properties by different effects like corrosion, vibration, strain and other natural or physical hazards. In this technique, object is located at the termination of the fiber. As the temperature is increased, the cavity will start glowing and behave like an optical source. This sensor can also be used to monitor the temperature under intense fields.

2.4.3 Application Based: In this case, the fiber optic sensor is classified as:

2.4.3.1 Physical Sensors: This type of sensor is used to detect the physical changes that occur on the sensor due to temperature, pressure, strain, acceleration etc.

2.4.3.2 Organic Sensors: This type of sensor is useful in the chemical field to analyze the presence of gas, pH value, concentration level of chemicals etc.

2.4.3.3 Biomedical Sensors: This type of sensor is used to measure the flow, glucose amount, oxygen in the blood, for monitoring cholesterol etc.

2.5 Advantages of Optical Fiber Sensor

The optoelectronic devices along with fiber optic sensor are nowadays indispensable for any information processing as well as discrete or measurement systems. Optoelectronics is one of the foremost technologies that have fundamentally changed the way people lived during the last thirty years. Nowadays, it is the foundation of all information processing and measurement systems used in diverse fields from communication to healthcare. In a broad sense, precise measurements of any measurands like pressure in blood and temperature is

short of information generation also. The uses of light in various information processing purposes is shown in Fig. 2.6, by different optoelectronic devices and systems which have several advantages as follows:

- **High Immunity to the Electromagnetic Interference:** In optoelectronic devices and systems the light quanta, i.e., photon being uncharged, does not experience disturbance by the neighbouring electrical discharge.
- **High Speed and Bandwidth:** The information carrying capacity of optical signal or optical bandwidth is relatively larger than the conventional electrical bandwidth due to extremely high velocity (~ 3×10^{10} cm/s) and very short-wave pulse (~ few femto sec) with high frequency (~ 10^{14} Hz) of light wave.
- **Non-Interference of Cross Over Light Signals:** This has overcome the limitations of closely spaced electrical contact points and help in the realization of high-density information processing systems.
- **Easy Integration of Light and Electrons:** The case for the integration of light and electrons in different semiconductors helps to design various optoelectronic devices and systems.

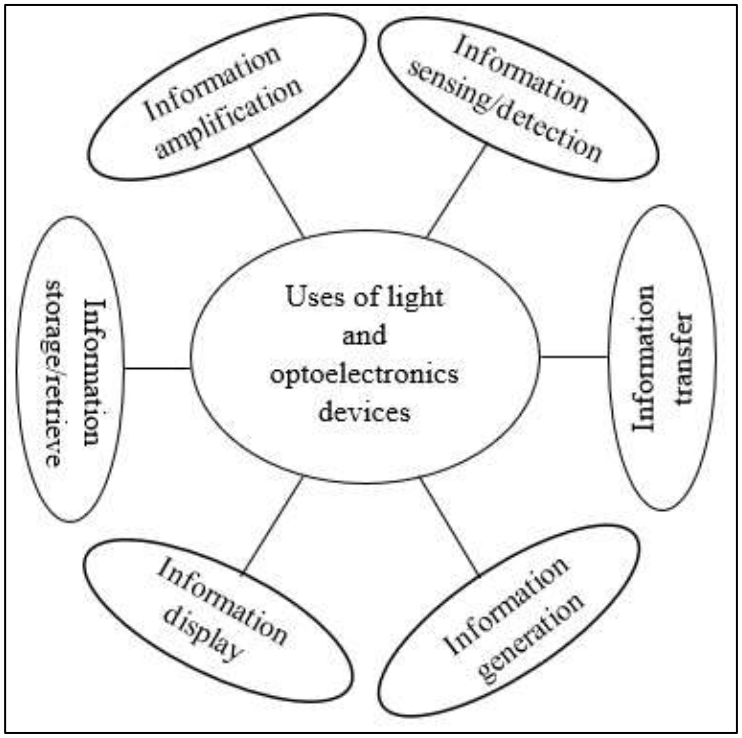

Figure 2.6: Areas of applications of light and optoelectronics devices in information processing application [16].

2.6 Health Monitoring of Civil Structures

Civil structures once built, starts to weaken with time. For economic reasons and human safety, it is important to maintain it safe and stable. It is crucial and mandatory to determine the time span, the purpose for which the building is being utilized and its strength to resist/withstand earthquakes, high speed winds etc. The method of understanding and tracing of any damage in a building and its extent of damage is known as SHM. Currently, this technique is gaining much popularity in the area of civil engineering. SHM is described as the use of non-deleterious methods for identifying and examining the health of the structure or any damage that has been caused over passage of time, the exact location of the damage and its extent. This technique is also used to determine the outcome of any damage that has been caused or is likely to occur. Although, this technique is a new method for sensing and analysing of civil structures, there are certain tests and evaluation methods which have been pre-defined for determining the strength of civil structures. The purpose of this technique is in line with the previous methods, however it leads in combining the new technologies into an efficient and smart apparatus. The details acquired from such apparatus can be used for preservation of structures and enhancing of safety of structures. Quick assessment of any structure, maintenance of old structures can be easily done using this technique.

2.6.1 Conventional Techniques of Health Monitoring of Civil Structures

Till date, the only means for identification of damage in civil structures is visual/physical inspection by skilled persons. Once the damage location is detected, evaluation is done and with the help of procedures such as eddy currents, radiography, thermal, ultrasonic, magnetic field or electro-magnetic impedance the exact damaged area and the extent of damage can be evaluated. A specimen of the damaged portion of the building may also be collected for testing/analysis in the laboratory. The prerequisite of this method is the approachability of the site which is to be examined. In some scenarios, the damaged part of the building might not be approachable or accessing the damaged part might need removing the upper layers. As such, this method of tracking is very tiresome and costly. Also, the trustworthiness of this method (visual/physical inspection) is largely dependent on the familiarity of the person conducting such inspection. For the last few years, several studies have tried to change the old method of inspection by new self executing methods which are efficient and can quickly inspect the condition of building. Along with this, the

proposal of using smart materials for structures was suggested as an option because they display high sensitivity to environmental change.

2.6.2 Fiber Optic Techniques for SHM

The demand of highly sensitive fiber optic sensors is growing day by day for various industrial application starting from monitoring the behaviour of precision structure such as ultrahigh quality optical telescope, precision tooling, robotic surgical instrument to SHM of a range of systems or mechanical products like bridges, dams, maritime structures, buildings etc. In addition to the physical strain, temperature fluctuation may also cause nanometre level deformation in those structures which can cause initiation of cracks and the reduction of lifespan as well as utility**.** Following are the different types of optical fiber sensors:

2.6.2.1 Reflection Type Sensors

This sensor is based on intensity modulated sensors where the sensors convert a physical parameter into change in intensity of light launched into the fiber intrinsically or extrinsically. The intensity of light arriving at the detector depends upon the position of the reflecting surface. The displacement of the reflecting surface causes a change in the intensity of light detected. Typically, a broadband source and multimode fiber are used for sensing. The measurement setup is shown in Fig. 2.7. This sensor arrangement is similar to a moveable reflector. Output power is proportional to displacement Δx; therefore, it is used as distance or pressure sensor.

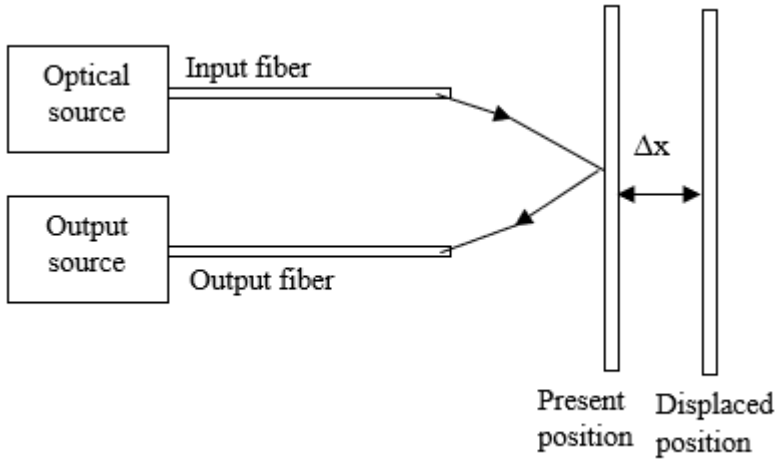

Figure 2.7: Intensity-modulated reflection type sensor.

2.6.2.2 Transmission Type Sensor

A fixed light is launched into one fiber and the second fiber undergoes displacement due to different measurand. The displacement may be longitudinal or axial, lateral or transmission and angular.

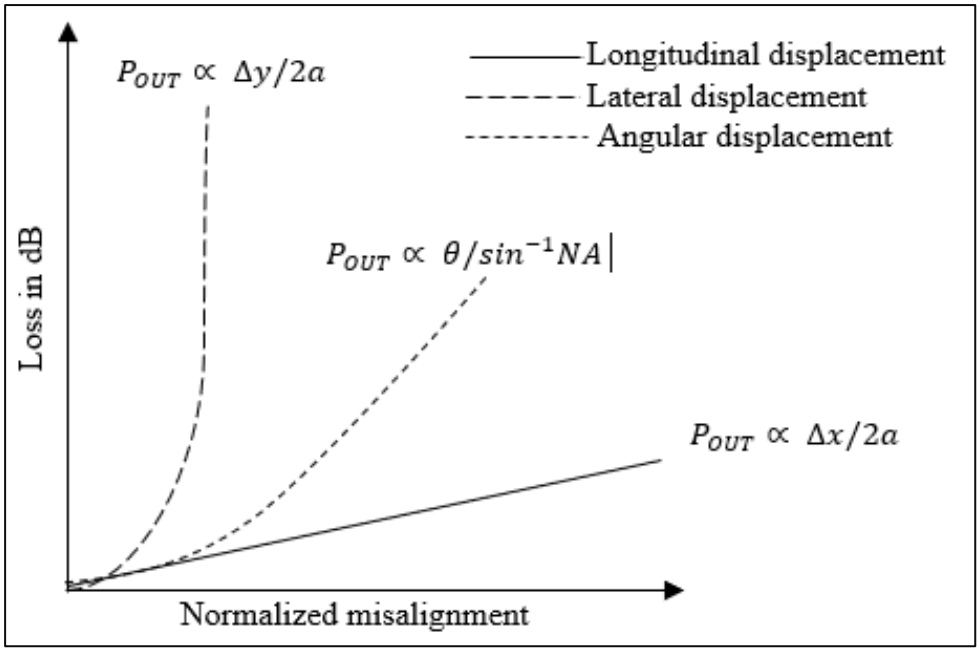

Figure 2.8: Sensitivity curves for different transmission type sensors.

Any parameter that can be caused either longitudinal or lateral or angular displacement can be measured with this sensor. However, as there is no reference signal for measurement. This measurement scheme suffers from light source intensity fluctuation, and the fiber loss varies. This can add error in the measurement. Figure 2.8 shows the sensitivity curve for different types of transmission types sensors. Lateral displacement is most sensitive but not linear throughout the operation range, while longitudinal displacement is less sensitive but gives linear output.

2.6.2.3 Micro Bending Sensor

Micro bending sensors are intrinsic sensor and simple setup of this sensor is shown in Fig. 2.9. The light launched into the fiber and its output is connected to an optical photodetector. In between the light source and detector, a microbending transducer is placed to sense the pressure. A microbend transducer has tapered teeth that produce microbends on the fiber when pressure is applied.

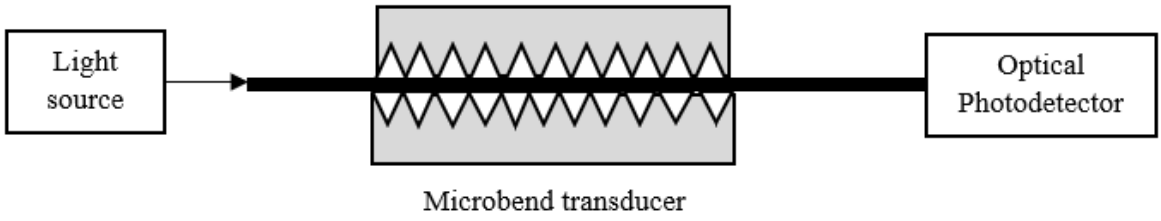

(a)

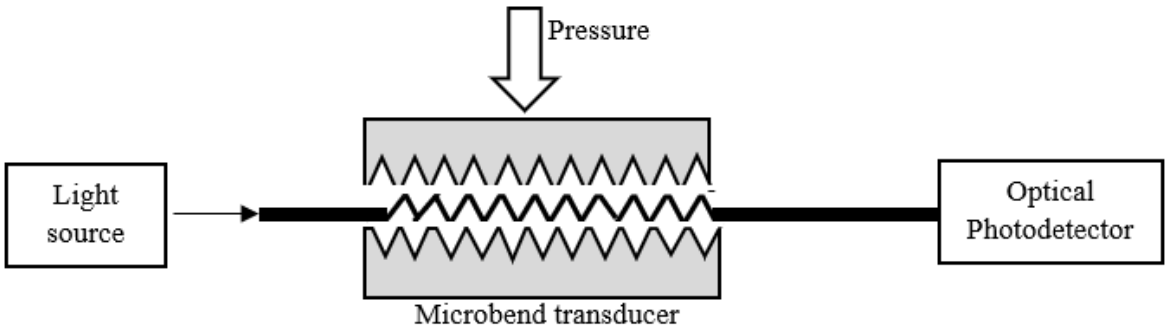

(b)

Figure 2.9: Microbending sensors with (a) no pressure (b) pressure.

Microbending results in the loss of higher order modes. With increase in pressure, microbending increases and the optical power received by photodetector decreases.

2.6.2.4 Evanescent Wave Fiber Sensor

The light energy profile of optical fiber is not confined to the core only; some energy penetrates the cladding and it is called an evanescent wave. This leaked optical energy is utilized for chemical sensing. When the cladding is etched, then this evanescent wave will communicate with the outside environment. The chemical absorbs light and the variation in light intensity is calibrated as the change in the concentration of the chemical. Evanescent wave fiber sensors can be used in biomedical applications.

2.6.2.5 Fiber Mach- Zehnder Interferometer Sensor

An interferometric sensor configuration consisting of a Mach- Zehnder interferometer is depicted in Fig. 2.10. The light of intensity I_0 is transmitted through the laser source into the fiber. Further, light is split using a 2×2 coupler having 50:50 coupling ratio. The equally divided light is sent through the sensing arm and reference arm.

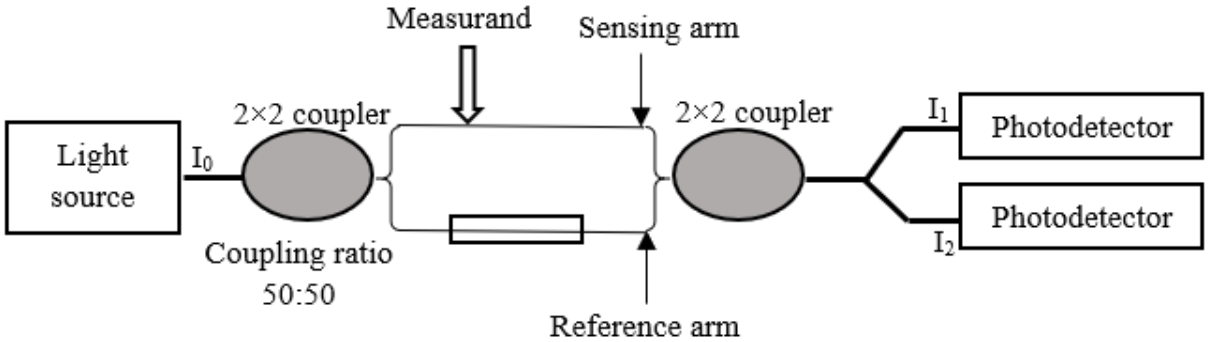

Figure 2.10: A fiber-optic Mach-Zehnder interferometer sensor.

The reference arm is shielded while the sensing arm is subject to the measurand directly. The measurand modulates the phase of light when any changes occur in its length, RI or both.

This creates a phase difference Δø between the light wave with intensity 'I_1' in the sensing arm and a light wave with intensity 'I_2' in the reference arm.

2.6.2.6 Fiber Fabry Perot Interferometer Sensor (FFPIS)

This is intrinsic type sensors which can detect a phase shift within a resonant cavity. These sensors consist of the piece of fiber that has reflective layers as shown in Fig. 2.11.

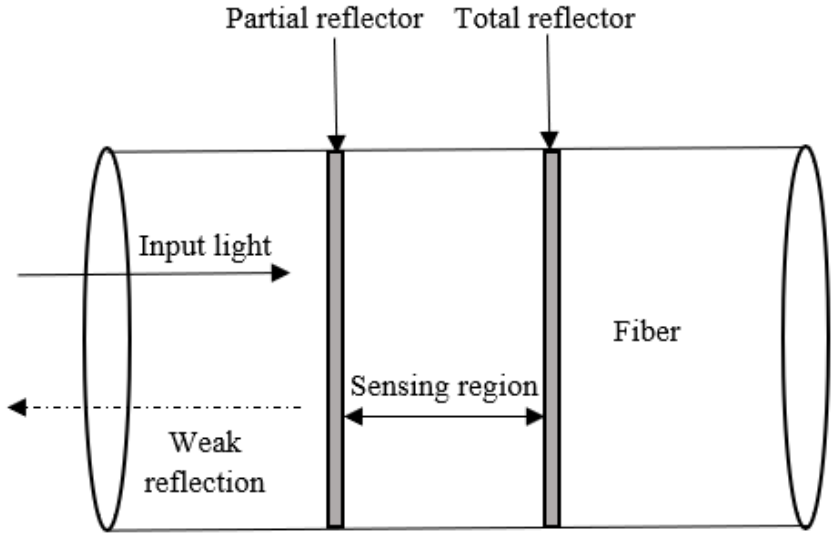

Figure 2.11: Fiber Fabry Perot sensor.

The two reflective layers form a cavity that acts as a sensing element. One layer is a partial reflector and the other is a total reflector. The sensor internal reflectors can be made by thin film deposition on the cleaved fiber end followed by fusion splicing. The Fabry-Perot interferometer has a series of resonances at characteristic wavelength defined by cavity length and refractive index when an exact number of half wavelengths of the light fit within the separation distance between the mirrors.

2.6.2.7 Fiber Bragg Grating Sensor

The gratings are the components of fiber, generally written in Ge-doped fiber using UV light. If Λ is grating pitch and n_{eff} is effective index of grating, then the reflected wavelength is called Bragg wavelength. The reflected wavelength is dependent upon the n_{eff} and regularity of the gratings. This sensor is used for the detection of wavelength shift from the reference wavelength due to the change in measurand. The reflective FBG sensor is represented in Fig. 2.12 where optical source is transmitting the light into the gratings from which the Bragg wavelength is reflected back.

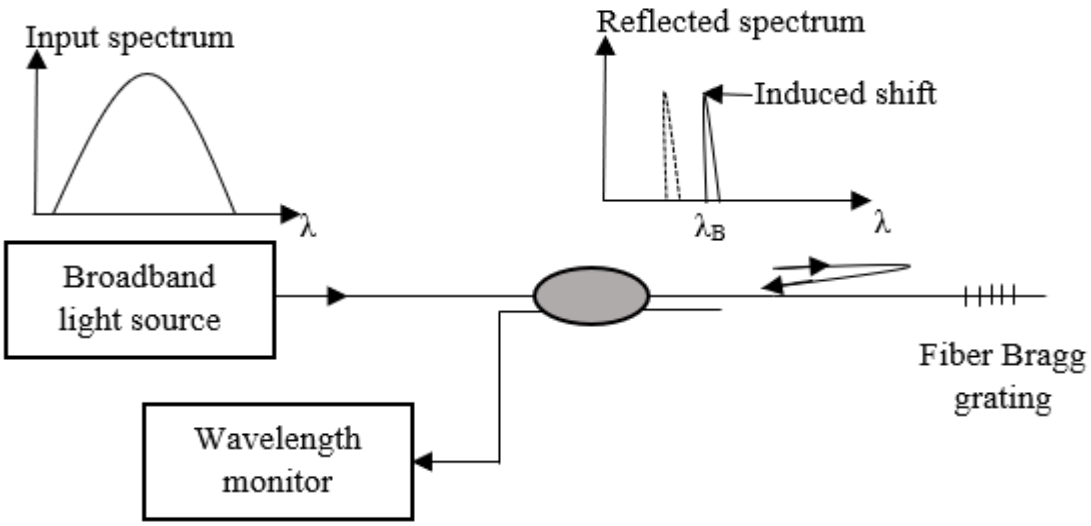

Figure 2.12: Diagram for Reflective Sensor.

The amplitude view of reflected wavelength and reference wavelength can be monitored through reflection spectra.

2.6.2.8 Polarization Fiber Sensor

The sensor can modulate the phase of light. The original signal and phase shifted signal interfere to modulate the light intensity so that phase shift is converted in terms of light intensity. A pressure sensor setup is shown in Fig. 2.13. A light signal having two polarization states is passed through the fiber sensor. The pressure signal changes the RI of sensing fiber and this in turn changes the polarization of light. Hence, there is a delay difference between the two polarization states.

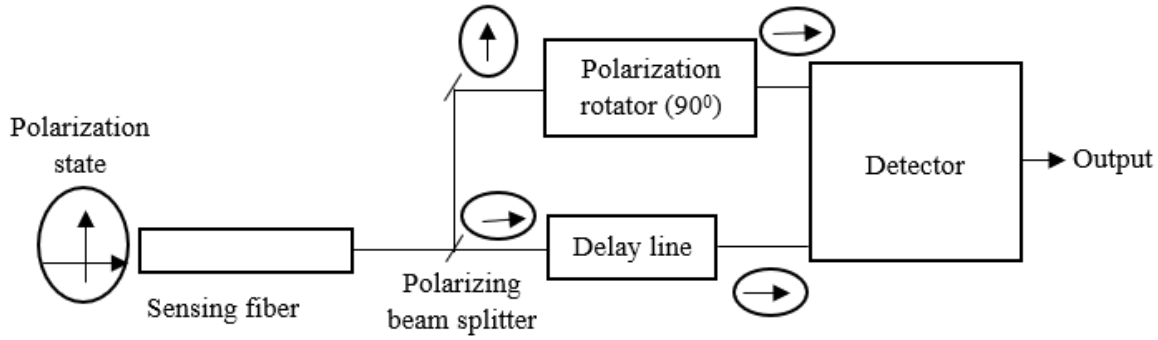

Figure 2.13: Polarization fiber sensor setup.

For measurement purpose, the two polarizations are separated by a beam splitter. One polarization is rotated by 90^0 and the path length of other is equalized after which both are combined. The output is high if there is no delay between the two and it is low if one is 180^0 behind the other.

2.7 Fiber Bragg Grating

Fiber grating is one of the main factors in the conventional and developing fields of fiber communication systems. In optical telecommunication system, the main disadvantage is on the component side for managing the light like coupling, in and out filtering etc. which mainly comes on bulk optics. Bulk optics have high losses, stringent tolerance for alignment, and huge size. These disadvantages are overcome using fiber gratings which have fewer losses, smaller in dimensions and cost-effective solution. Their applications also spread into the area of optical fiber sensing. Fiber grating are non-conducting equipment where some percentage of light is reflected back (called Bragg wavelength) and rest of the light is transmitted to the fiber through the gratings using the fundamental principle of Fresnel reflection.

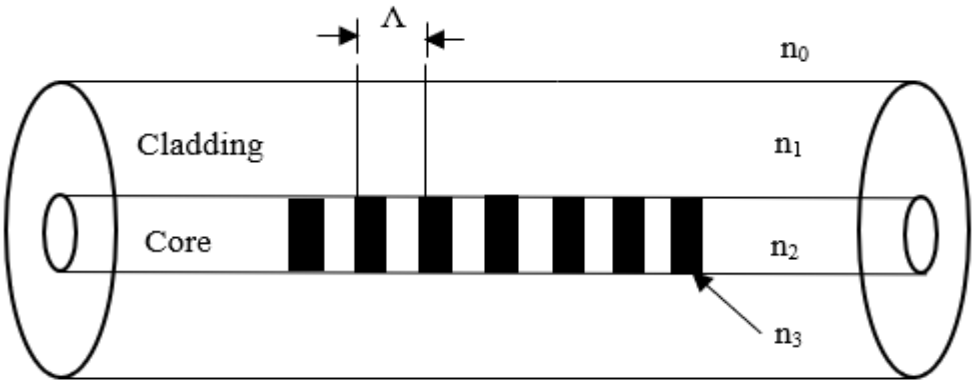

Figure 2.14: Fiber Bragg grating structure.

In FBG symmetrical breaking of RI is established in the core to make the gratings and these breakings scatter the wavelength as shown in Fig. 2.14. The Bragg wavelength is reflected back every time when the light strikes an area of the higher refractive index. If Λ is the grating pitch, n_{eff} is the effective RI and λ_B is Bragg wavelength and is defined as:

$$\lambda_B = 2n_{eff}\Lambda \qquad (2.\ 1)$$

where

$$n_{eff} = \frac{n_2 + n_3}{2} \qquad (2.\ 2)$$

Here n_2 and n_3 are the refractive indices.

Following are a few related important terms of FBG:

2.7.1 Core and Cladding Mode Coupling

The travelling of the light through the waveguide in terms of guided EM waves is called the modes of waveguide. In the fiber cladding, core boundary condition is guiding to

coupling between magnetic and electric field components and every mode has its particular propagation constant value. If symmetrical breaking is introduced in the fiber, then modes will interchange its power level and this is called mode coupling. The fiber gratings are divided into two categories where one is Bragg gratings and another is transmission gratings. In Bragg gratings type the coupling arises between the modes which propagate in different directions. In transmission gratings, the coupling arises in the same direction.

The effects of incident light on grating and angle are defined as [5]:

$$n\,sin\theta_2 = n\,sin\theta_1 + m(\lambda/\Lambda) \qquad (2.\ 3)$$

Where n is the RI of core, θ_1: incidence angle, θ_2: diffraction wave angle, m: order of diffraction. Figure 2.15 illustrate reflection by Bragg grating of a mode with a bounce angle θ_1 into the same mode travelling in the opposite direction with a bounce angle $\theta_2 = -\theta_1$. And the β is the z- component of wave propagation constant 'k' and is the main parameter in describing fiber modes, which is written as follow [13]:

$$\beta = (2\pi/\lambda)n_{eff} \qquad (2.\ 4)$$

Where $n_{eff} = n_{co}\sin\theta$. The mode remains guided as long as β satisfies the condition $n_{cl}k < \beta < n_{co}k$, where n_{co} and n_{cl} are core and cladding refractive indices and $k = 2\pi/\lambda$.

The boundary between truly guided modes and leaky modes is defined by the cut-off condition $\beta = n_{cl}k$. As soon as β becomes smaller than $n_{cl}k$, power leaks out of the core into cladding region.

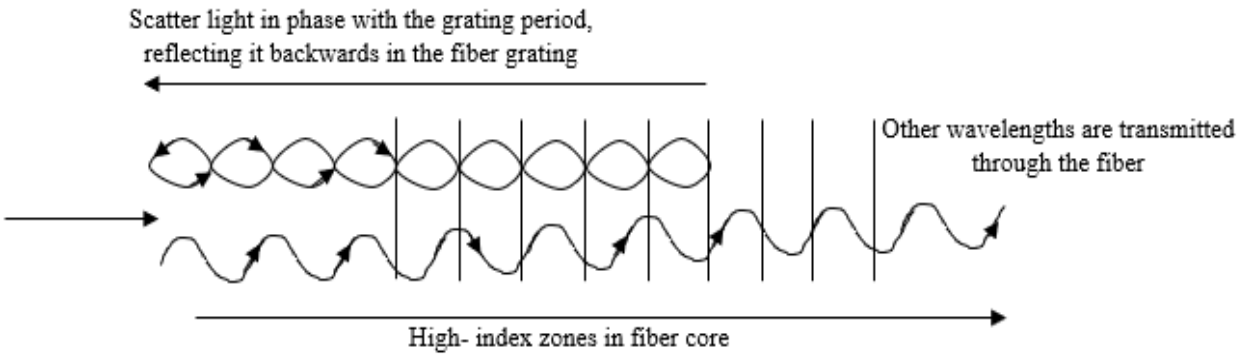

Figure 2.15: Diagram for FBG bounces back Bragg wavelength and communicates rest of the wavelength [16].

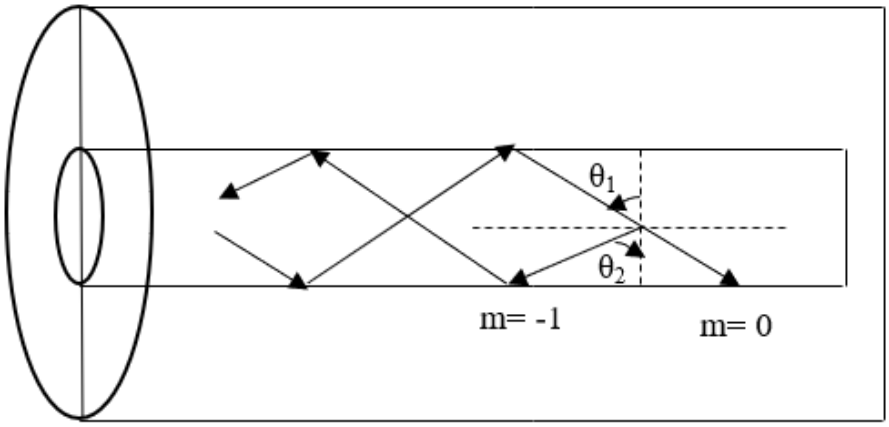

Figure 2.16:Core mode Bragg reflection by an FBG.

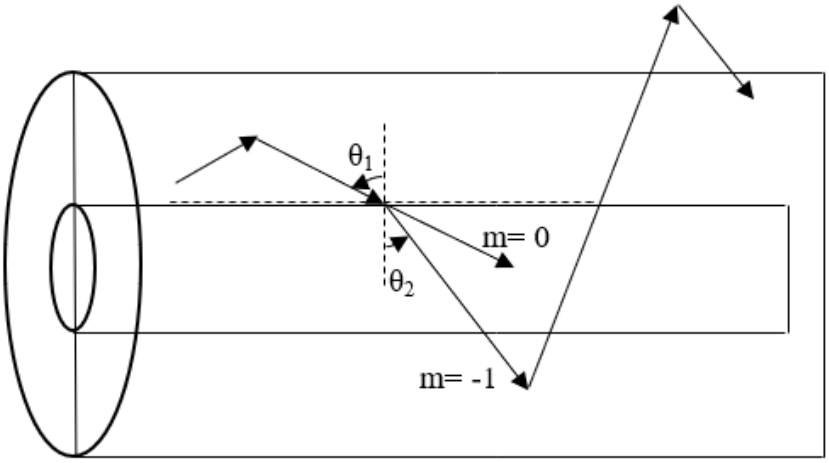

Figure 2.17: Cladding mode coupling by long-period grating [18].

We find that the resonant wavelength for reflection of a mode of index n_{eff1} into a mode of index n_{eff2} is:

$$\lambda = (n_{eff1} + n_{eff2})\Lambda \qquad (2.5)$$

If the two modes are identical, we get the familiar result for Bragg reflection:

$$\lambda = 2n_{eff}\Lambda$$

Diffraction by a transmission grating of a mode with a bounce angle θ_1 into a co-propagation mode with a bounce angle of θ_2 is illustrated in Fig. 2.16. In this illustration, the first mode is a core mode whereas the second is a cladding mode. Since, here $\beta_2 > 0$, the resonant wavelength for a transmission grating is:

$$\lambda = (n_{eff1} - n_{eff2})\Lambda \qquad (2.6)$$

2.7.2 Grating Types

Based on change in RI profile and grating pitch the grating is divided into various categories as shown in Fig. 2.18.

1. Uniform Grating Shape

For uniform short period FBG, the refractive index perturbation is given by:

$$n(z) = n_{co} + \Delta n_0 A(z) n_d(z) \qquad (2.7)$$

where n_{co} is the core RI, $n_d(z)$ is the index variation function, Δn_0 is the maximum index variation, and $A(z)$ is denotes to apodization function. For uniform FBG with no apodization index the variation function $n_d(z)$ is given by:

$$n_d(z) = \frac{\cos 2\pi z}{\Lambda} \qquad (2.8)$$

where Λ is the constant grating period.

2. Long- Period Fiber Grating Shape

Long-period fiber grating (LPFGs) typically have grating periods of the order of 100 μm to 1mm and are therefore much easier to manufacture. An LPFG can couple the forward propagating core mode to one or a few of the forward propagating core mode to one or a few of the forward propagating cladding modes. Using couple mode theory, the transmission characteristics can be monitored. The sensitivity of LPFG is dependent on nonlinear effects of modes. The LPFG can be used for exploration of tunable equipment and sensors. By influencing the scattering characteristics, the bandwidth can be expanded. Also, by varying the coupling factor and grating period or by introducing phase shifts along the grating more advanced transmission characteristics are obtained.

(a)

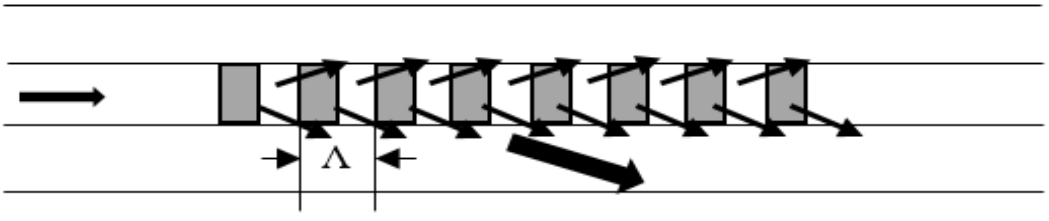

(b)

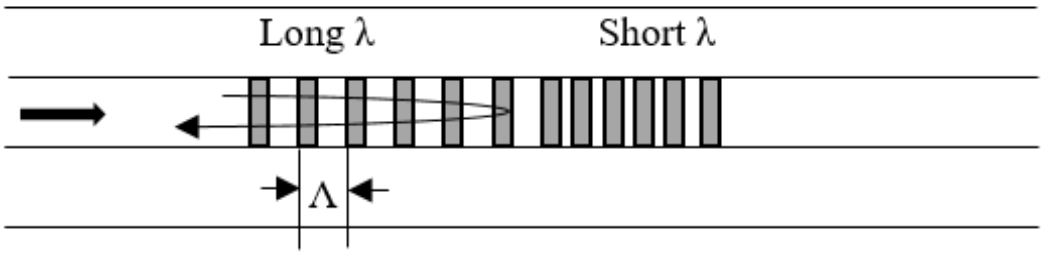

(c)

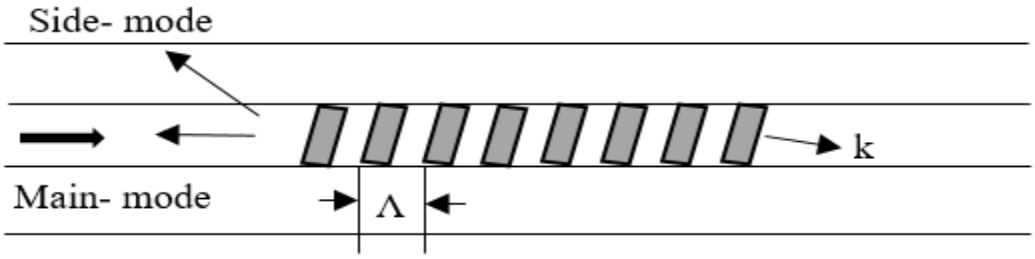

(d)

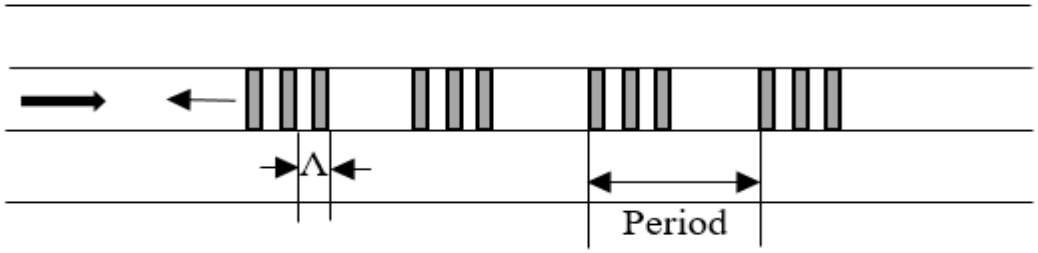

(e)

Figure 2.18: Types of fiber grating: (a) UFBG, (b) LPFG, (c) CFBG, (d) TFBG, (e) SFBG.

3. Chirped Fiber Grating Shape (CFBG)

The RI profile of the grating is reshaped as a linear variation in the grating pitch and the resulting grating is said to the chirped. When any change occurs in physical parameters of sensor then the grating period and signal spectrum gets changed.

4. Tilted fiber grating Shape

The variation of RI occurs at an angle to the optical axis. The angle of tilt has an effect on the reflected wavelength and the bandwidth. This grating combines three factors i.e. transmitted mode, reflected mode for the core and reflected mode for cladding. The resonant wavelength for each mode depends differentially on external perturbations and thus can be used to make the fiber grating into a multimodal sensor.

5. Sampled Fiber Grating Shape

A sampled fiber grating has the property of reflecting a number of wavelength components with uniform wavelength order.

2.8 Literature Survey

2.8.1 Sensitivity Measurements in Optical Sensing

Kim *et al.* [14] proposed a FBG laser sensor with semiconductor optical amplifier (SOA) over erbium-doped fiber laser because SOA generates multiple wavelength operations. Experimentally, eight sensing points were sensed and it was shown that the proposed sensor was good at multiple point sensing.

Guo *et al.* [15] proposed long distance fiber sensor system using broadband source and Raman amplifier. Number of sensors were increased using Intensity and wavelength division multiplexing (IWDM) technique. Four FBGs were used in this work and Raman amplifier was used to increase the sensitivity of sensing signal for long distance. It was observed that Bragg wavelength is accurately detected at 25km with good quality factor.

Zhou *et al.* [16] used the FBG strain sensor for 3D structural strain detection for pavement structure. They investigated the two vertical sensor and third one is transverse sensor. The proposed sensor was embedded in highway pavement structure and studied it for various application including monitoring the strain field. They optimized the sensor assembly for valuable applications and to reduce the observation error. From the experimental result it was observed that there is 60% less load on vertical sensors than transverse sensor.

Bai *et al.* [17] designed central wavelength demodulation system of FBG distributed sensor. Using proposed sensor experimental work was done to monitor the health of structure of the smart reinforced concrete. The comparison of observed result with traditional strain measurement was discussed and the proposed sensor gave us better performance over traditional sensor in terms of immunity to EMI, easy to make distributed sensor network and remote monitoring.

Lima *et al.* [18] proposed the FBGs sensor for structural health monitoring (named as the church of Santa CASA DA Misericordia of Aveiro). Total nineteen sensors were installed to identify the structural damages and observe the vibration, displacement as a result of thermomechanical processes. This experiment was done to predict a probable dangerous situation for the structure and also gather the data which will be useful for future planning.

Hassan *et al.* [19] measured the corrosion with the help of strain and temperature parameters using FBG based sensor. They performed the experiment on reinforcement rebar. They monitored the growth of corrosion by observing the wavelength shift and obtained maximum 1 nm wavelength shifting, which is less sensitive.

Han *et al.* [20] presented FBG moisture sensor using SOA based fiber laser where two FBGs sensors were used as a resonator mirror. The optical power is measured for the detection of

moisture level in environmental chamber. They varied the RH value from 30% to 80% and it is reported that as the humidity level increased the optical power decreases accordingly. From the results, it is recommended that the proposed sensor has excellent sensing feature in continuous monitoring, long term measuring, temperature compensation and maximum power fluctuations.

Kister *et al.* [21] continuously monitored the strength of West Mill bridge which is in Oxfordshire, United Kingdom. They tested the bridge under different conditions to evaluate the performance of sensor for SHM. They applied different bending tests to predict the deformation of the bridge. They also checked the performance of optical sensors after three years and observed that placed optical sensors give acceptable results to any load.

Capoluongo *et al.* [22] sensed the variation of dynamic features using FBG sensor and the implementation was done on two steel bar (joined to each other) in presences of artificial impairment. As a result, it was shown that FBG has an ability to retrieve the modal shapes in better arrangement with reference sensors up to 1.5 kHz frequency.

Paolozzi *et al.* [23] used optical sensor to analyse the dynamic variation of a composite wing beam. The experiment was done on proposed structure to obtain the strain frequency response and resonant frequencies. Sun *et al.* [24] shows the measurements of dynamic strain using conventional strain gauges and FBG's. Dynamic and static loading tests were executed to authenticate the superiority and possibility of using packaged FBG accelerometers and FBG as reusable strain sensors. It was reported that most of the working frequency of strain sensor fulfills the necessity of dynamic strain measurement. Strain sensor measured the maximum strain and it agrees with the electric strain gauges.

Takeda *et al.* [25] performed the SHM on composite wing structure using FBG sensor. Seven sensors are used to complete the experiment of fatigue tests and impact damages. The deformations are monitored by observing the changes in output spectrum of sensor. During this experiment the change in strain value is observed with the help of shifting in wavelength chart.

Sekine *et al.* [10] identified the shapes and place of deformation (crack) in aircraft panels. FBG sensor was used to detect the damages in aircraft panels and repaired with patches. FBG sensor were mounted at different locations on the surface of model and the reflection spectrum was observed through grating period. As a result, deformation was identified by minimizing the difference between calculated reflection spectrum and detected deformation.

Zhao *et al.* [26] proposed displacement sensor to monitor the beam using interrogation method. They observed the wavelength shifting using proposed sensor and compared the

results with conventional interrogation methods. They make the system cheaper than conventional interrogation methods with the help of blazed FBG and fiber optic array, and infrared linear detector. They received and recorded the elements using fiber optic array and infrared linear detector. From the investigation they suggested that proposed sensors are suitable for small displacement measurement applications.

Chan *et al.* [27] investigated the FBG sensors to monitor Tsing Ma Bridge (TMB). Forty FBG sensors were installed to monitor the performance under both railway and highway loads as well as comparing the results with conventional structural health monitoring system. They experimentally proved that FBG sensors give us better performance than conventional sensors.

In addition to these some work pertaining to the field of sensitivity issue in optical sensing are tabulated in table 2.2.

Table 2.2: Sensitivity in optical sensing

Reference [year]	**Wavelength**	**Techniques**	**Purpose**	**Sensitivity**
Ferreira *et al.* [2017][28]	325 nm	Fabry Perot cavity-based polymer FBG & fast Fourier transform	Sense refractive index and temperature	$-1.94\ RIU^{-1}$
Jia *et al.* [2017][29]	1525 nm 1550 nm 1580 nm	Fabry Perot interferometer	RI sensor for high temperature application	~1546 nm/RIU
Chavez *et al.* [2013][30]	976nm 1064nm	Yb doped fiber	Temperature monitoring	--
Zhu *et al.* [2017] [31]	1547.3 nm 1539.5 nm	Dual FBG sensor	Accelerometer monitoring	9.4 pm/g
Kim *et al.* [2017] [32]	---	Polymide FBG sensor	Enhance the maximum strain monitoring for prestressed concrete	2.36%
Wang *et al.* [2017][7]	1539.906 nm 1541.899 nm 1543.816 nm 1545.827 nm	FBG based sensitivity adjustable	Two-dimensional vibration monitoring	X and Y directions resides in 16.096 pm/g ~ 152.290 pm/g and 16.398pm/g ~ 150.680

				pm/g, respectively.
Almubaied *et al.* [2017] [33]	1544.762 nm	FBG strain sensor	Corrosion monitoring of reinforced concrete	0.3 nm
Zhang *et al.* [2012][34]	1543	FBG sensor	Pressure Measurements	20 pm/kpsi
Huang *et al.* [2012][35]	1550	Chirped FBG Sensor	Stress	0.08 nm
Linag *et al.* [2005][36]	1519.868 nm	FBG sensor	Refractive Index	0.5 nm

2.8.2 Simultaneous Monitoring in Optical Sensing

Ramakrishan *et al.* [37] proposed a polarimetric sensors based on an acrylate coated polarization maintaining photonic crystal fiber (PM-PCF), a coating stripped PM-PCF and FBG sensor to monitor strain, thermally induced strain and temperature, respectively. These sensors were embedded on glass fiber reinforced composite material. After experiment they suggested that proposed sensor configuration can be used in composite material SHM application.

Jung *et al.* [38] demonstrated an FBG with erbium doped fiber amplifier (EDFA) which can simultaneously measure the strain and temperature. The parameters of FBG and EDFA were optimized at different Bragg wavelengths and amplifier lengths (or pumping powers) respectively. It was reported that the performance of strain and temperature can be observed by monitoring the transmission dip shift and subtracting the temperature effect from it.

Luo *et al.* [39] proposed etched FBG coated with polyimide to detect the salinity and temperature simultaneously. Refractive index and temperature of salinity was measured with the use of cladding mode resonance wavelength (CMRWs) and fundamental mode resonance wavelengths (FMRWs). From the experimental results it was shows that, FMRW and CMRW have the detection sensitivities of 15.407 and 125.92 nm/RIU for RI and 0.0312 and 0.0435 nm/°C for temperature, respectively.

Kang *et al.* [40] proposed FBG and Extrinsic Fabry Perot interferometer (EFPI) sensor to monitor strain, temperature and vibration simultaneously for aluminum beam with the help of wavelength swept fiber laser (WSFL) and laser diode. Aluminum beam was placed in a thermal chamber, further strain and temperature were monitored using FBG sensor while simultaneously vibration was measured using EFPI sensor by laser diode.

Enckell *et al.* [41] proposed stimulated Brillouin scattering optical fibers to monitor distributed strain and temperature on Gotaalv Bridge in Sweden. Optical sensors were installed on the whole length of bridge further measured the strain profile and detected the cracks that are wider than 0.5mm.

Massaroni *et al.* [42] fabricated three FBG based sensors to monitor Relative Humidity (RH) and temperature in mechanical ventilation. Two FBG sensors were coated with agar and one sensor is coated agarose layer. Temperature measurement was simply performed by commercial FBG sensor that is insensitive to RH. It was reported that when value of RH increases the spectra of three FBG coated sensors shift towards the higher wavelength. This analysis has been performed at different values of RH (about 15% and about 40%) at constant temperature 20^{o}C.

Kim *et al.* [43] proposed a FBG sensor to measure the dynamic strain on concrete beam. Diode driver, photo diode and super luminescence diode (SLD) are considered as a detector. Cyclic load up to 14 ton was applied on the beam and the response of the proposed sensor was monitored. They compared the data with strain gauge and experimentally it was observed that both sensors show good coincident response to the applied loads.

Xu *et al.* [44] proposed FBG sensor to measure the temperature and strain at same time. The sensor is divided into two parts, one is coated area and another one is uncoated area. The variation of strain was measured at constant temperature 20^{o}C and it is observed that wavelength spacing increases with applied strain. Further, variation of temperature (5 to 50^{o}C) was measured at fixed strain value 470$\mu\varepsilon$. From the results it was shown that, uncoated area was less sensitive to temperature and more sensitive to strain than coated area.

In addition to these, some work pertaining to the field simultaneous monitoring issue in optical sensing are tabulated in table 2.3.

Table 2. 3 Simultaneous Monitoring in optical sensing

Reference [year]	**Wavelength**	**Parameters Investigated**	**Sensing Method**	**Outcome**
Cheng *et al.* [2006] [45]	1540 nm 1545 nm 1550 nm 1555 nm	Static Strain and Temperature	FBG sensor and Genetic algorithm, two pair FBGs	They observed variation of error value with change in strain and temperature. They achieved maximum error from 27.68 to 97.23% and 9.32 to 17.7% for strain and temperature profile respectively.

Lee *et al.* [2010][46]	1562.5 nm	Temperature, strain, refractive index	Etched-Core Fiber Bragg Grating Sensors	Demonstrated simultaneous measurement by exciting multiple order modes in an etched-core FBG sensor. They achieved maximum wavelength shifts: 3 nm, 7nm and 13 nm for 1^{st}, 2^{nd} and 3^{rd} mode at different refractive indices. -0.5, -0.65 and -1.2 nm for 1^{st}, 2^{nd} and 3^{rd} mode due to change in temperature.
Park *et al.* [2010][47]	1532.23 nm 1556.517 nm	Strain and Temperature	Normal and Reverse index fiber Bragg grating Sensor	They achieved maximum wavelength shift: 9nm for both normal and reverse index fiber sensor for strain value. 1.3nm and 1.25 nm for normal and reverse index fiber sensor for strain value for temperature value, respectively.
Wu *et al.* [2016][48]	1548.08 nm 1547.94 nm	Gas pressure and Temperature	FBG and Fabry Perot cavity	They monitor the gas pressure and temperature simultaneously using FBG and FPC sensor and sensitivity of the sensor was also calculated as: 4.063pm/kPa and 4.071pm/kPa for FBG and FPC, respectively. 0.87pm/^{o}C and 0.83 pm/^{o}C for FBG and FPC, respectively.
Dreyer *et al.* [2018] [49]	1538.5 nm 1540.5 nm 1544.5 nm	Temperature, vibration	FBG sensor	Temperature and vibration were measured simultaneously in a hydroelectric generator. They achieved 10 pm/°C temperature sensitivity coefficient between room temperature and above 60 °C and 7.19 pm/g vibration sensitivity in a frequency range between 5 Hz and 1 kHz.

2.8.3 Continuous Monitoring in Optical Sensing

Thakur *et al.* [50] proposed polarization maintaining photonic crystal fiber (PCF) for structural health monitoring of composite beam. Vibration was tested in the frequency range 1-50Hz using proposed sensor. Antunes *et al.* [51] monitored the deformation of structure with optical displacement sensors. Horizontal cyclic force was applied by hydraulic actuator to full scale adobe wall and monitored by thirteen sensors which are implemented on structure. It was demonstrated that, the feasibility of applying static optical FBG sensors to study the behavior and performance of civil engineering infrastructures even for extreme loading events.

Triana *et al.* [52] measured the strain in metal structures. The strain coefficient of 1.19 pm/με was determined from FBG sensors which was fabricated at Universidad Politecnica de Valencia. Bremer *et al.* [53] proposed a fiber optic crack sensor and two moisture sensors to monitor crack and moisture in concrete structures. Optical sensors were embedded in concrete structures for evaluation and measured the attenuation of fiber depending on crack size. From the result it was shown that, when RH values were applied it gives us linear response with respect to wavelength shift (maximum wavelength shift 0.5 nm). The crack size i.e. 1.4mm is also detected during experiment by proposed crack sensor.

Lu *et al.* [54] used FBG sensor to detect the strength of reinforced concrete (RC) beam. They used Carbon fiber reinforced polymers (CFRP) to enhance the strength of RC beam. Further, strain change of CFRP was calculated through monitoring the wavelength changes of FBG sensors. Roveri *et al.* [55] used grating based fiber sensors to monitor the strain and vibration on four lines railway track. Fifty sensors were used to monitor the track continuously for six months. They observed the strain value during daily passenger rail transport with roughly speed 90km/h. They achieve maximum 50 με strain value for the 44^{th} train passage.

Table 2.4: Continuous monitoring in optical sensing

Reference [year]	Detection	Sensor Type	Wavelength Shift	Remark
Lau *et al.* [2001][57]	Strain	FBG Sensor	1.5 nm	Not temperature compensation
Sheng *et al.* [2009] [58]	Strain	FBG Sensor	1 nm	Less sensitive
Shen *et al.* [2015] [59]	Strain	FBG Sensor	0.8 nm	Less sensitive
Bremer *et al.* [2017] [60]	Strain	FBG Sensor	0.3 nm	Less sensitive
Feng *et al.* [2015] [61]	Vibration	FBG Sensor	19 nm	Not temperature compensation
Ding *et al.* [2010] [62]	Humidity	FBG Sensor	0.4 nm	Less sensitive

Miquel *et al.* [2016] [63]	Strain and temperature	FBG Sensor	3 nm for strain 1.2 nm for temperature	Less sensitive
Obaton *et al.* [2013][64]	Liquid level	Tilted shape FBG	12 nm	High sensitive in case of liquid level measurement

Zheng *et al.* [56] monitored the corrosion in steel rebars under the concrete structure using FBG sensor. They calculated the corrosion rate (0.5%) using FBG parameters and changes in diameter of rebar. Islam *et al.* [12] monitored the degree of corrosion on reinforcing steel rod in moist condition using FBG sensor. Sensitivity was also calculated for different cladding resonance. They achieved highest sensitivity 36.7pm/h and lowest 7.3pm/h for high and low cladding modes.

From the extensive literature survey, it can be concluded that there is a definite need to carry out research in the area of FBG. The investigations required in the field of FBG for communication systems should encompass the area of simulation of FBG and its validation using theoretical and experimental works. The wavelength shift in FBG on simulated external perturbation using a wideband source also needs to be observed leading to the design of FBG Interrogator for Sensor/Communication systems.

2.9 Gaps in Present Study

This section lists the common limitations encountered while dealing with optical fiber sensing systems. This would make the reader realize the importance of these drawbacks and elucidate the reasons for attempts at solutions to these problems.

1) Potential of optical sensors to provide high sensitivity with optimized results is an open area of research.
2) Optical sensor technology is best alternative to give the fast response. Further, there is need to increase the sensitivity with cost effective solutions.
3) Till now various grating based optical sensors are illustrated for health monitoring of civil structures but other low-cost sensors such as SPR, PCF, hybrid optical sensor etc. can also be used for the same and better results will be predicted because of its high sensitivity and fast response.
4) Various investigations have been done on fiber Bragg grating as a sensor, but we can also use uniform, chirped and tilted fiber Bragg grating shapes for better system performance.

Chapter 3

Design of an Optical Refractive Indexed Sensor for Chemical Detection

3.1 Introduction

In this chapter, the first research objective which is to propose a model of optical sensor to increase sensitivity in terms of RI, wavelength shifting and OSNR has been addressed. The optical RI sensor is proposed to detect the presence of $Ca(OH)_2$ and $Mg(OH)_2$ chemicals to monitor portlandite. Portlandite is one of the main reasons which causes spalling, corrosion and cracking in structures which eventually affects its health. If proposed chemical concentrations are detected in the concrete structure, it is possible to detect the presence of portlandite at early stage. In this work, two RI sensors are proposed, one is etched cladding sensor (uncoated sensor) and another one is highly sensitive sensor (ITO coated sensor). ITO coating is used on etched cladding sensor to increase the sensitivity. The results of proposed sensors are presented in terms of wavelength shifting, OSNR and intensity of light. To implement and analyse this work, OptiFDTD software is used.

3.2 Design of Optical Refractive Index Sensor

Numerous studies have been conducted on portlandite monitoring such as carbonation with carbon dioxide, thermogravimetry, chemical analysis and gamma densitometry [78-79]. But these studies have some limitations like manual monitoring, less flexible and less sensitive which can be subdued by using an optical sensor for continuous monitoring of chemical reactions in structures which are responsible for formation of portlandite.

In this work, we have used FBG based cladding etched sensors i.e. without (uncoated sensor) and with ITO coating layer (coated sensor), see Fig. 3.1. The designing part of the sensor is divided into four steps:

In Step 1, a single mode optical fiber is designed with 1.449 and 1.444 refractive index of core and cladding respectively. In Step 2, the uniform gratings are formed in the fiber core with grating pitch of 535nm. Under step 3, some part of cladding is etched at that area where gratings are presented for the detection of proposed chemicals. Further, in Step 4, the sensitivity is increased using ITO coating on the cladding etched area of core. To observe the sensitivity levels of the proposed sensors, the results from both sensors are compared

with respect to the same concentration level. Figure 3.2 and Fig. 3.4 shows the distribution of RI within the core for uncoated and coated sensors respectively. The light propagation along with the core is also obtained for uncoated and coated sensor shown in Fig. 3.3 and 3.5.

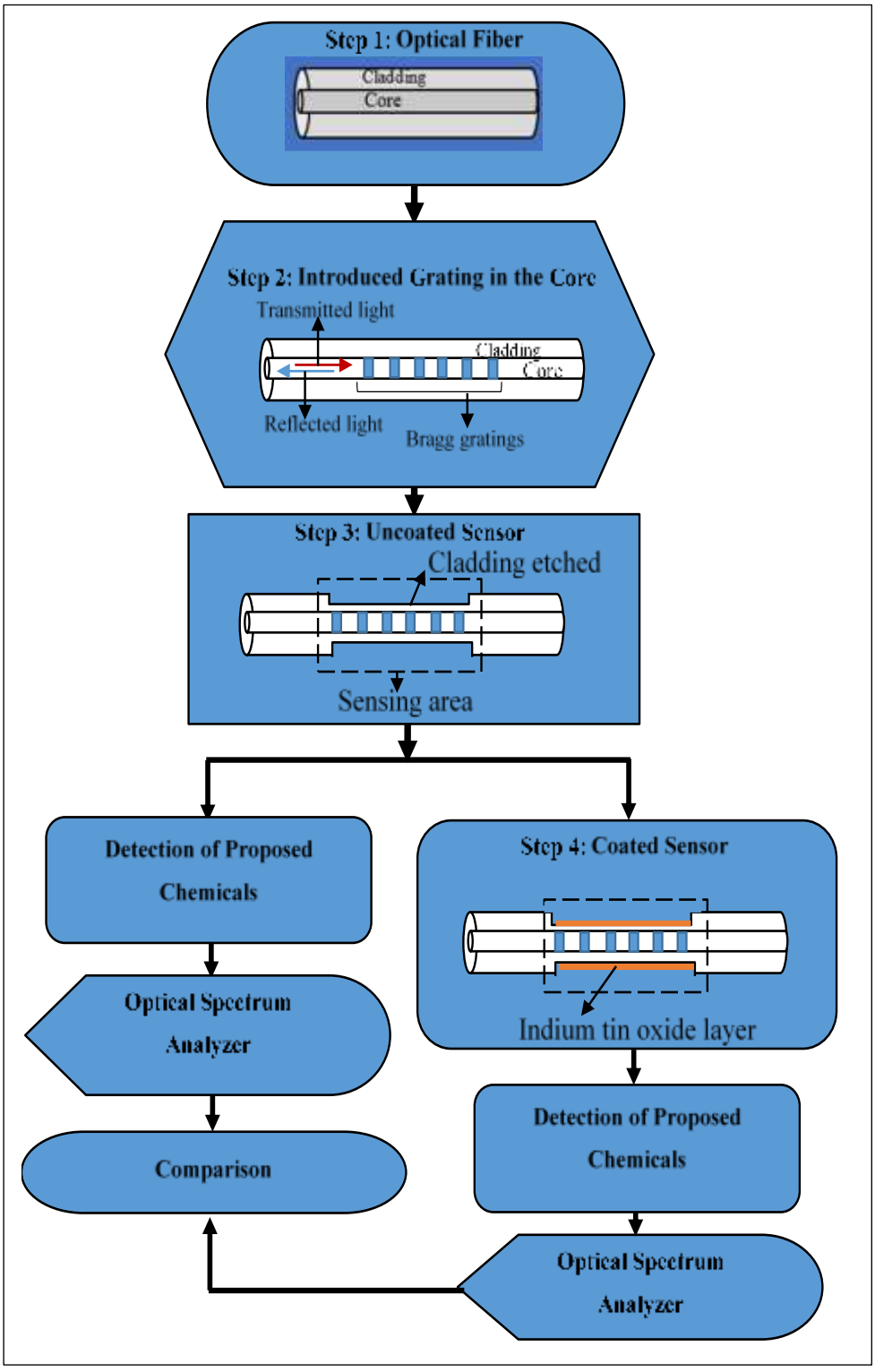

Figure 3.1: Design steps of proposed refractive index sensor for chemical detection.

From these Figures, it is cleary seen that the light is properly transmitted through the core with high intensity power. In the shown refractive index profiles, different colors represents the values of refractive indexs of cladding, core and gratings.

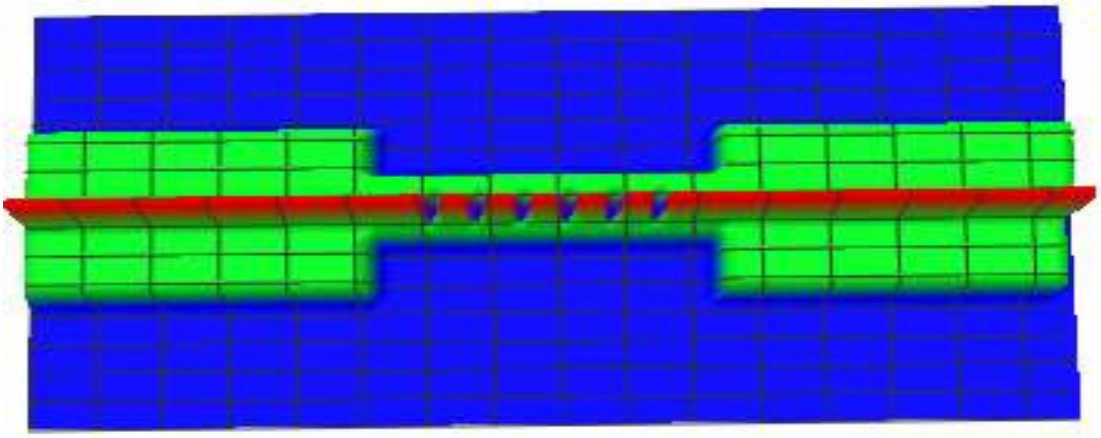

Figure 3.2 Refractive index profile of uncoated sensor.

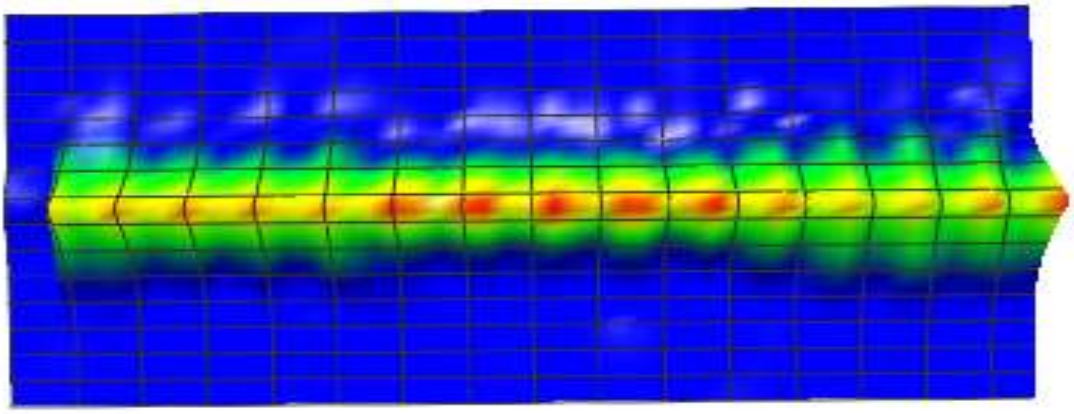

Figure 3.3: Propagation of light through core for uncoated sensor.

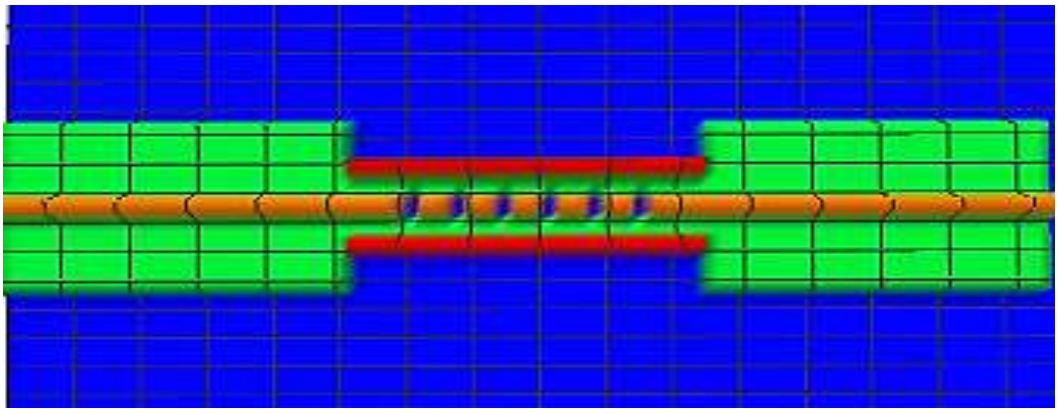

Figure 3.4 Refractive index profile of coated sensor.

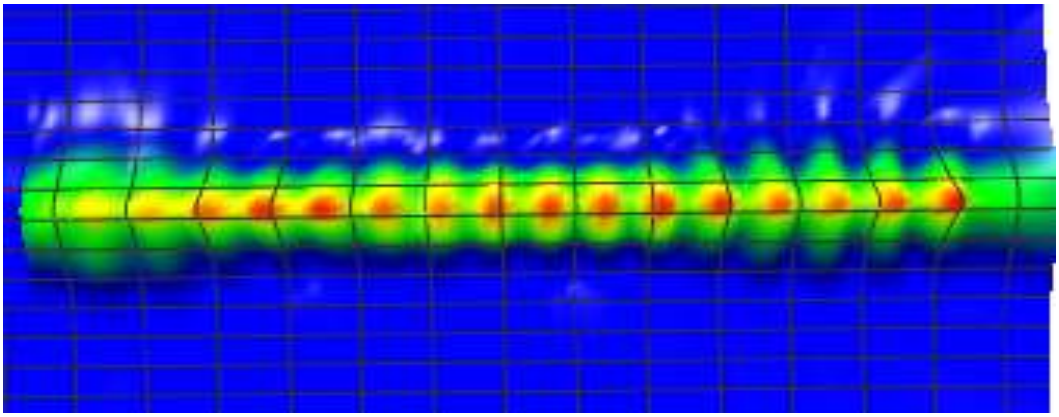

Figure 3.5: Propagation of light through core for coated sensor.

The effective refractive index variations through the core can be observed in light propagation spectrum where the light is properly transmitted along the core with existing modes.

3.2.1 Results and Discussions

Using proposed sensors, the values of refractive index are analysed with respect to different concentration levels of chemicals, see Fig. 3.6. From the graph it can be observed that, as we increase the concentration level of chemicals, the intensity of light is increases accordingly. We have used reflectometer to measure the refractive index and concentration of liquids, gels and solids which is shown in fig. 3.6(a). Refractometers determine the refractive index with an accuracy of up to ± 0.00002 nD, within a measuring range of 1.26 nD to 1.72 nD and a temperature range from 4 °C to 125 °C. The high accuracy of up to ± 0.03 °C is achieved by precise internal Peltier temperature control. The optical bench is sealed and temperature-stabilized to protect it from outside influences.

(a)

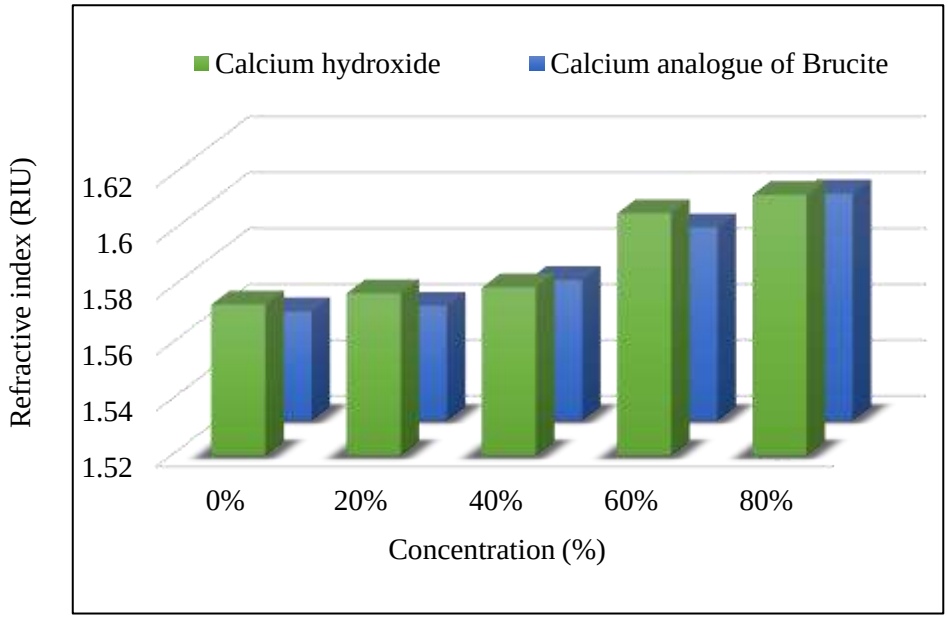

(b)

Figure 3.6: (a) Reflectometer to measure the refractive index at different concentration of level (b)Variations in RI with respect to chemical concentrations.

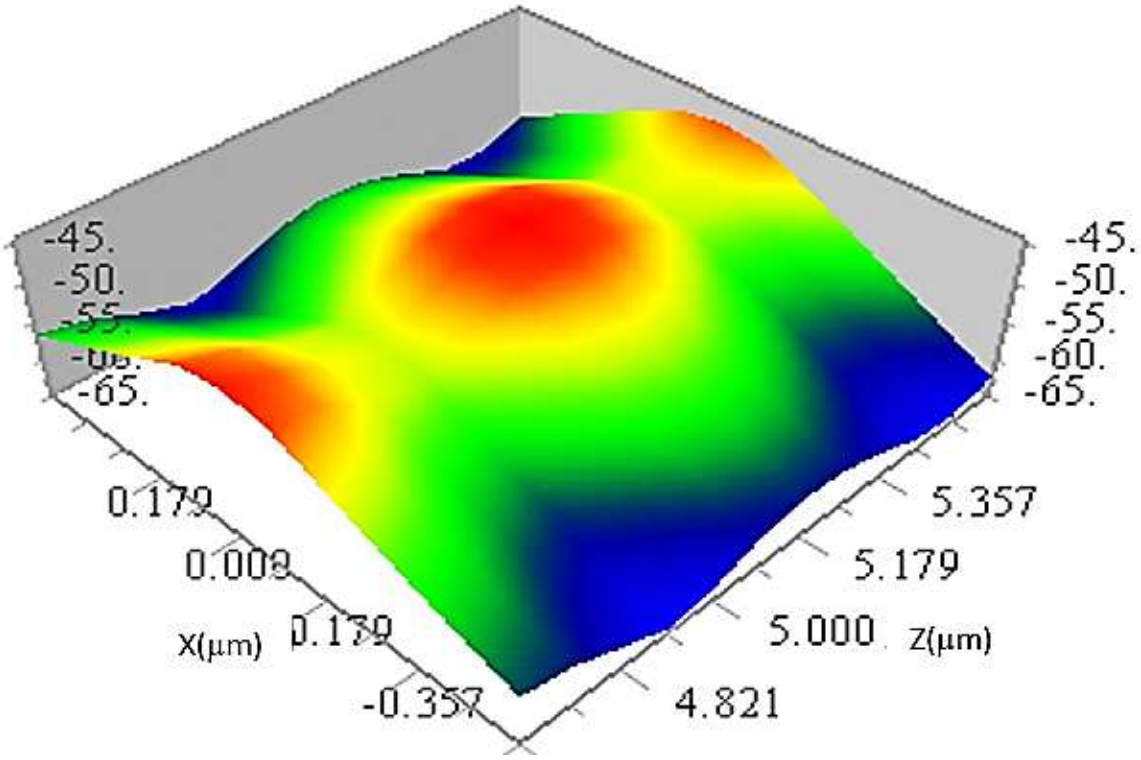

Figure 3.7: Transmitted field pattern for uncoated sensor.

The presence of these chemicals is detected with the help of transmitted field patterns and it can be seen that the sensors induces the variation in light when any changes are arising in the

concentration of chemicals. The transmission field pattern for uncoated sensor is shown in Fig. 3.7 to Fig. 3.9 and it can be observed that the light moves when the proposed chemicals are detected by active area of sensor.

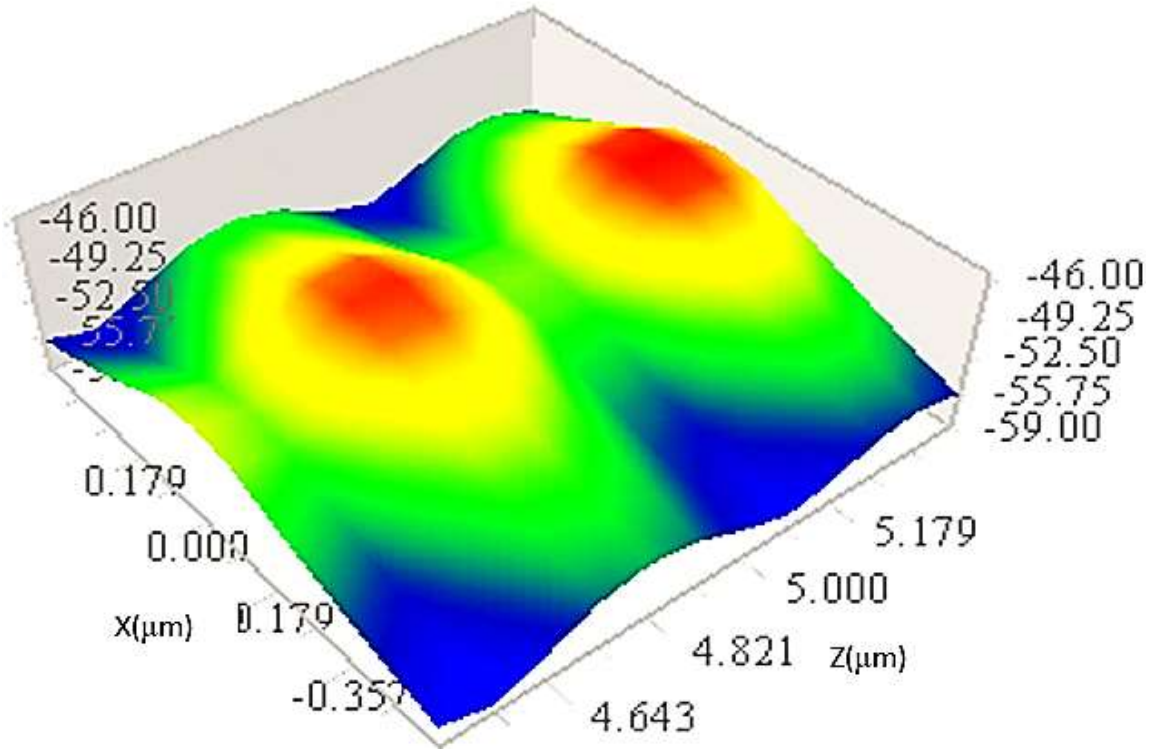

Figure 3.8: Transmitted field pattern for uncoated sensor with the presence of $Ca(OH)_2$.

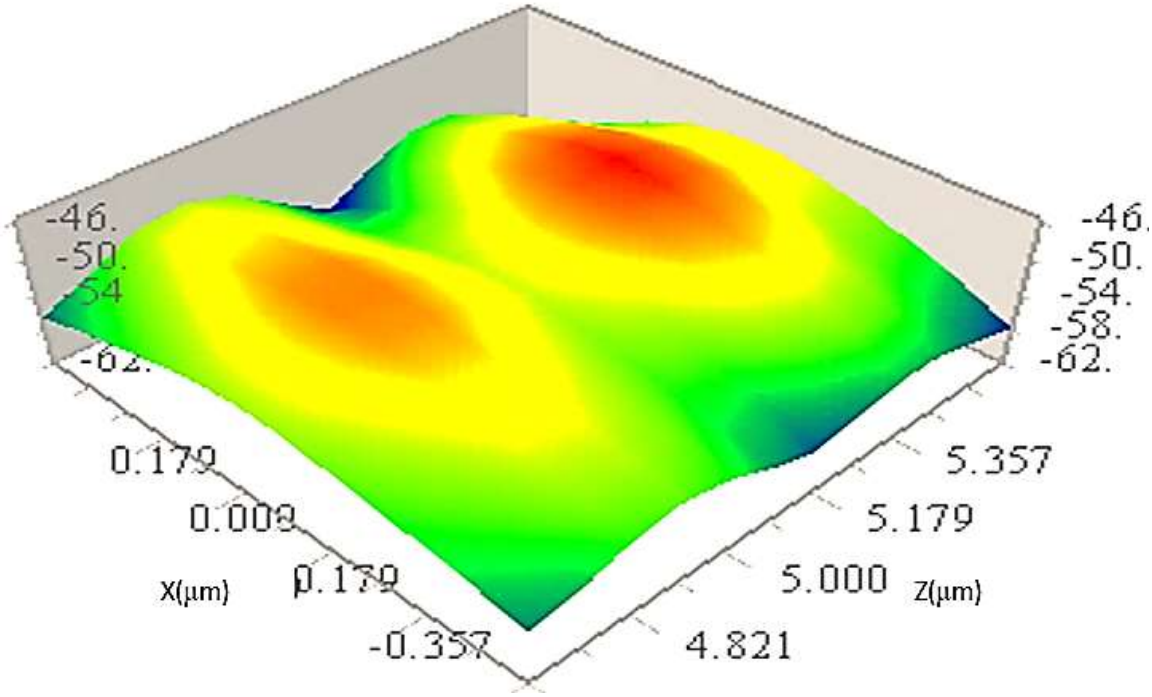

Figure 3.9: Transmitted field pattern for uncoated sensor with the presence of $Mg(OH)_2$.

Similarly, the transmission field patterns are also taken for coated sensor which are shown in Fig. 3.10 to 3.12. From these patterns it can be observed that an intensity of light changes when chemicals are detected in the sensing area.

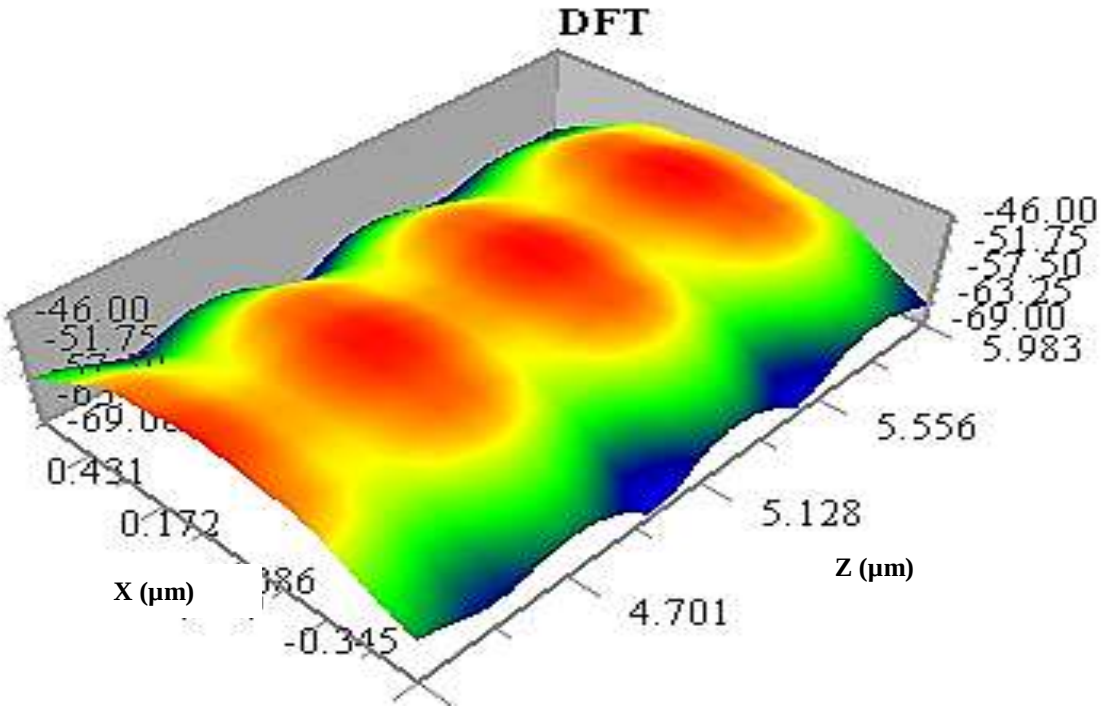

Figure 3.10: Transmitted field pattern for coated sensor.

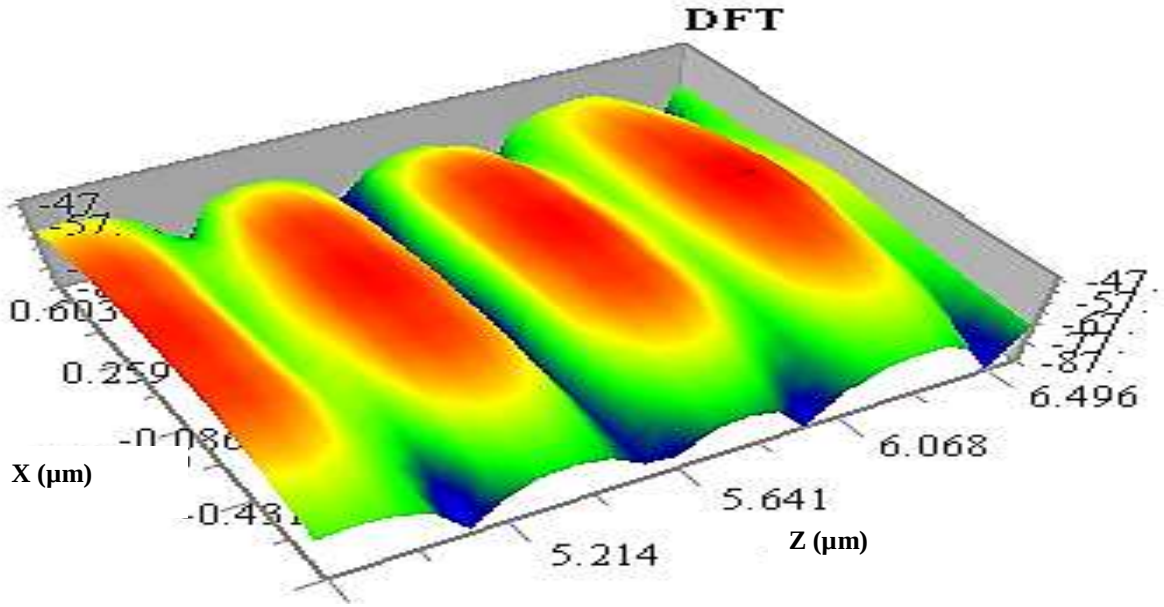

Figure 3.11: Transmitted field pattern for coated sensor with the presence of Ca $(OH)_2$.

The variation in intensity of light is observed at different concenration levels of chemicals for uncoated and coated sensor which is shown in Fig. 3.13 to 3.20, respectively. From the

graphs 3.13, 3.15, 3.17 and 3.19 it can be seen that as we increase the concentration level of chemicals the intensity of light changes incrementally. From the Fig. 3.14, 3.16, 3.18 and 3.20, it can be seen that as we increase the concentration level of the chemical, the wavelength is shifting toward right direction.

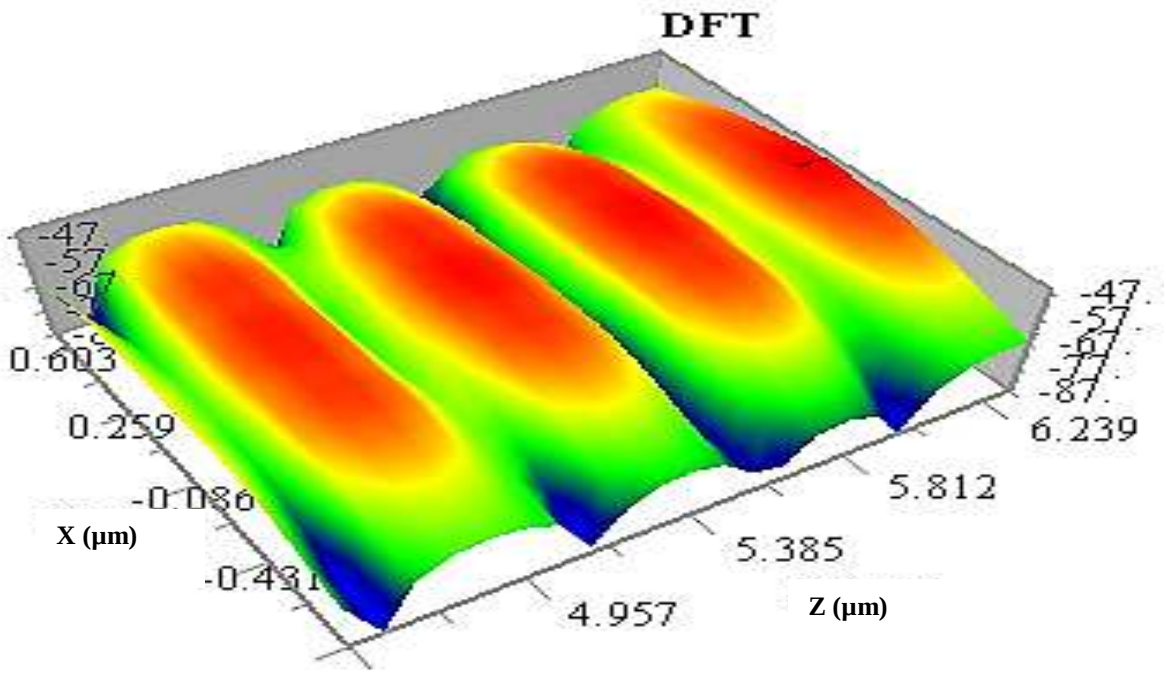

Figure 3.12:Transmitted field pattern for coated sensor with the presence of $Mg(OH)_2$.

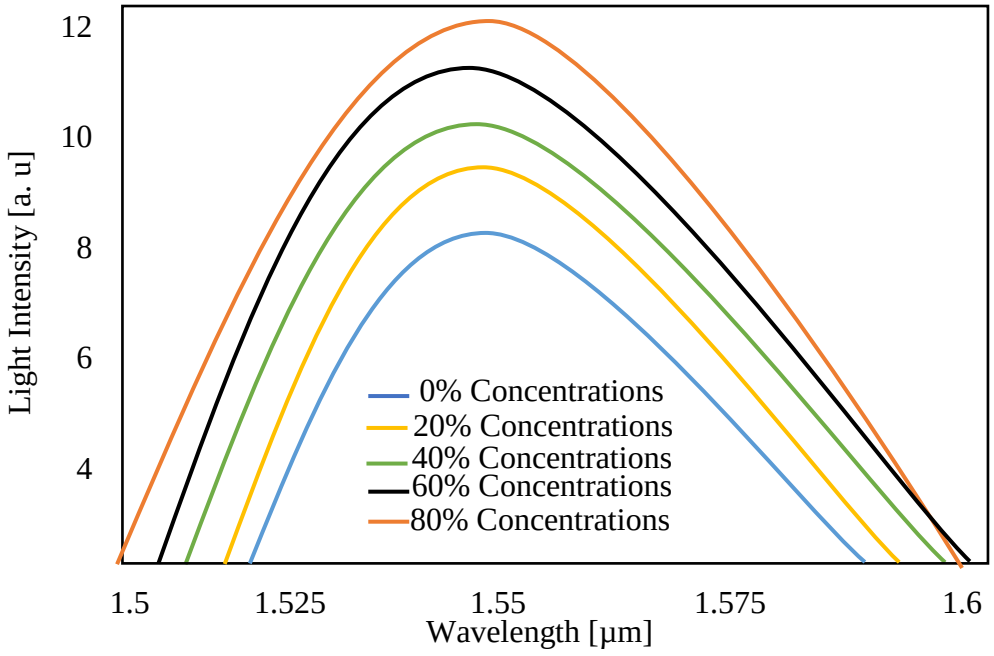

Figure 3.13: Variations in intensity of light as a function of wavelength for uncoated sensor with respect to different concentration levels of $Ca(OH)_2$.

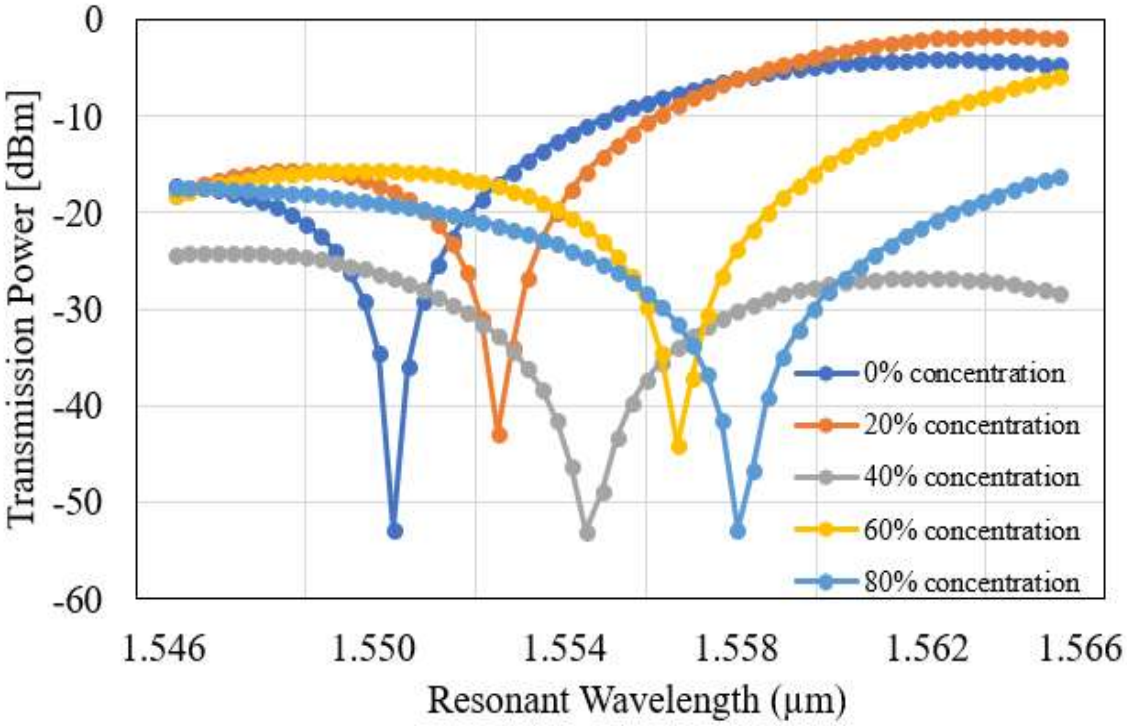

Figure 3.14: Variation in transmittance power as a function of resonant wavelength for uncoated sensor with respect to different concentration levels of $Ca(OH)_2$.

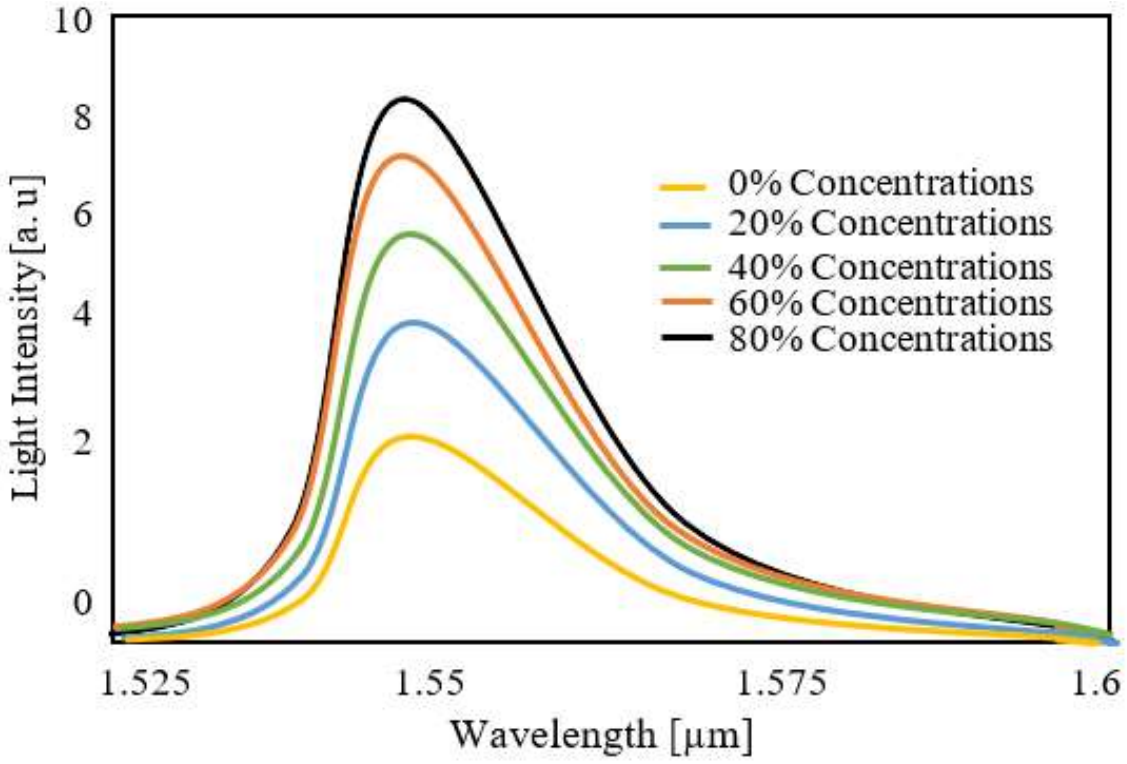

Figure 3.15: Variations in intensity of light as a function of wavelength for uncoated sensor with respect to different concentration levels of $Mg(OH)_2$.

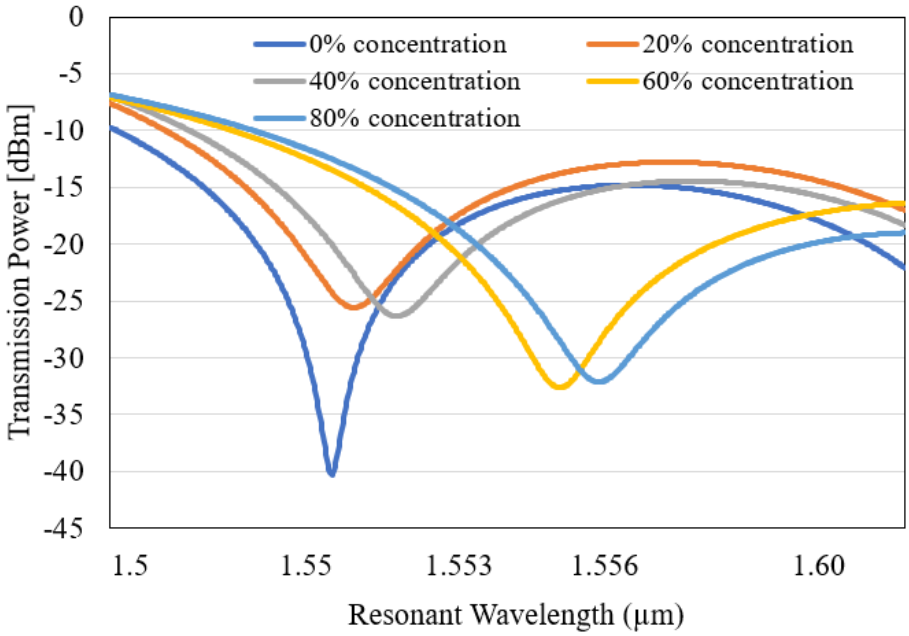

Figure 3.16: Variation in transmittance power as a function of resonant wavelength for uncoated sensor with respect to different concentration levels of $Mg(OH)_2$.

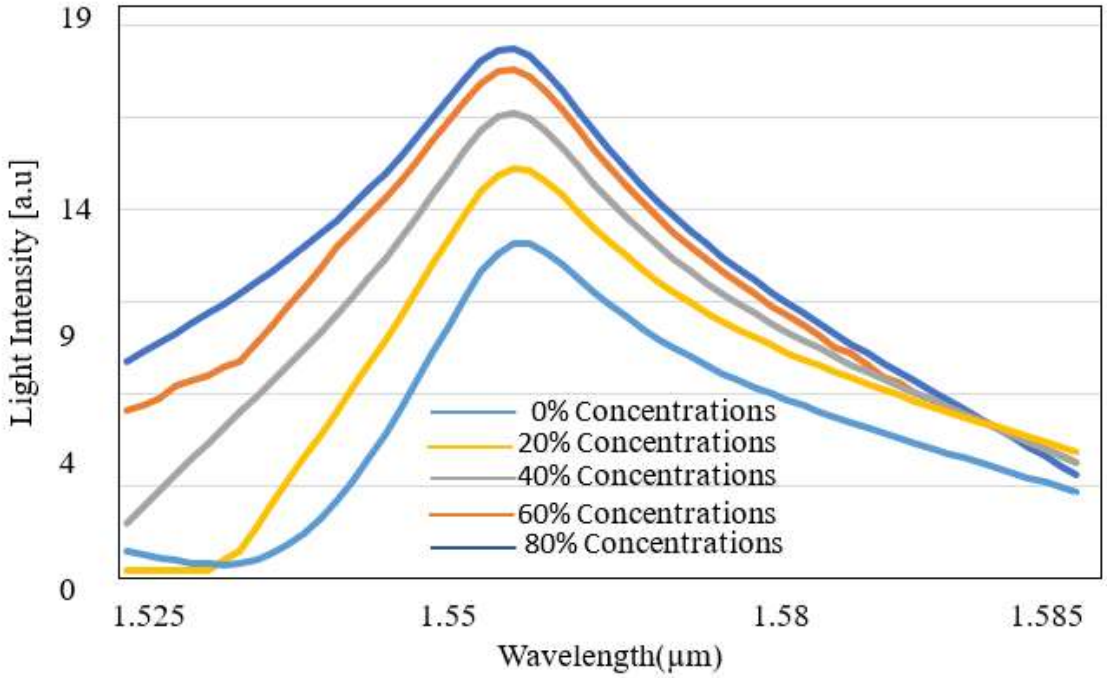

Figure 3.17: Variations in intensity of light as a function of wavelength for coated sensor with respect to different concentration levels of $Ca(OH)_2$.

The maximum wavelength shifts of 8 nm and 6 nm are obtained for $Ca(OH)_2$ and $Mg(OH)_2$ respectively, using uncoated sensor. The maximum wavelength shift of 12 nm and 10 nm are achieved for $Ca(OH)_2$ and $Mg(OH)_2$, respectively using coated sensor. From the graphs it can be concluded that coated sensor shows better performance compared to uncoated sensor in terms of sensitivity.

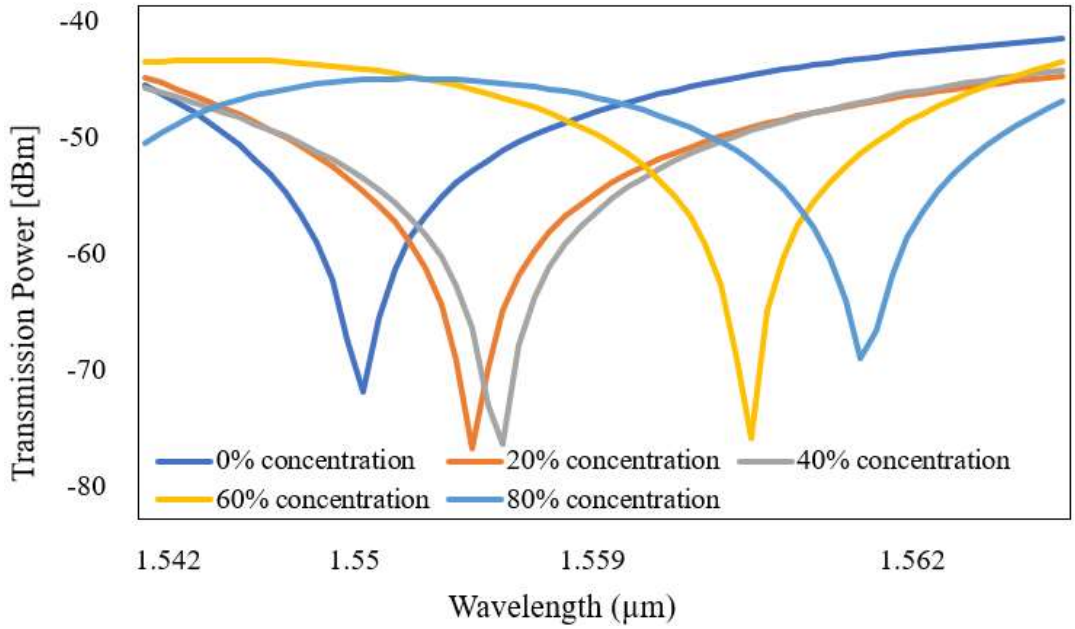

Figure 3.18: Variation in transmittance power as a function of resonant wavelength for coated sensor with respect to different concentration levels of $Ca(OH)_2$.

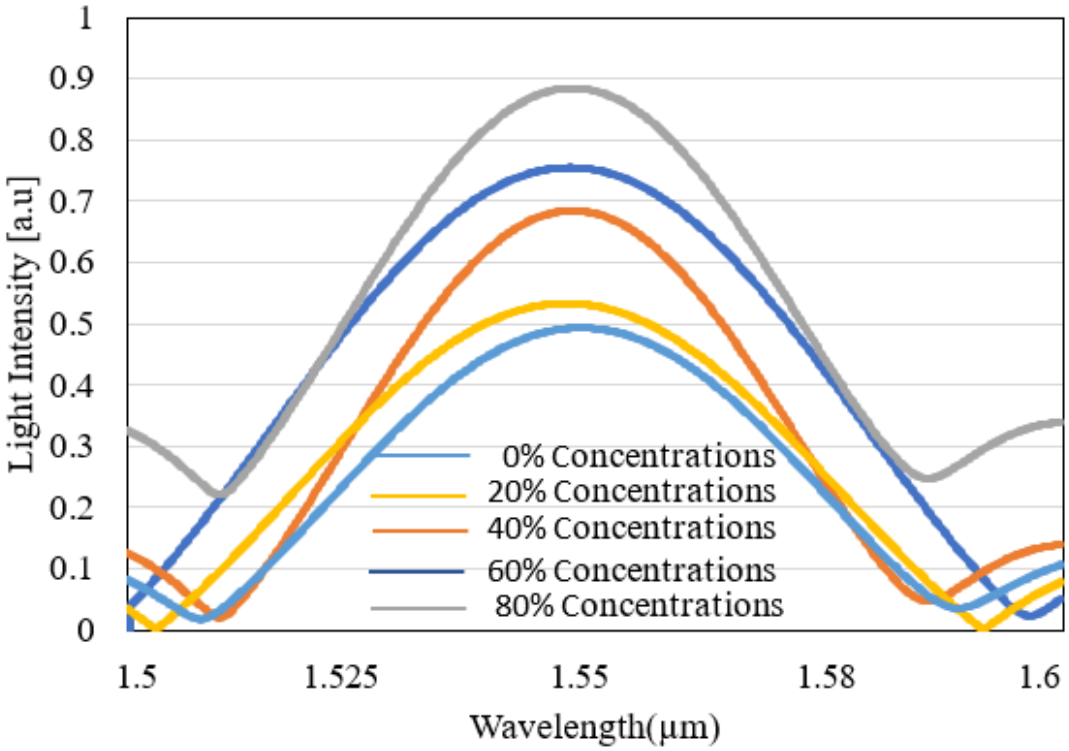

Figure 3.19: Variations in intensity of light as a function of wavelength for coated sensor with respect to different concentration levels of $Mg(OH)_2$.

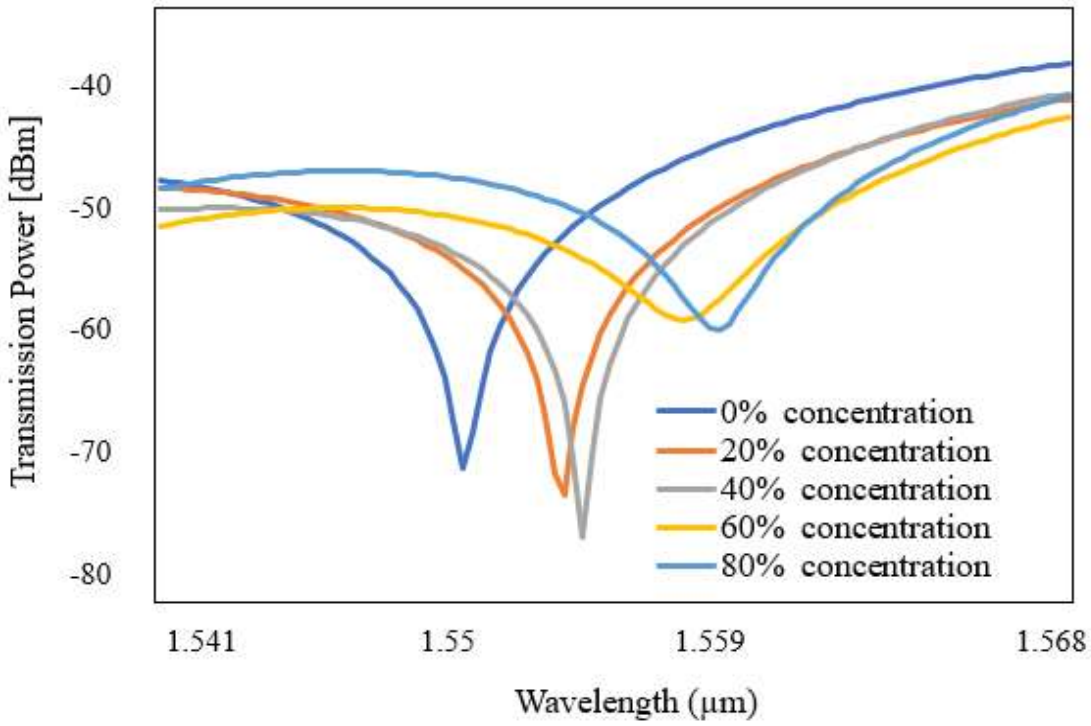

Figure 3.20: Variation in transmittance power as a function of resonant wavelength for coated sensor with respect to different concentration levels of $Mg(OH)_2$.

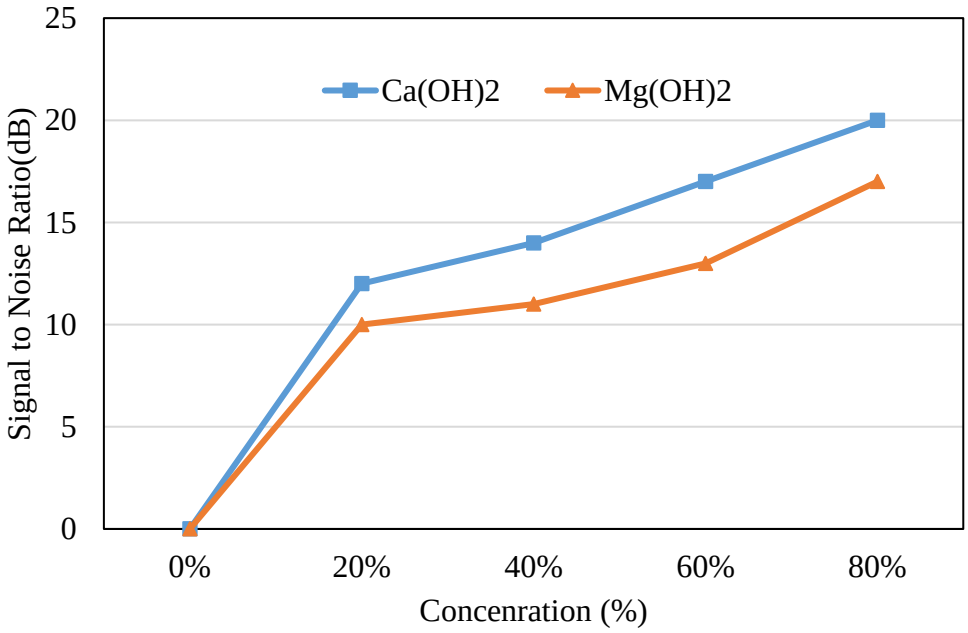

Figure 3.21: OSNR variation for different concentration levels of chemicals using uncoated sensor.

In the optical domain it is important to observe the OSNR because it suggests a degree of impairment and provides a qualitative description of the receiver performance when optical signal is carried by a transmission system. Figure 3.21 and 3.22 shows the OSNR

performance of proposed sensors at different chemical concentration levels. From the results it can be attained that a higher OSNR is observed for the coated sensor as compared to uncoated sensor. By comparison of the results for OSNR value it can be seen that the coated sensor is superior for detection of chemicals with higher signal power and lesser noise. For better clarity the graph is also plotted between refractive index, concertation level and observed the wavelength shift which is shown in fig. 3.23.

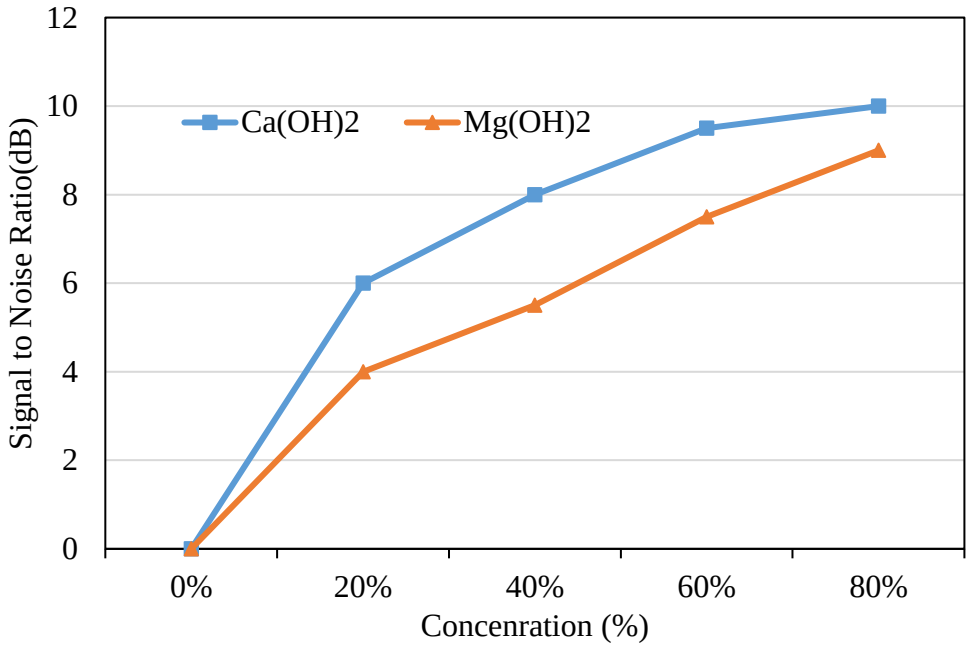

Figure 3.22: OSNR variation for different concentration levels of chemicals using coated sensor.

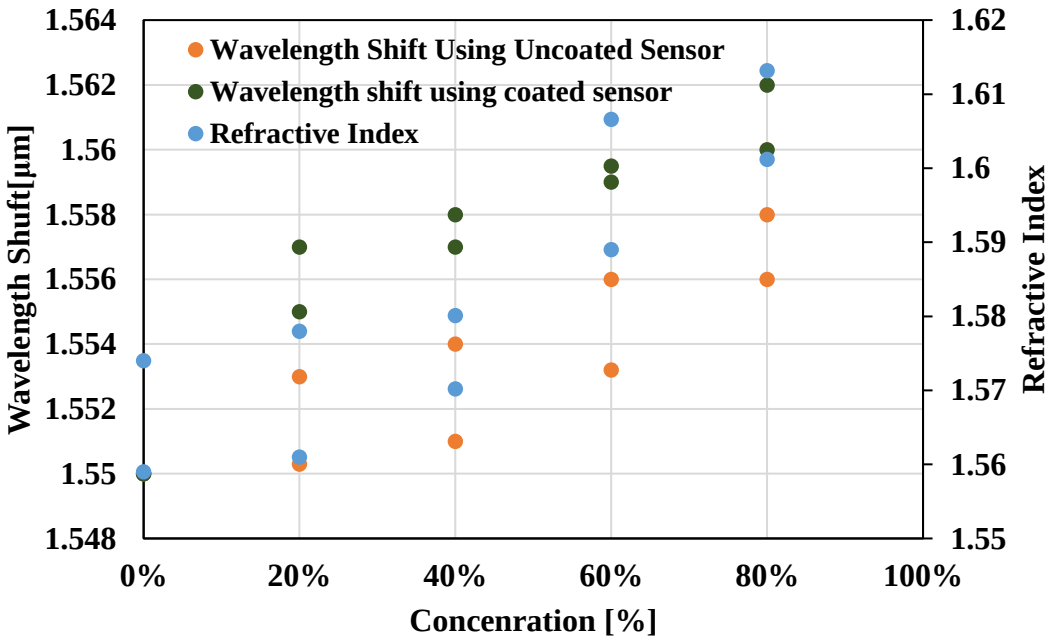

Figure 3.23: Change in shift in wavelength with respect to RI and concentration level of chemical for uncoated and coated sensor.

3.3 Conclusion

In this Chapter, we have presented that presence of Ca $(OH)_2$ and Mg $(OH)_2$ are the main reasons behind the formation of portlandite in civil structures. If these chemicals can be detected at earlier stage then possible and appropriate actions can be taken. To sense and monitor these chemicals, we have proposed optical uncoated and coated refractive index sensors. In uncoated sensor, cladding is etched near to the core (active area) where gratings are inserted. In coated sensor, ITO layer is used for coating on etched cladding sensor to enhance the performance in terms of wavelength shifting, intensity of light and OSNR. In conclusion, we have successfully detected the both chemicals even with different concentration levels. The maximum shift of wavelength i.e. 8 nm and 6nm using uncoated sensor and 12 nm and 10 nm using coated sensor for $Ca(OH)_2$ and $Mg(OH)_2$ are observed, respectively. OSNR is also analysed to observe the noise level of proposed sensors and it is observed that high OSNR (lesser noise) is achieved with the coated sensor.

Chapter 4

Optimization of Optical Sensor to Enhance the Sensitivity

4.1 Introduction

Initially in Section 4.2, for better understanding, we have performed Various on commercially available FBG optical sensor to monitor the strain value at different civil structures, the detail of these experiments is reported in chapter 6. From these experimentations, we have observed maximum wavelength shift of 7 nm which is less and need to be improved. In this chapter, to increase the sensitivity of FBG sensors, multiple parameters are optimized by implementing GA. The sensitivity is increased in terms of wavelength shift with the combination of optimized parameters i.e. Poisson's ratio, P_{11} and P_{12}. After optimization, we have achieved 38.16 nm of wavelength shift.

In next step, a hybrid optical sensor is proposed (see Section 4.3) to sense the strain, temperature and vibration. The sensor is designed by modifying the conventional ring resonator to increase the sensitivity. The modification is done with the help of Bragg gratings which are inserted in ring loop. Four uniform gratings are inserted after constant period called superstructure uniform grating shape. Further, the proposed sensor is used to monitor different deformations which occurs in the civil structure due to natural or physical hazards. These deformations are observed with the help of transmission power spectrum, overlap integral and wavelength shifting graphs.

4.2 Optimization of Optical Sensor to Increase the Sensitivity

The unique and promising advantages of optical fiber sensors make them useful for effective SHM to maintain the health of civil structures with speedy and cheaper solutions [86-90]. Various schemes have been used for SHM of civil structures using optical fiber sensors [52], [71] but FBG sensor are mostly used [64-65], [91]. Several parameters such as grating length and grating shape can control the performance of an FBG. The optical fiber sensor based on FBG for SHM was proposed by Morey *et al.* in 1989 [72]. The FBG sensor follows the Fresnel reflection principle where the light may reflect and refracts at the interface. The structure of FBG is shown in Fig. 1.12 (Chapter 1)**.** In this system, Bragg wavelength equation 1.1 is considered for the designing [73]. The variation of Bragg wavelength due to change in strain and temperature is expressed as [37]:

$$\Delta\lambda_b = K_\varepsilon.\Delta\varepsilon \qquad (4.\ 1)$$

Where $\Delta\lambda_b$ is change in wavlength, K_ε is factor of strain senstivity, $\Delta\varepsilon$ is variation in strain (0.2145 (1/με)).

Further K_ε is expressed as [56], [74]:

$$K_\varepsilon = (1-P_e)\,\lambda_b \tag{4. 2}$$

And the effective photo-elastic coefficient (P_e) is defined as [74]:

$$P_e = \frac{n^2}{2}(P_{12} - \nu(P_{11} + P_{12}) \tag{4. 3}$$

From equation 4.2 and 4.3 we have equation (4.4) [72]:

$$K_\varepsilon = \left[1 - \frac{n^2}{2}\left(P_{12} - \nu\left(P_{11} + P_{12}\right)\right)\right]\lambda_b \tag{4. 4}$$

Where, n: Refractive index (1.46), P_{ij} is Photo-elastic factor (P_{11},P_{12}); range: 0.1-2.0, V: Poisson's ratio; range: 0.1- 2.0, λ_b: Bragg wavelength (1550nm)

Put equation (4.4) in (4.1):

$$\Delta\lambda_b = \left[\left(1 - \frac{n^2}{2}(P_{12} - \nu(P_{11} + P_{12})\right)\right]\lambda_b\Delta\varepsilon \tag{4. 5}$$

The equation 4.5 shows the shift in wavelength with respect to strain.

4.2.1 Optimization of Optical Sensor using GA

The procedure for optimization of proposed sensor is sectioned into the four stages, the flow chart diagram is represented in Fig.4.1.

Stage 1: Initial population of GA and the range is generated for the selected parameters of FBG and in stage 2 number of generations i.e. 10 is counted with the help of counter at the starting and every generation moves towards the required results iteratively. Stage 3: The fitness value (which represents to maximum wavelength shift) is evaluated by calling subprogram on passing the different combination of parameters which are to be optimized. For whole population, the group of parameters are passed one by one to the subprogram within the function call. Step 4: An array of wavelength shift values is taken as the fitness respective to all current population parameters. Depending on a small probability, a random value for chromosomes are chosen through tournament selection which is set to 75% value. A crossover (fixed to 80%) method is used to obtain pairs of new chromosome from these selected chromosomes [20]. Finally, a new enhanced population is obtained when each of the new chromosomes undergo mutation operation (2.5%). Until, the final generation is reached, stages 3 and 4 are repeated. It is observed that with the progression of generations there is an increase in wavelength shift.

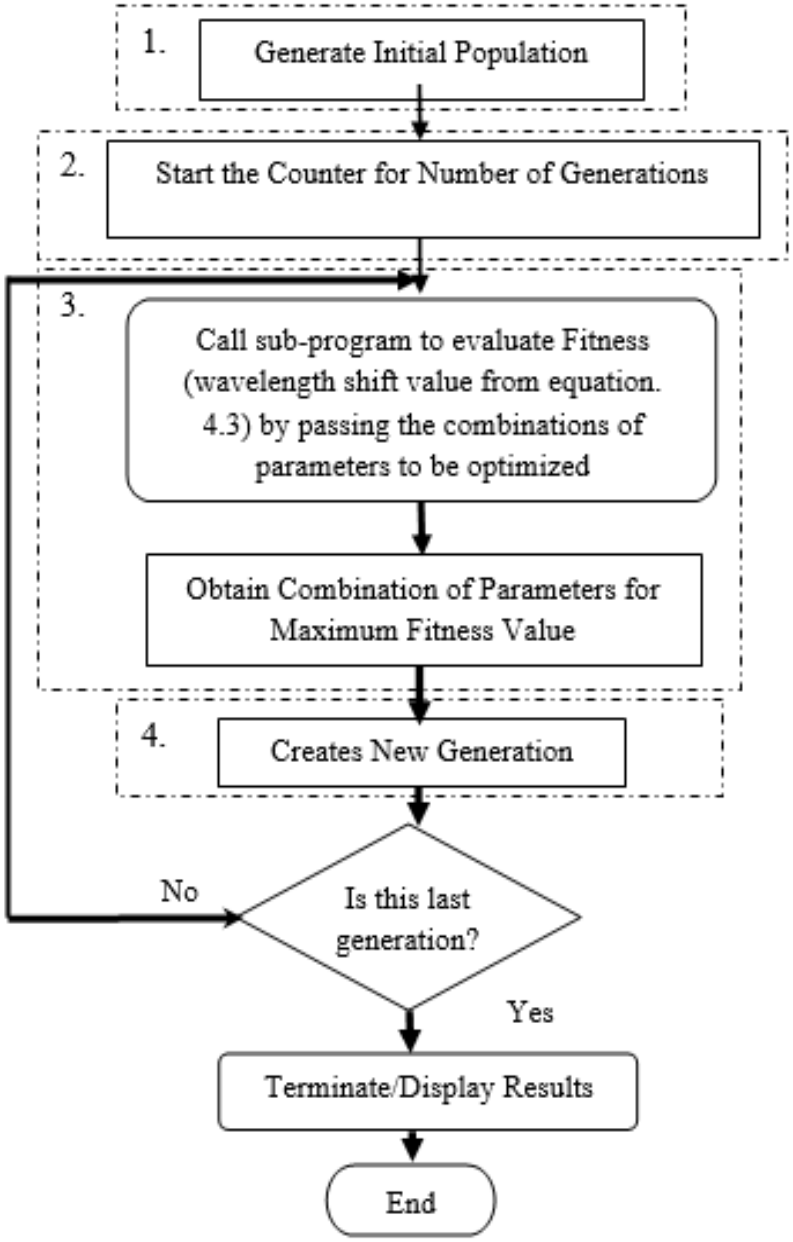

Figure 4.1: Basic flow diagram of GA applied for optical sensor optimization.

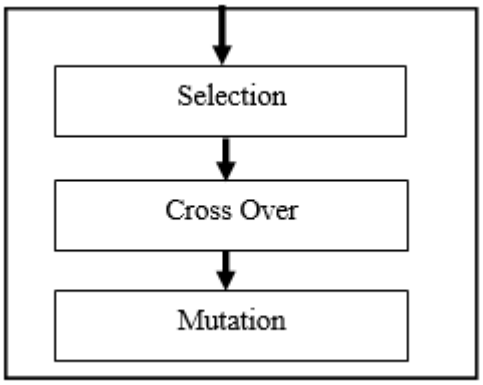

Figure 4.2: New created generation in GA.

As all the three methods are collectively present in the proposed method for employing GA, a very few generations get involved in the process and no further modification is required. The remaining parameters of GA, FBG and related to equation 4.5 are described in Table 4.1 to 4.3. For this optimization, the strain and temperature are taken as constant to check the sensitivity by varying the FBG parameters. After completion of algorithm, different convergences are observed in terms of wavelength shifting against proposed parameters.

Table 4.1: Parameters for the GA

Parameter	Value
Cross over probability	80%
Mutation probability	2.5%
Tournament selection parameter	75%
Number of generations	10
Population	30 individuals
Fitness function	Maximum wavelength shift

Table 4.2: Range of values for FBG parameters

Parameter	Value
Poisson's ratio	0.1 - 2.0
Photo-elastic coefficient (P_{11})	0.1 - 2.0
Photo-elastic coefficient (P_{12})	0.1 - 2.0

Table 4.3: Values of parameters associated with equation (4.5)

Parameter	Description	Value
N	Refractive index	1.46
λ_B	Bragg wavelength	1550 nm
$\Delta\varepsilon$	Strain change	0.2145 ($1/\mu\varepsilon$)
ΔT	Temperature change optic coefficient	25^0 C

In the 2D plots, the shift value is plotted versus a single parameter, but in each case the shift is obtained with the particular combination of the four optimized parameters. After optimization it can be observed that the sensitivity (in the term of wavelength shift) of FBG has been enhanced to 38.16 nm. After completion of optimization process, it is observed that the proposed FBG provides maximum wavelength shift (near 38.16 nm) with poisson's ratio of 1.94, silica photo elastic coefficient p11 of 1.994, and silica photo elastic coefficient p12 of 1.8103.

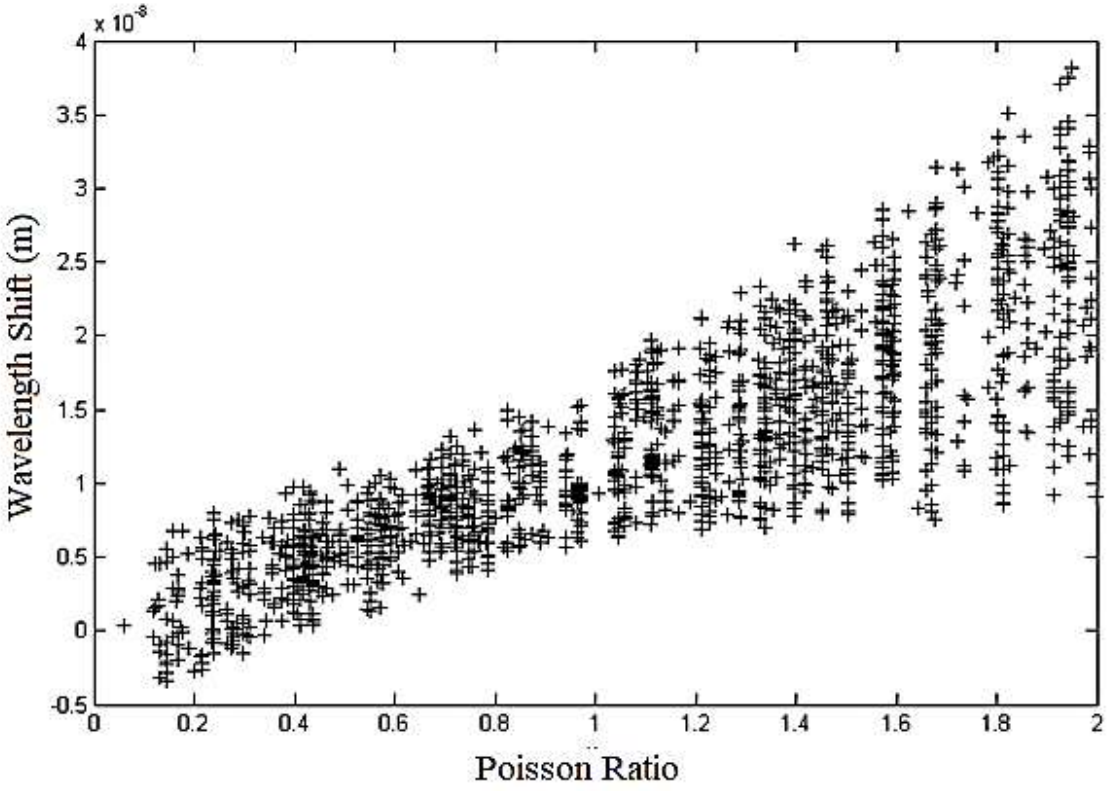

Figure 4.3: Convergence of the GA obtained for Poisson Ratio.

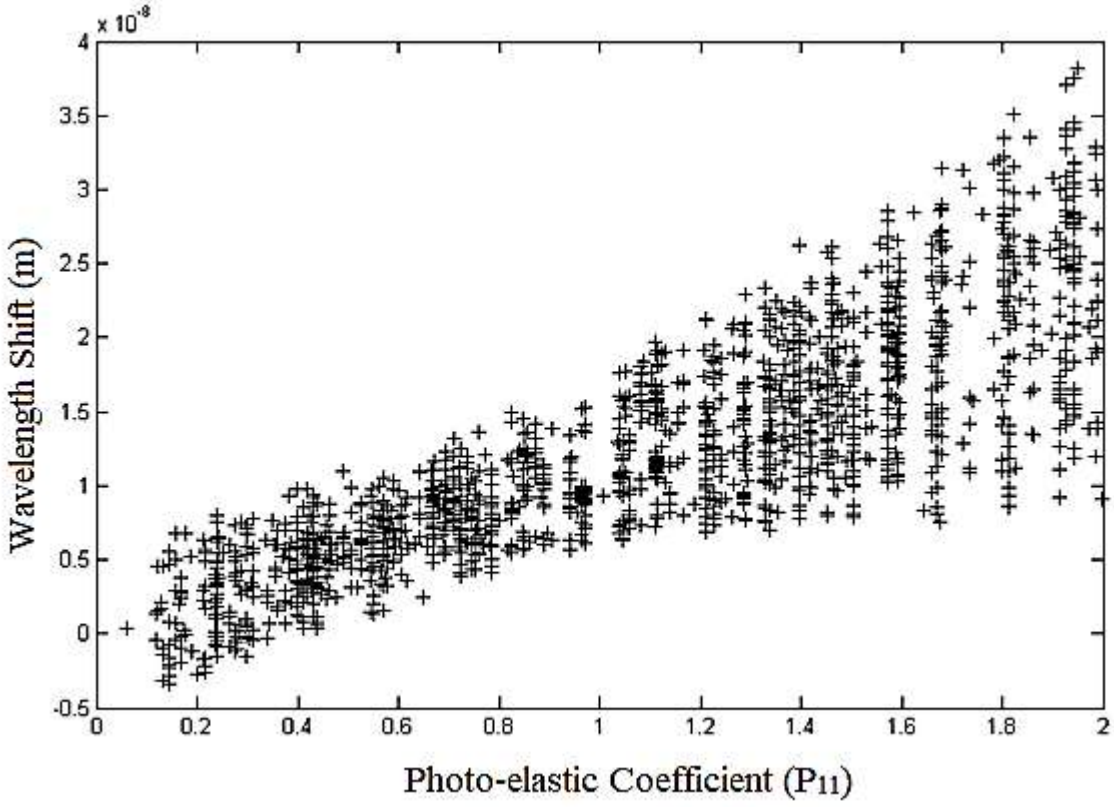

Figure 4.4: Convergence of the GA obtained for Silica photo elastic coefficient P_{11}.

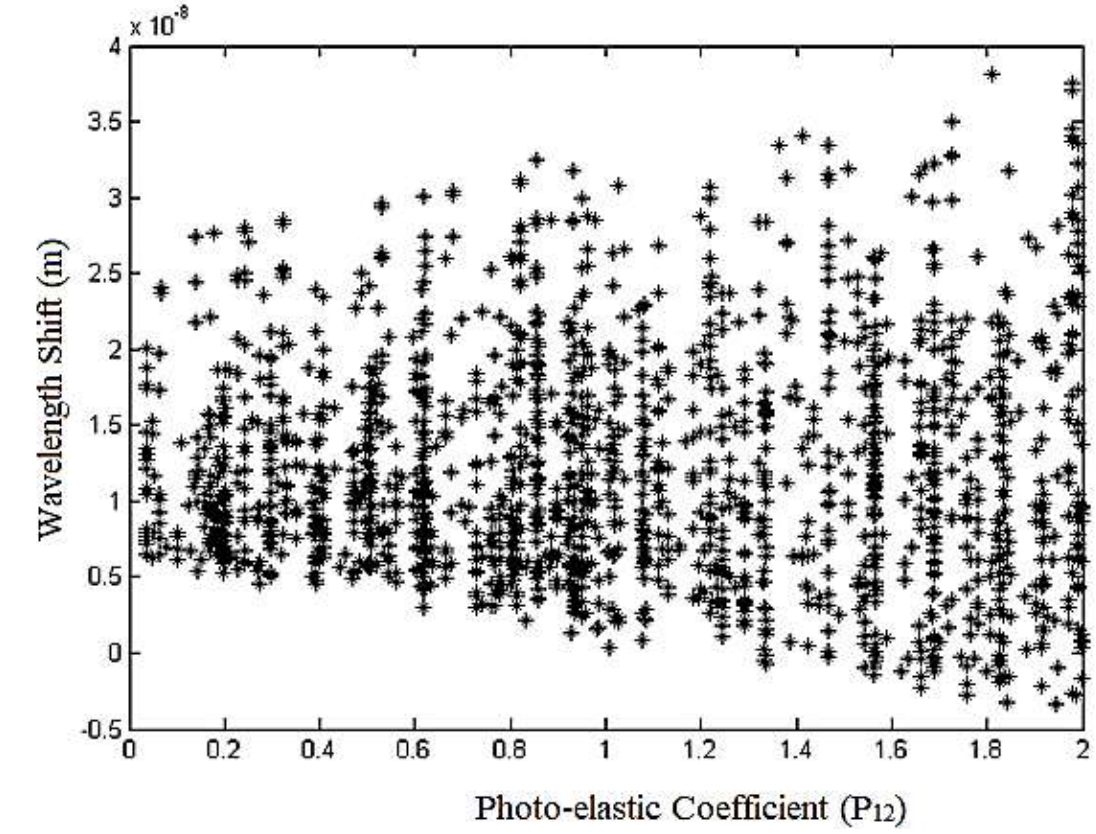

Figure 4.5: Convergence of the GA obtained for Silica photo elastic coefficient P_{12}.

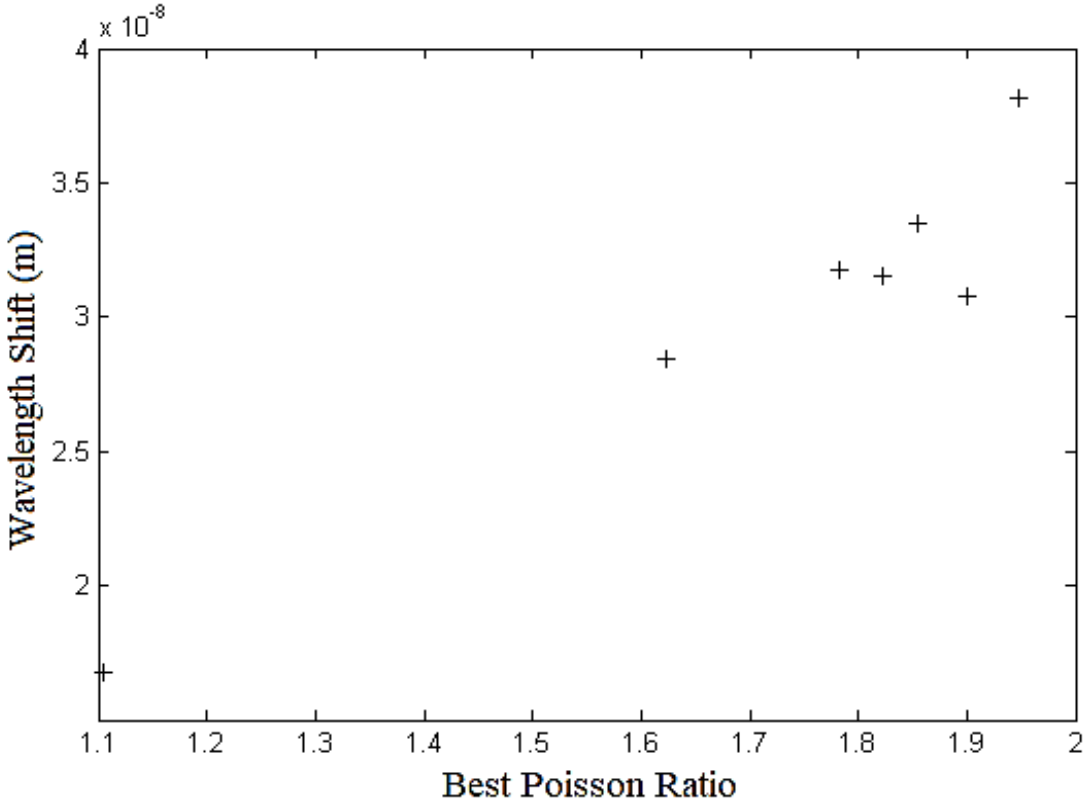

Figure 4. 6: Best Result obtained for Poisson ratio after optimization.

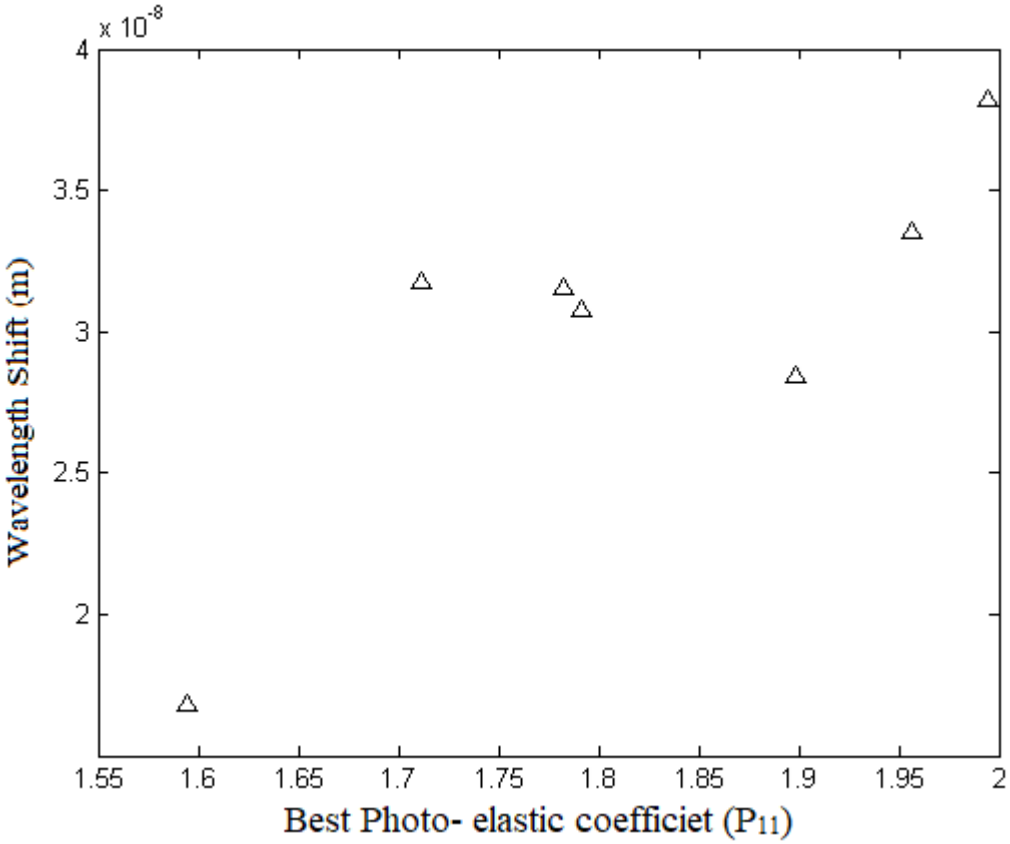

Figure 4.7: Best Result obtained for P_{11} after optimization

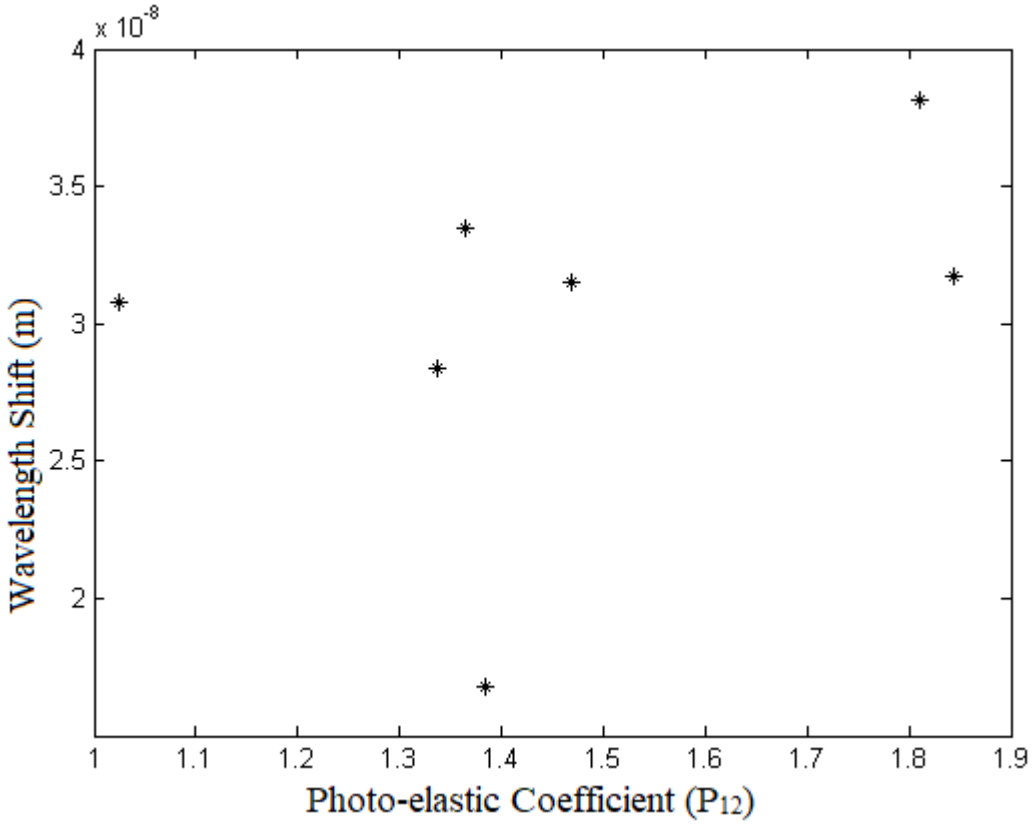

Figure 4.8: Best Result obtained for P_{12} after optimization

The existing FBG provides large wavelength shift by just optimizing the parameters and no any impurity or advanced material/fabrication process is used to increase the sensitivity, which yield the cost effectiveness. For better clarity the graphs the best result obtained is shown in fig.4.6 to 4.8. The few results obtained from GA with respect to wavelength change are described by Table 4.4.

Table 4. 4: Results obtained from different combination of proposed parameters

Case	Poisson's ratio	P_{11}	P_{12}	Wavelength shift (nm)
1.	1.105	1.5940	1.3846	16.794
2.	1.623	1.8983	1.3349	28.403
3.	1.9004	1.7916	1.0251	30.7916
4.	1.8220	1.7828	1.4682	31.5295
5.	1.7825	1.7117	1.8449	31.757
6.	1.8545	1.9568	1.3637	33.489
7.	1.9484	1.9948	1.8103	38.168

4.3 Design of HOS to Measure Strain, Vibration and Temperature

In literature, many techniques for measuring temperature, gas, liquid and refractive index for life sciences research, bio- chemical, chemical sensing application and food industry have been reported with conventional ring resonator [95-99]. It can be further expanded to civil applications also. In civil industry, the deformation in structures can be sensed with the help of optical sensors. In this section, the previous reported techniques have been extended by reducing the overlapping of integral using HOS and increasing transmittance power. We have proposed two types of waveguides, one is Ring Resonator (RR) and another is hybrid optical waveguide. An optical RR seems to be a hoop (ring) shaped waveguide which is illustrated in Fig. 4.9. The proposed sensor is optimized at different radius of the ring resonator i.e. 0.7 μm, 1.2 μm, 1.7 μm, 2.2 μm, 2.7 μm, 3.2 μm, 3.7 μm, 4.2 μm and 4.7μm to increase the sensitivity for physical measurands.

From the results, it is observed that 4.7 μm radius gives us better result in terms of transmittance power and quality factor of the light, see Fig. 4.17. In ring waveguide four Bragg gratings are inserted to detect different parameters. These gratings are formed uniformly with 2.7 μm grating period which is represented in Fig.4.10.

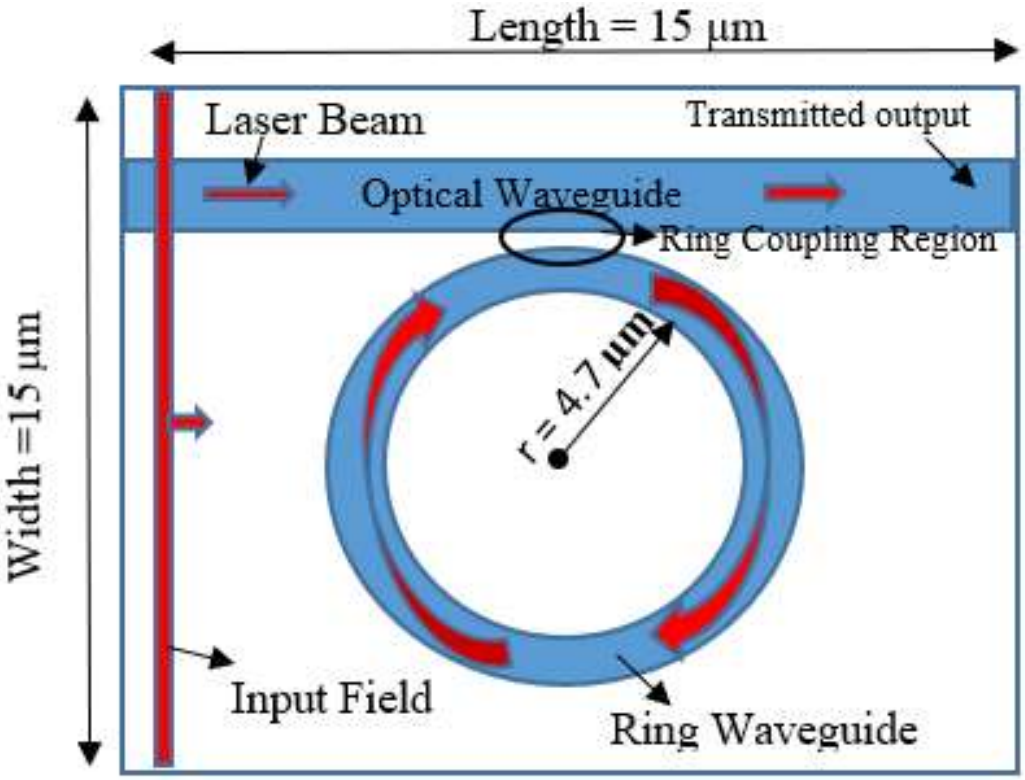

Figure 4.9 System setup for RR sensor.

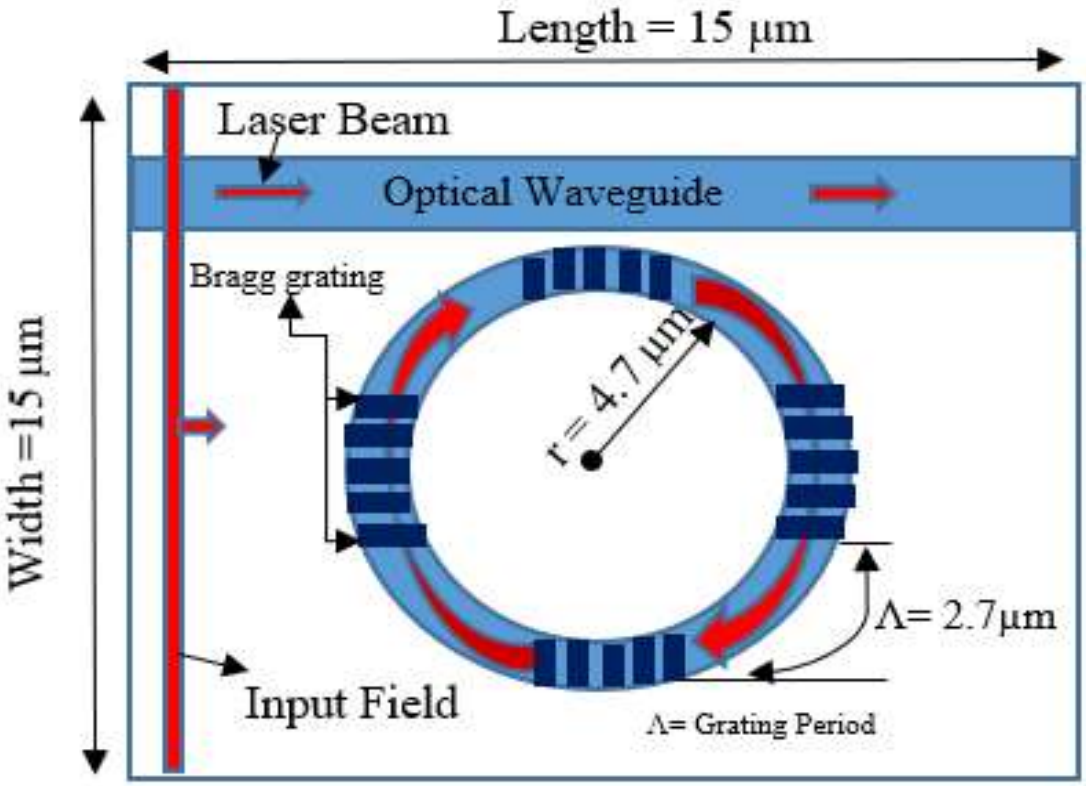

Figure 4.10: Structure of HOS.

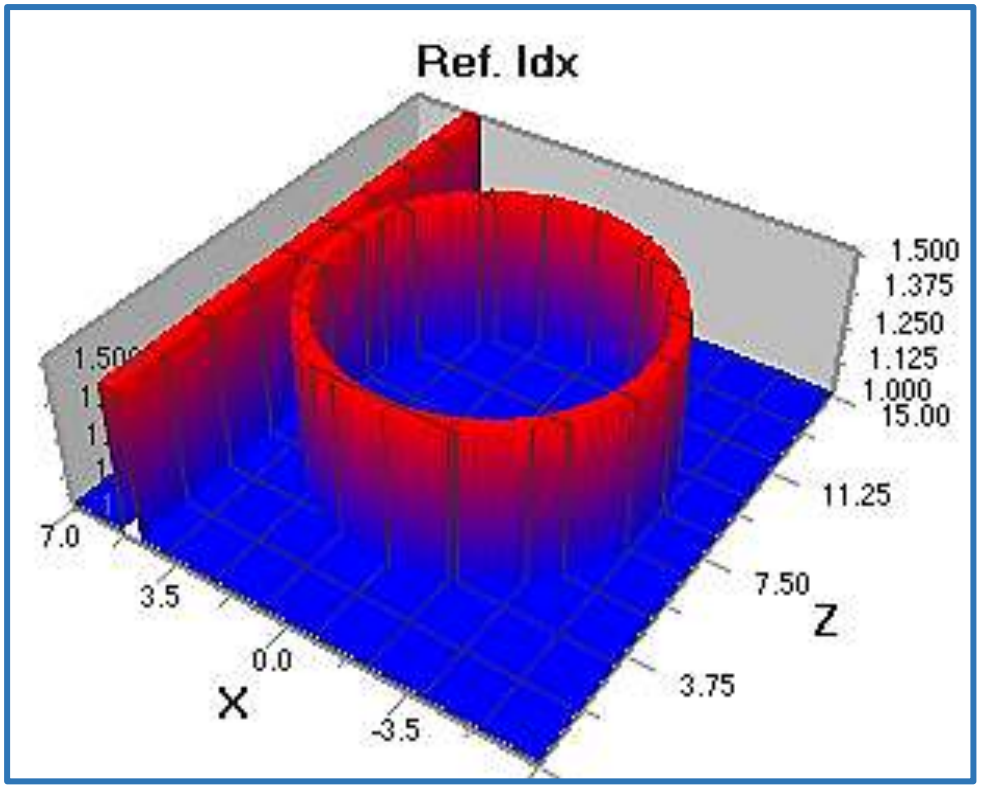

Figure 4.11: Refractive Index profile of RR sensor.

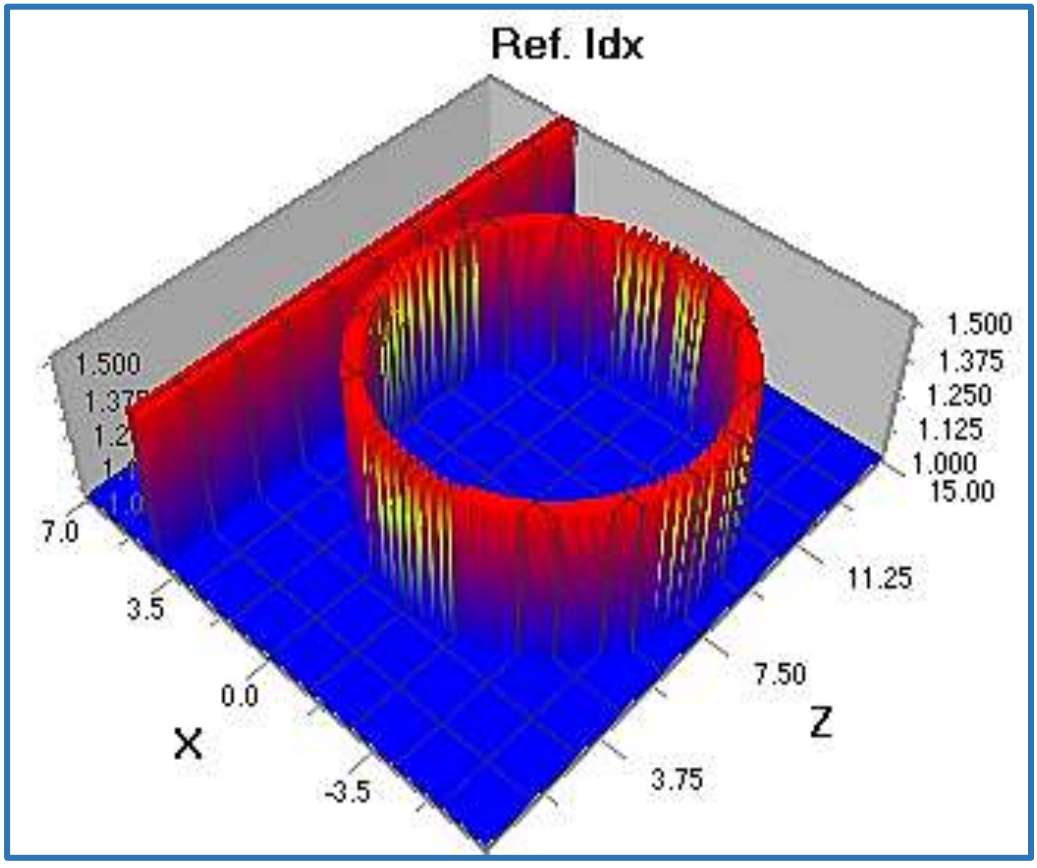

Figure 4.12: Refractive Index Profile of HOS.

When the light is transmitted from the input field, the light is splitted into two directions. Some part of light travels through the ring resonator and remaining part propagates through optical waveguide. When the light falls on the grating and sensor is exposed to different deformation then Bragg wavelength is reflected back to the photodetector where the behaviour of light is observed. The shifting in wavelength received at output side helps in sensing these deformations. The RI profile of RR sensor and of HOS along the length and width of wafer can be seen in Fig.4.11 and 4.12.

4.3.1 Results and Discussion

The image view of electric field distributions of proposed sensors is shown in Fig. 4.13 to Fig. 4.14. It can be seen that the HOS shows better distribution of electric field as compared to RR. The Poynting vector patterns are also obtained to monitor the power value and scattering of light through the both sensors, see Fig. 4.15 and 4.16. It reveals that the proposed HOS performs superior as in comparison to simple ring resonator because it provided better results in terms of high speed of energy flow in an EM wave, distribution of light and power level.

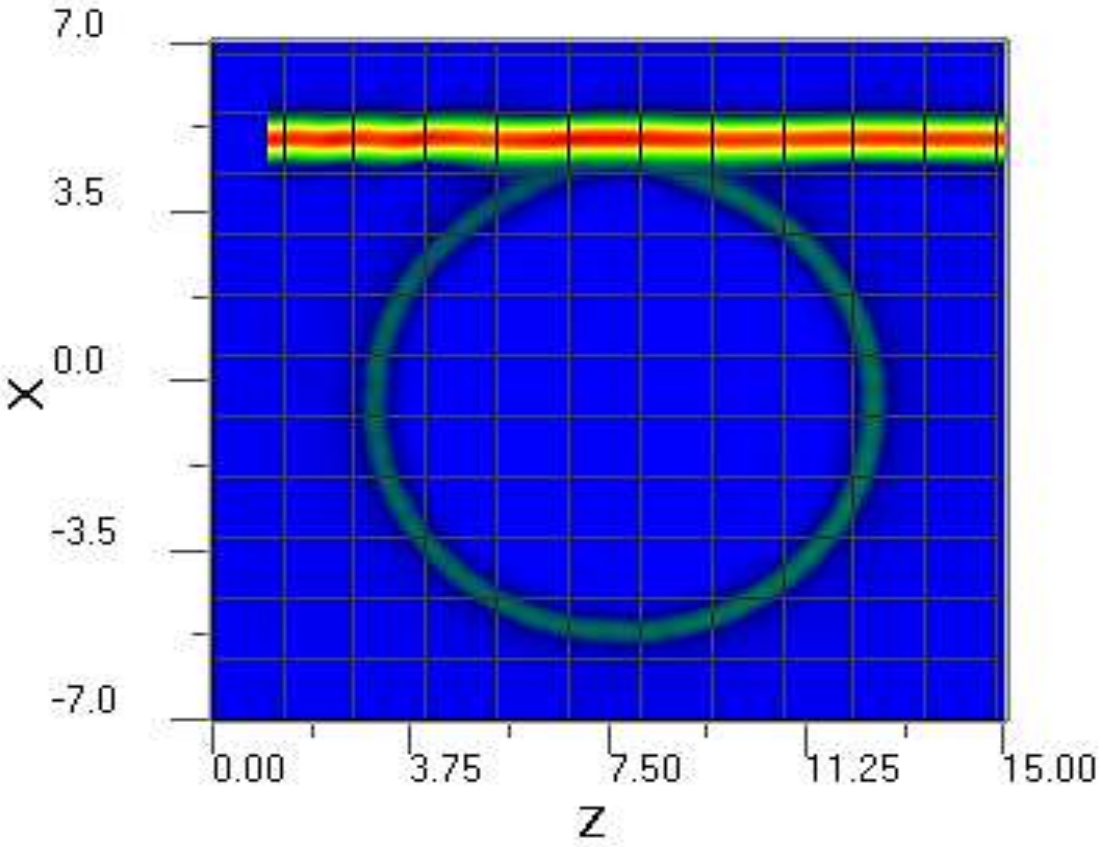

Figure 4.13: Electric field distribution of Ring Resonator.

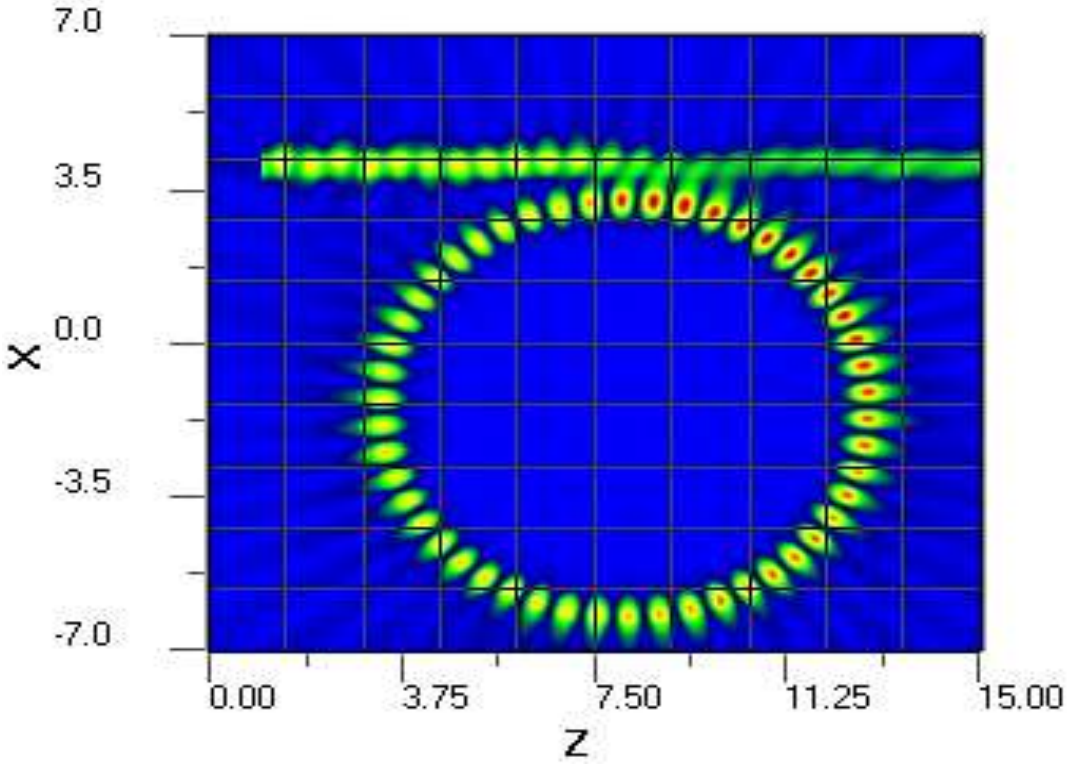

Figure 4.14 Electric field distribution of HOS.

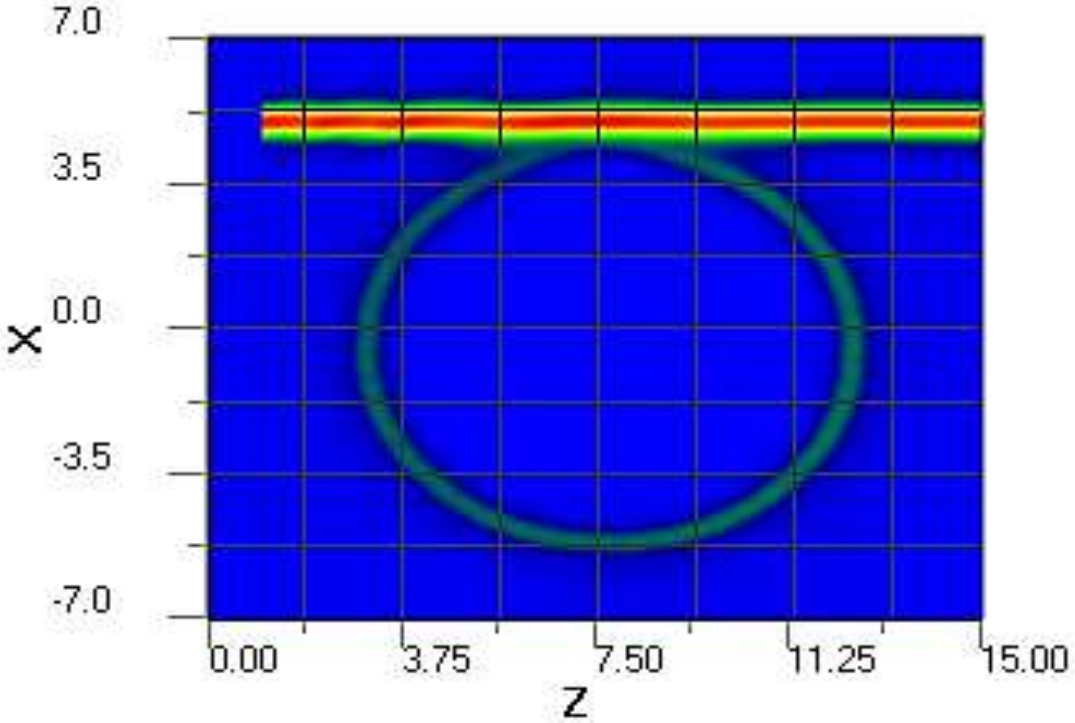

Figure 4.15: Poynting vector patron of RR sensor.

The graphs for transmittance power against different frequencies are also obtained at different position of waveguide to monitor the acceptable power. It must be large enough to drive cascaded components. The high transmittance power is good for structure sensing

application because these types of sensors can be useful for large structure. The graphs for transmittance power are shown in Fig. 4.17 to 4.20.

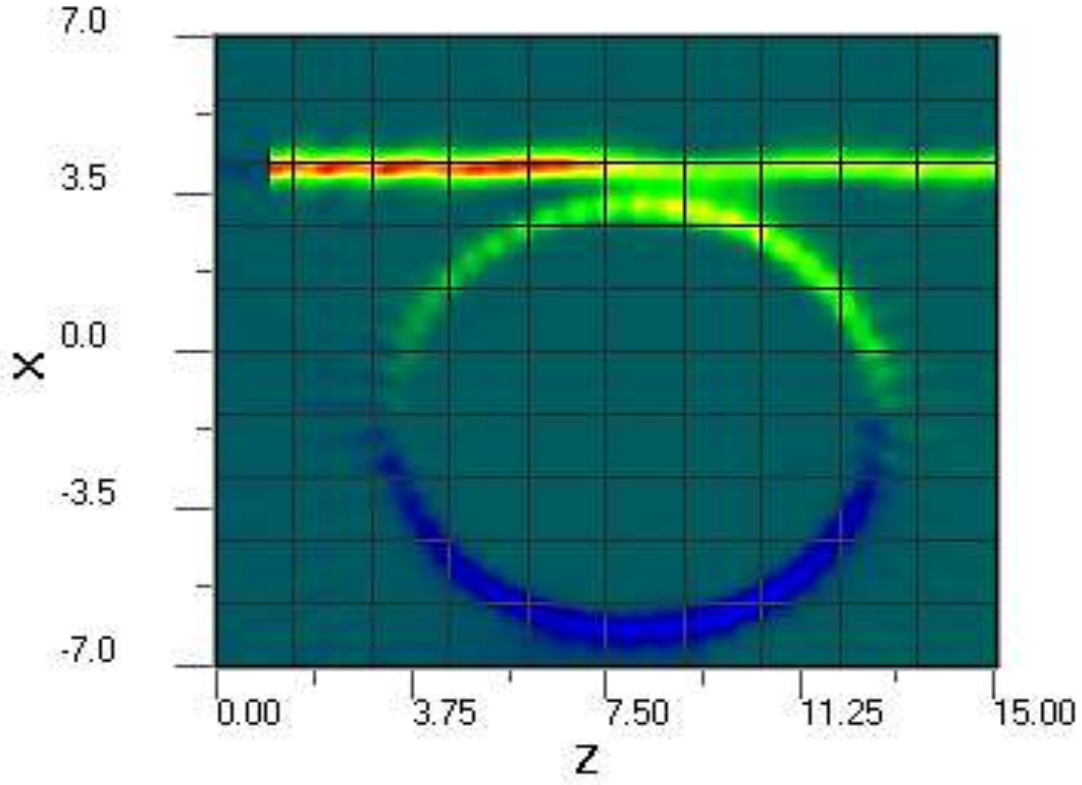

Figure 4.16: Poynting vector pattern of HOS.

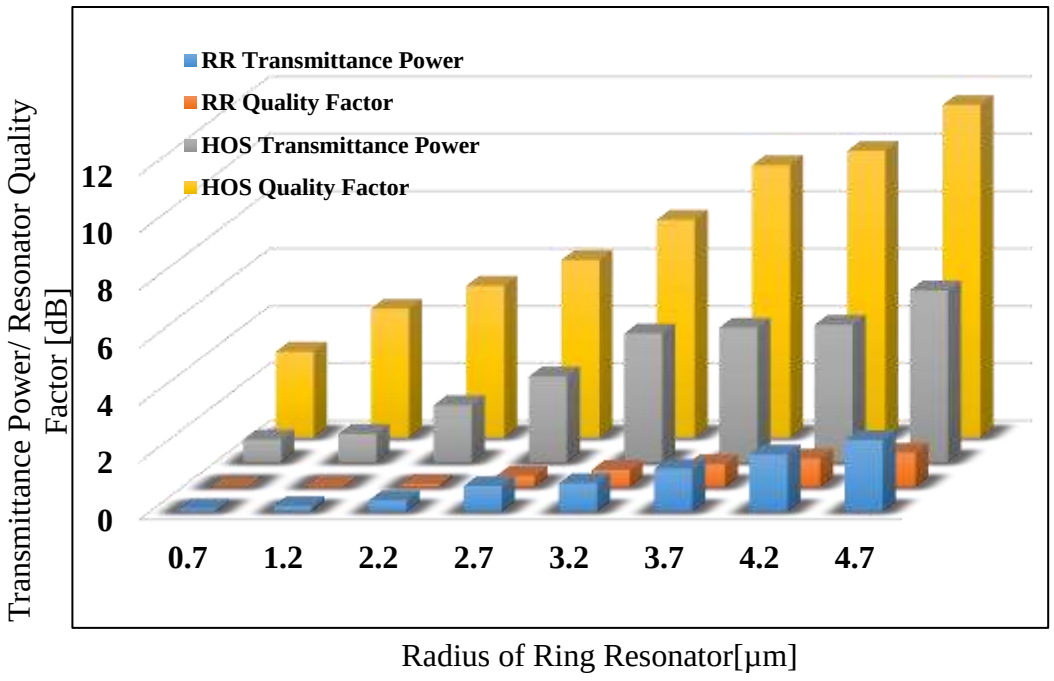

Figure 4.17: Transmittance power and quality factor for HOS.

From these patterns it is observed that the transmitted light power increased as it travelled along the waveguide. Further, the overlap within the frequencies is also obtained because it is a significant aspect to examine the performance of optical sensor. The integral overlapping is calculated and it is reported that it must be as small as possible. The overlap factor with respect to horizontal distance of waveguide is indicated in Fig. 4.21. It reveals that the HOS gives improved performance than ring resonator with acceptable overlap factor.

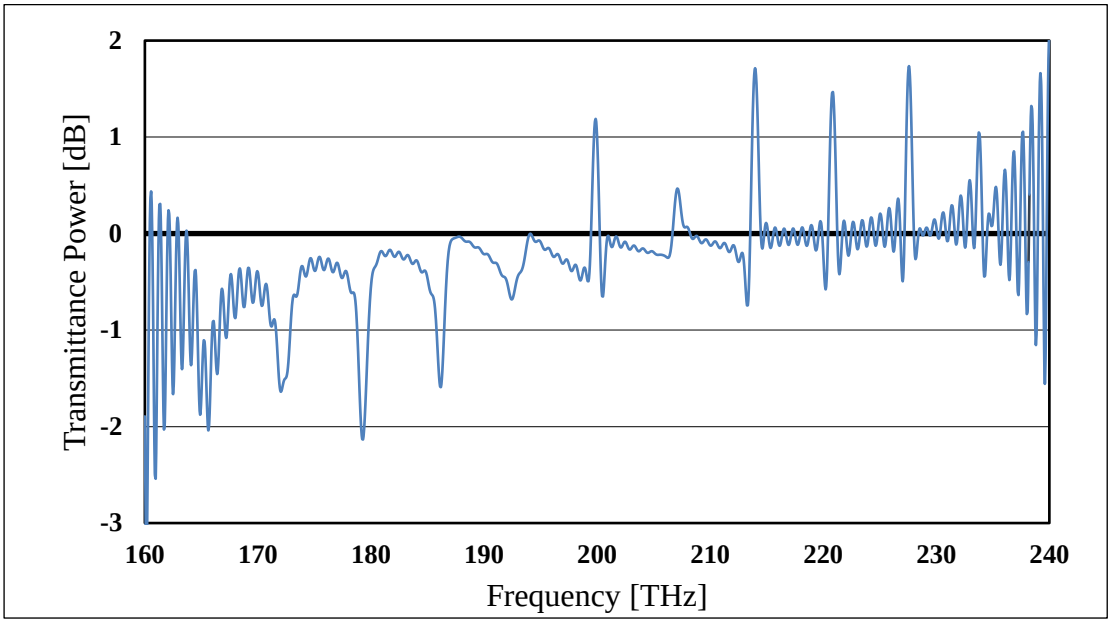

Figure 4.18: Transmittance power of HOS at 2.56 µm.

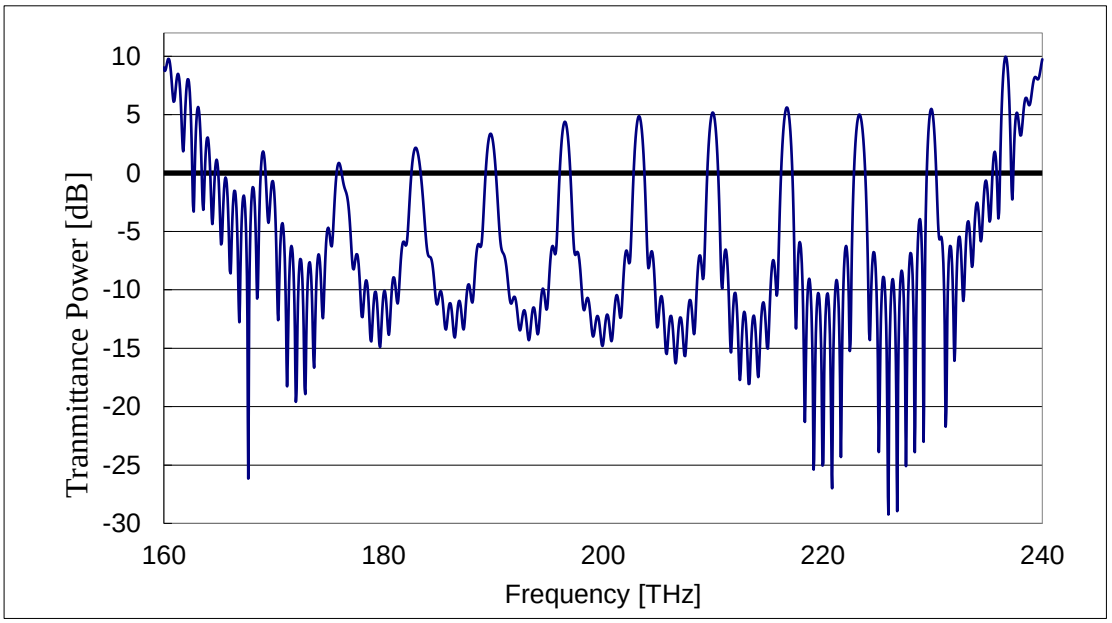

Figure 4.19:Transmittance power of HOS at 8.13 µm.

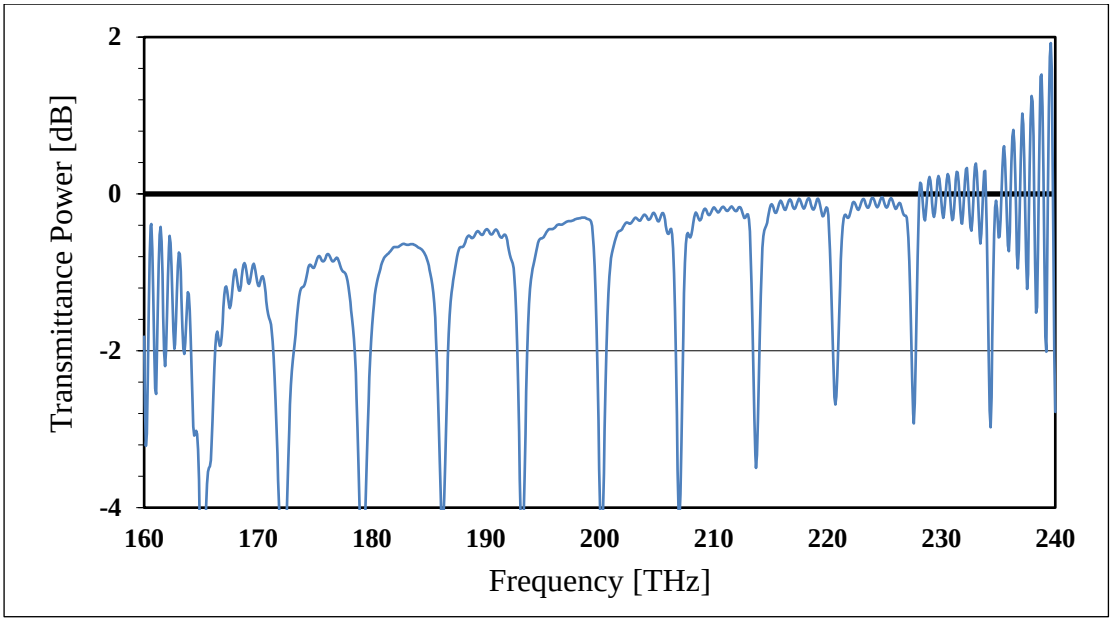

Figure 4.20: Transmittance power of HOS at 13.27 µm.

Further, optimization of sensors is done with different grating material. For RR sensor, we have observed no response (0 nm wavelength shift) even for all values of applied vibration, temperature and strain, see Fig. 4.21 to 4.24. It means that it is not suitable for monitoring the health of civil structures. When different grating materials (MgF_2 and SiO_2) are introduced in ring resonator, then performance of the sensor is enhanced with noticeable change in wavelength shift from 0.2nm to 0.4nm for MgF_2 and 0.3 to 1 nm for SiO_2 at different values of strain from 50 to 850με, respectively, see Fig. 4.22.

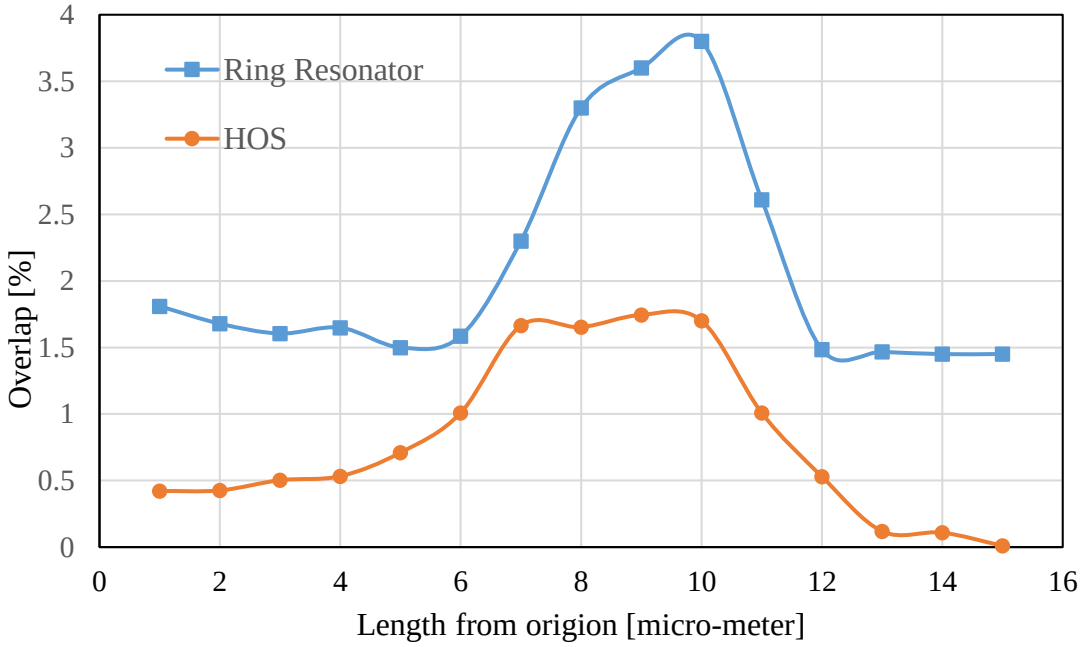

Figure 4.21: Overlap integral with respect to waveguide length.

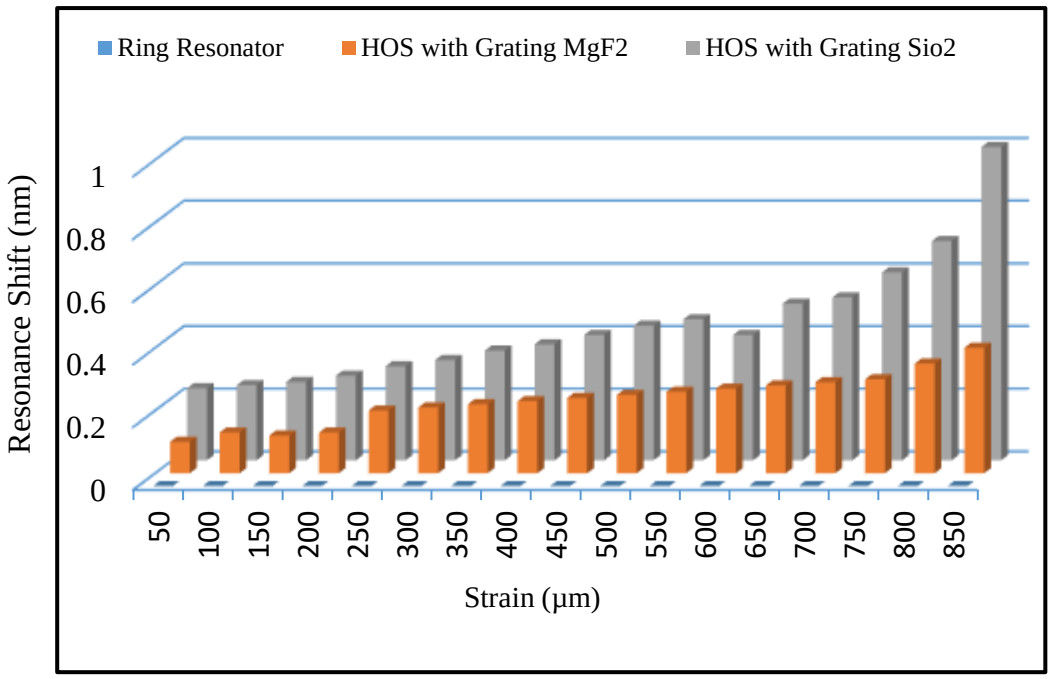

Figure 4.22: Shift in wavelength with respect to different strain value.

For varying temperature, the proposed sensor shows change in wavelength shift from 0.5 nm to 4 nm and 2 nm to 7 nm for MgF_2 and SiO_2 respectively which is shown in Fig. 4.23. Further, the proposed sensor is used to perform the vibration measurement and it reveals that the wavelength shifts from 2 nm to 6 nm and 7 nm to 13 nm for MgF_2 and SiO_2 respectively.

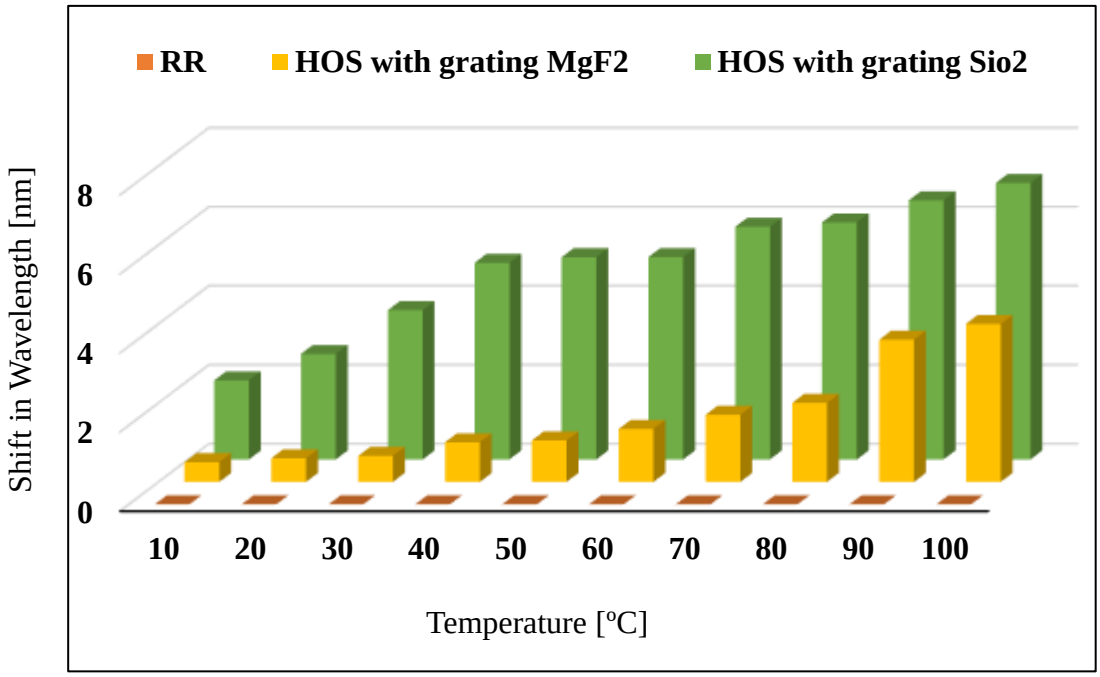

Figure 4.23: Variation in wavelength with respect to temperature.

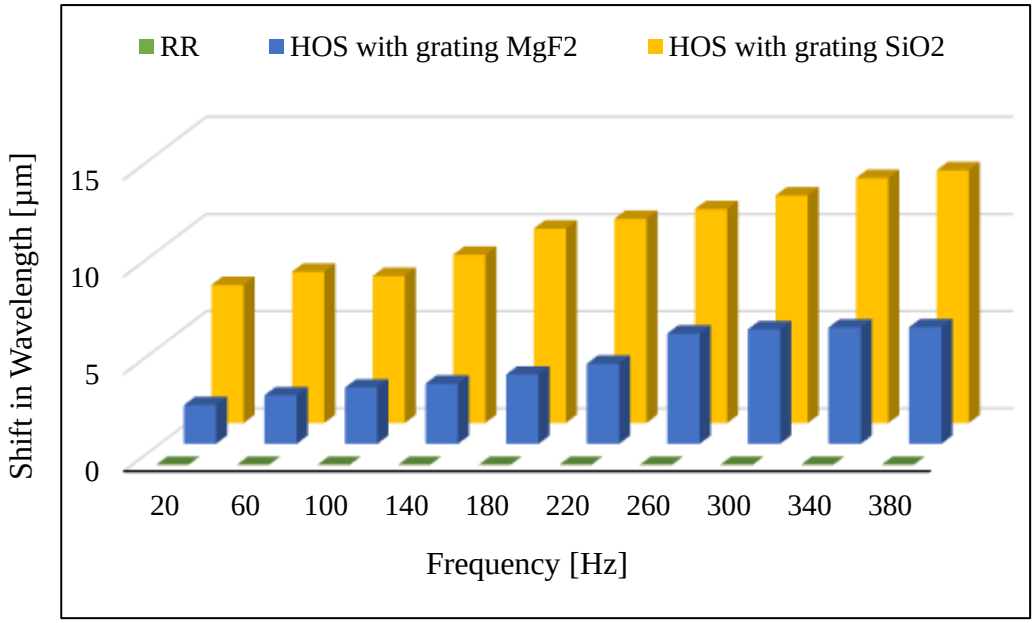

Figure 4.24: Change in wavelength at different level of vibration.

From all the above observations, the HOS projected is recommended for monitoring the physical parameters in civil structure applications.

4.4 Conclusion

In this chapter, different parameters of FBG sensor are optimized using GA to increase the senstivity in terms of wavelength shifting. We implement GA because it has the ability to optimize mutiple parameters simultaneously with maximum possible combinations of selected parameters to get the desired results. In chapter 6 various experiments have been performed on strain monitoring, from where it has been observed that as the value of load is increased the corresponding value of strain also increases proportionally and maximum 7nm shift is achieved. But, it also reveals that the sensitivity is less and need to be improved and in this chapter we have enhanced the performance of sensor using GA with maximum wavelength change of 38.16 nm. It has also been reported that the combination of Poisson's ratio, P_{11} and P_{12} with values of 1.94, 1.994 and 1.8103, respectively gives better results.

Further, ring resonator sensor with uniform superstructure Bragg gratings and conventional ring resonator has been proposed to monitor the vibration, strain and temperature on same time. The sensor has been optimized with different diameters of ring resonator and with different grating materials to enhance the performance in terms of wavelength shifting. Further, gratings are inserted in the ring loop and optimized it with different grating material to again increase the sensitivity of the sensor. Various results, such

as transmittance power, quality factor, overlap integrall and change in wavelengths has been taken to observe the sensor performance. The proposed sensor gives desired results using 4.7μm diameter of ring resonator with SiO_2 grating material and observed 7nm wavelength shift. From the results it has been reported that HOS gives better results when it is compared with conventional RR sensor.

Chapter 5

Impact of Different Grating Shapes of Fiber Bragg Grating on Sensitivity of Optical Sensor

5.1 Introduction

This Chapter deals with the third objective of thesis work, which is to investigate the FBG sensor with different grating shapes to enhance the performance. In this work, we have checked the impact of UFBG, TFBG and SFBG shape, grating lengths (30,000, 40,000 and 50,000 µm) and refractive indices (1, 1.33 and 1.46) on sensitivity of FBG optical sensor. The shift in wavelength, transmittivity, reflectivity, amplitude and received power with respect to mentioned parameters have been observed and analyzed.

5.2 System Setup to Increase the Sensitivity of FBG Sensor

Three Bragg gratings i.e. UFBG, TFBG and SFBG are used in the system setup for studying there effects. We have used Single Mode Fiber (SMF) having core radius 1 µm and cladding radius 10 µm in which FBG gratings are introduced. We have taken content RI values of cladding i.e 1.45 and core. The core having different gratings shapes the RI values are set to i.e. 1.46, 1.33, 1 for UFBG, TFBG and SFBG respectively. These three gratings shapes are simulated individually while other parameters are same.

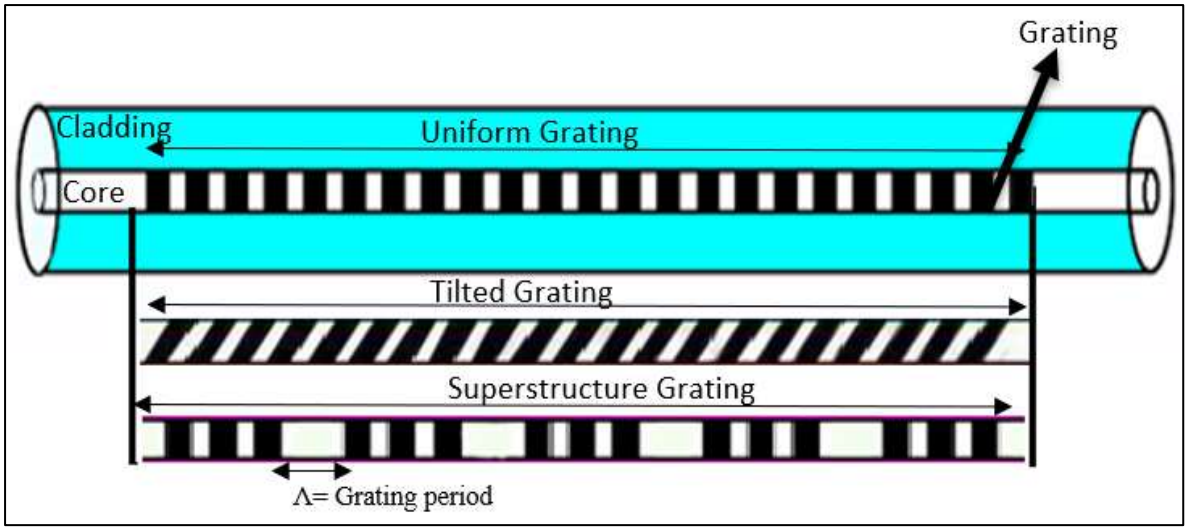

Figure 5.1: FBG sensor with different grating shapes.

5.3 Results and Discussion

In this system, the value of core RI is varied during the simulation to get better result. Propagation of light through the systems having different grating shapes are shown in Fig.

5.2(a)- 5.2(c), from where it can be seen that the light travels through the core and grating accurately. The light travels with different shapes have been observed with respect to uniform, tilted and superstructure Bragg grating shapes. Wavelength shift as a function of strain values is also observed at different grating shape, grating length and RI values, see Fig. 5.3 to 5.5.

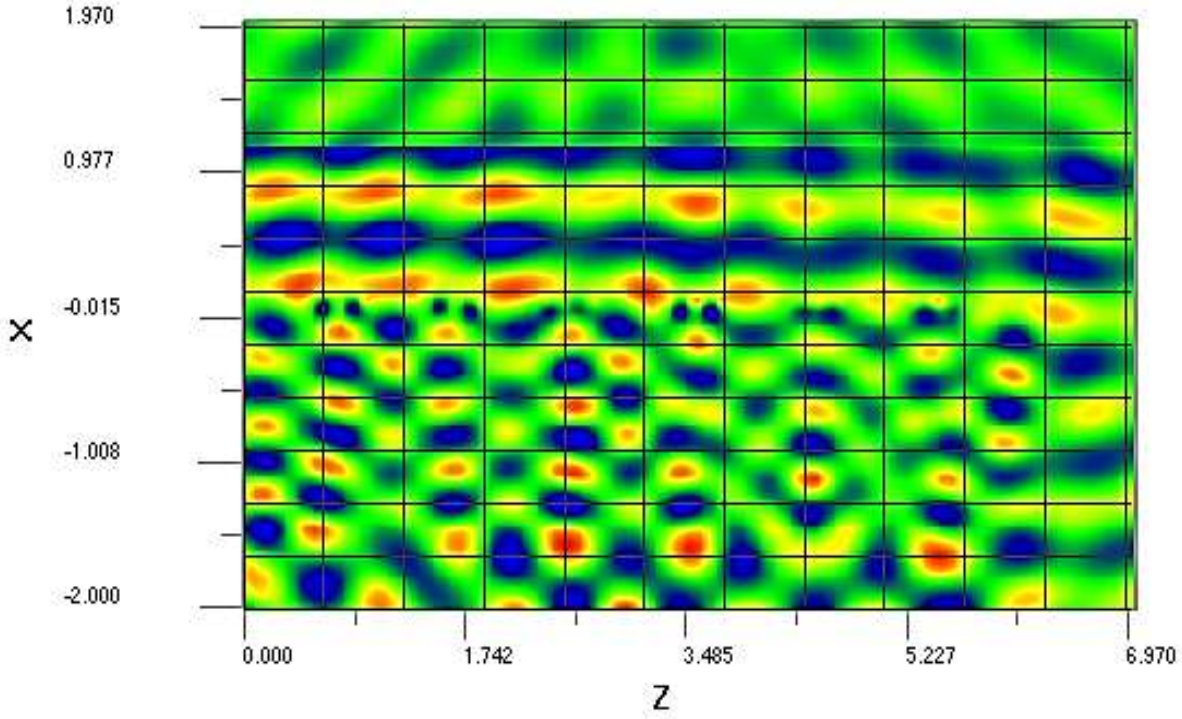

(a)

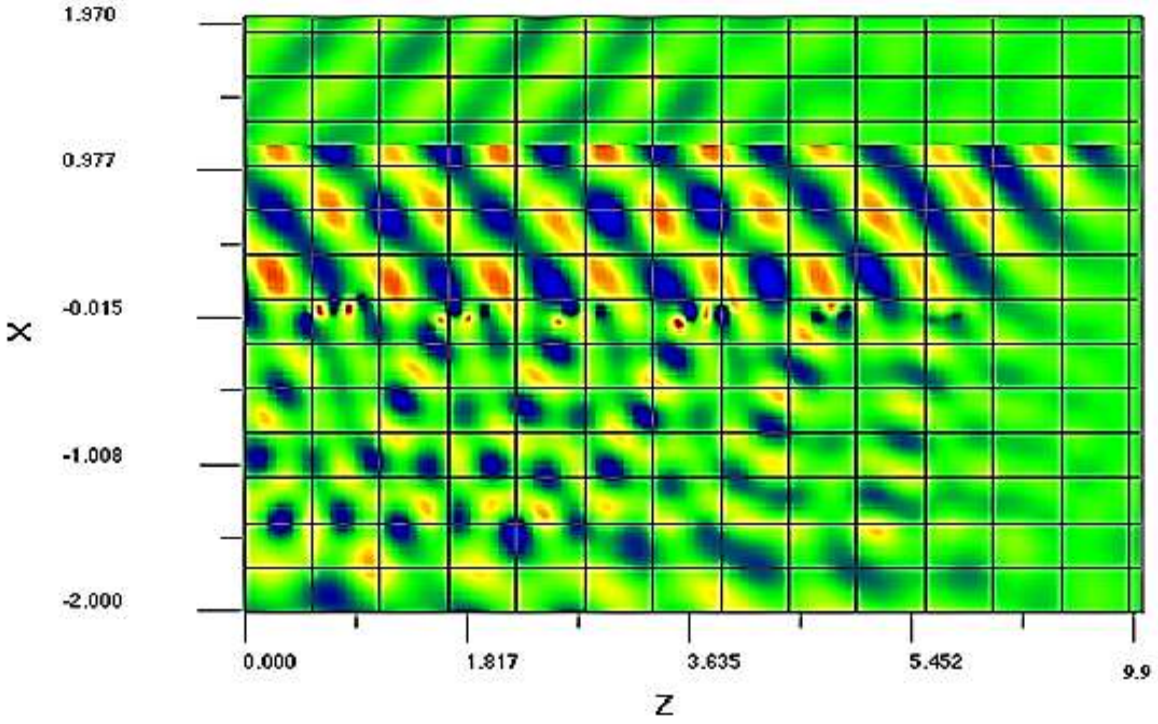

(b)

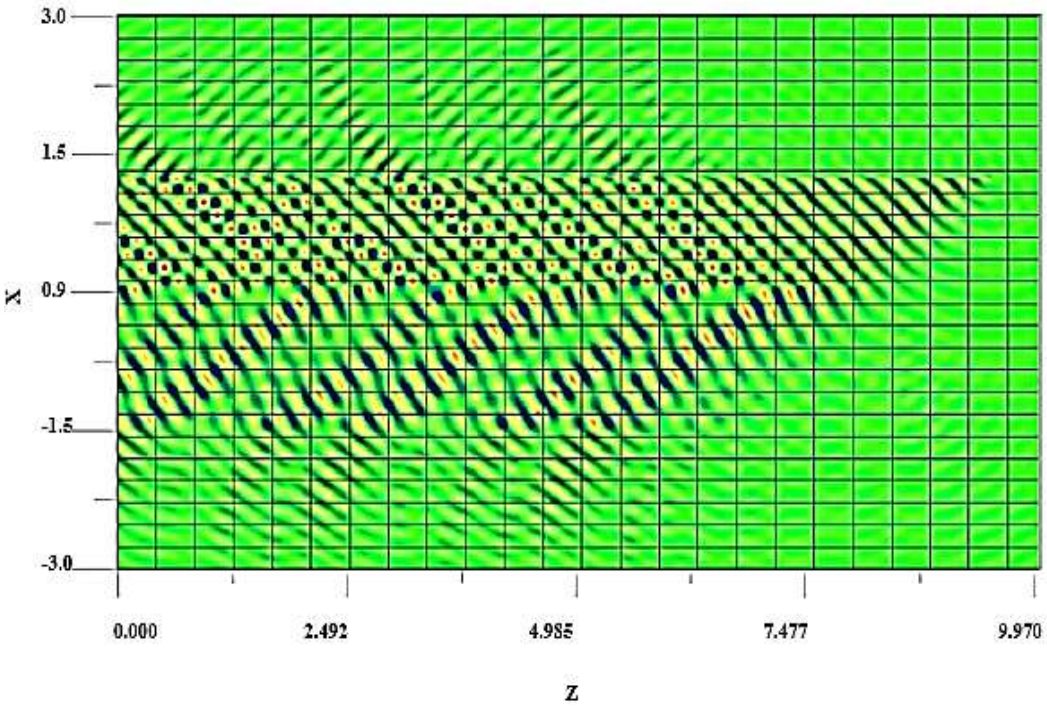

(c)

Figure 5.2:Light propagation through: (a) UFBG (b) TFBG (c) SFBG.

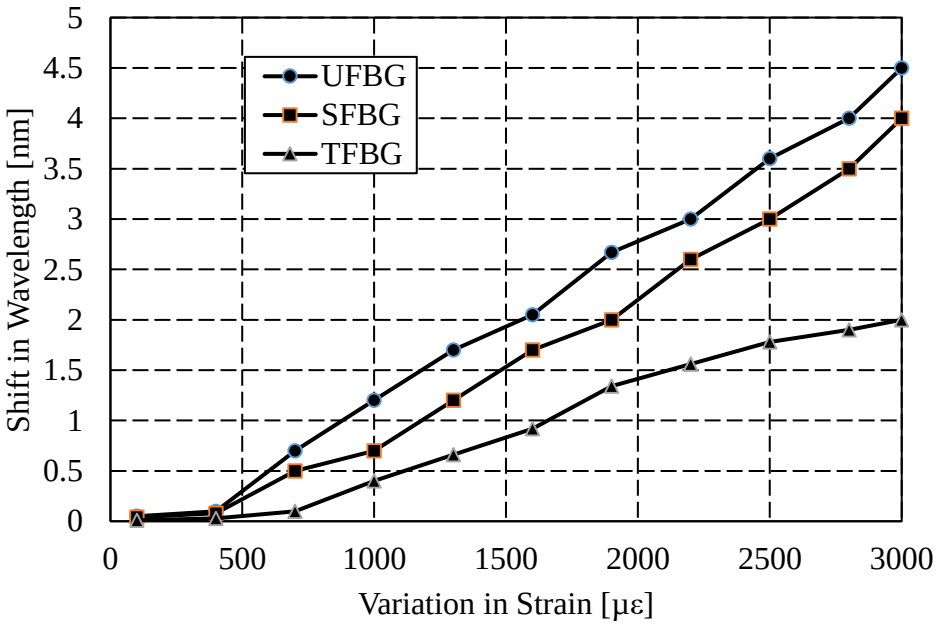

Figure 5.3: Wavelength shifting due to strain for different grating shapes.

In further simulations the best grating shape is chosen and then the results have been analysed with respect to different grating length. After having best grating shape and length, we have checked the performance as a function of refractive index. The idea is to find the best combinations of these parameters to enhance the sensitivity of proposed sensor. As per the mentioned methodology, after performing several simulations, as a result the range of the

sensor has increase from 4.5 nm to 6 nm with respect to uniform grating shape, 50000µm of grating length and 1.44 of refractive index.

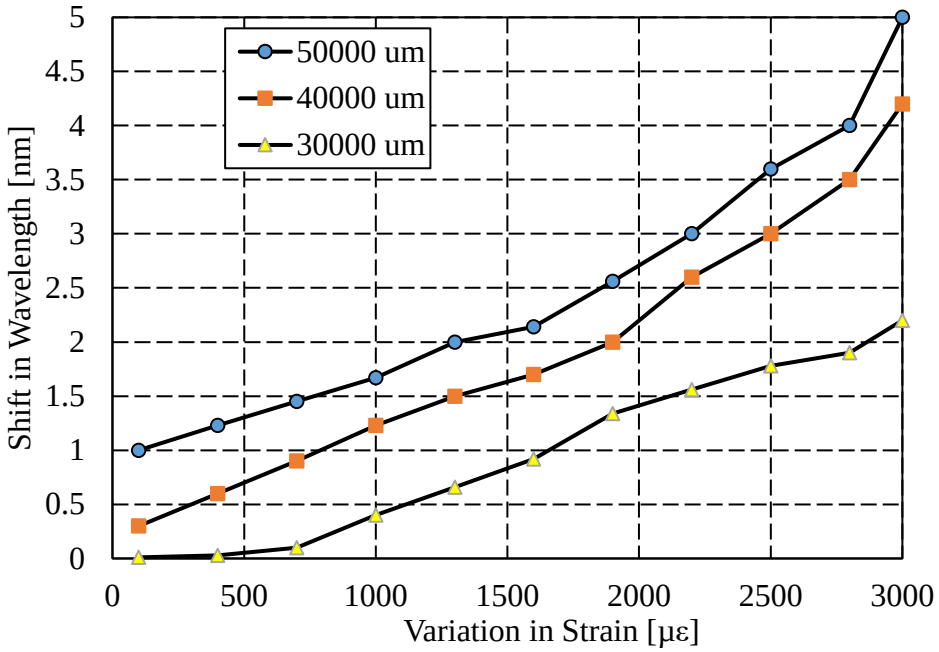

Figure 5.4: Wavelength shifting due to strain for different grating length.

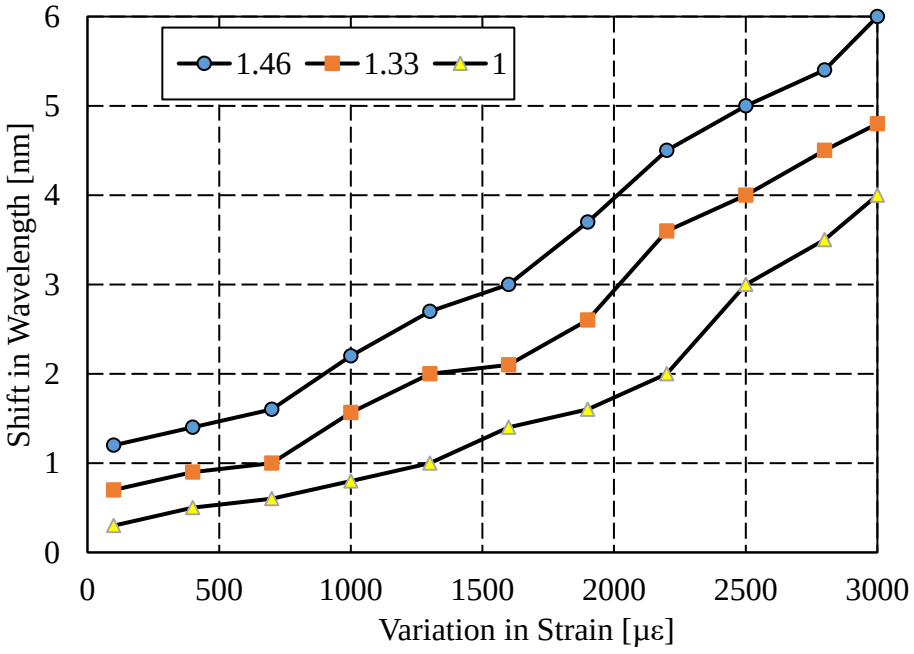

Figure 5.5: Wavelength shift with respect to change in strain for different values of RI.

Further, the grating shapes are investigated for far field applications. After the investigation, tilted shape provided good performance with maximum amplitude (0.467 a. u.) over uniform and superstructure shape having values of 0.0467 a. u and 0.0383 a. u, respectively. The coupling efficiency (CE) is also measured as 5.622%, 0.466% and 0.012%

for TFBG, SFBG and UFBG, respectively. The sensitivity of proposed sensor for far field applications is determined by evaluating its performance of reflection spectra. The reflection and sensitivity are directly proportional to each other, it means if reflectivity is high then the sensor is more sensitive.

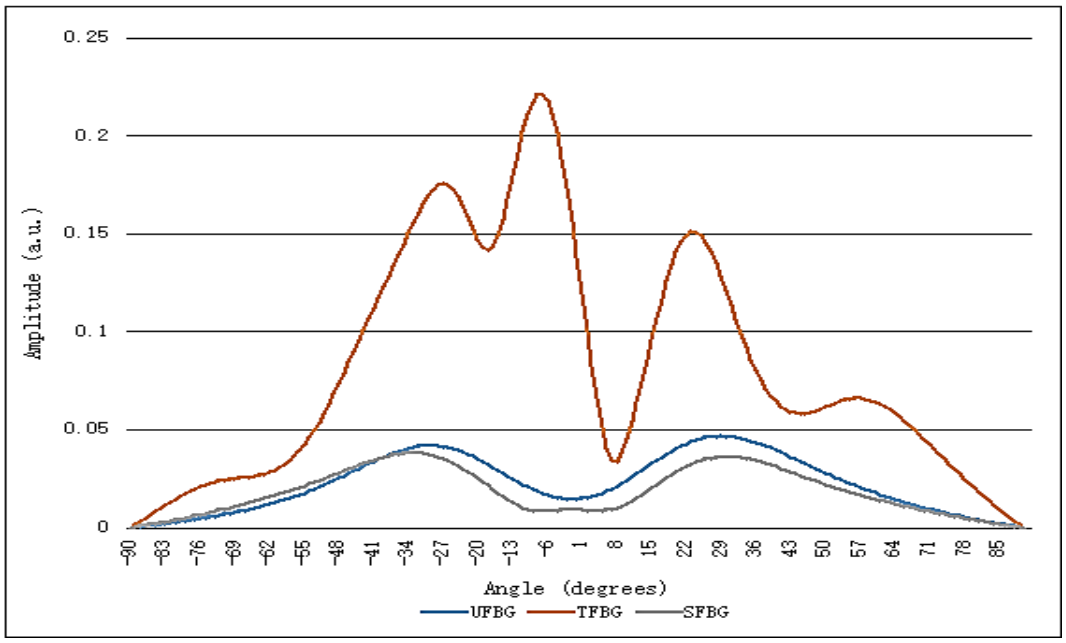

Figure 5.6: Amplitude variation of the guided light.

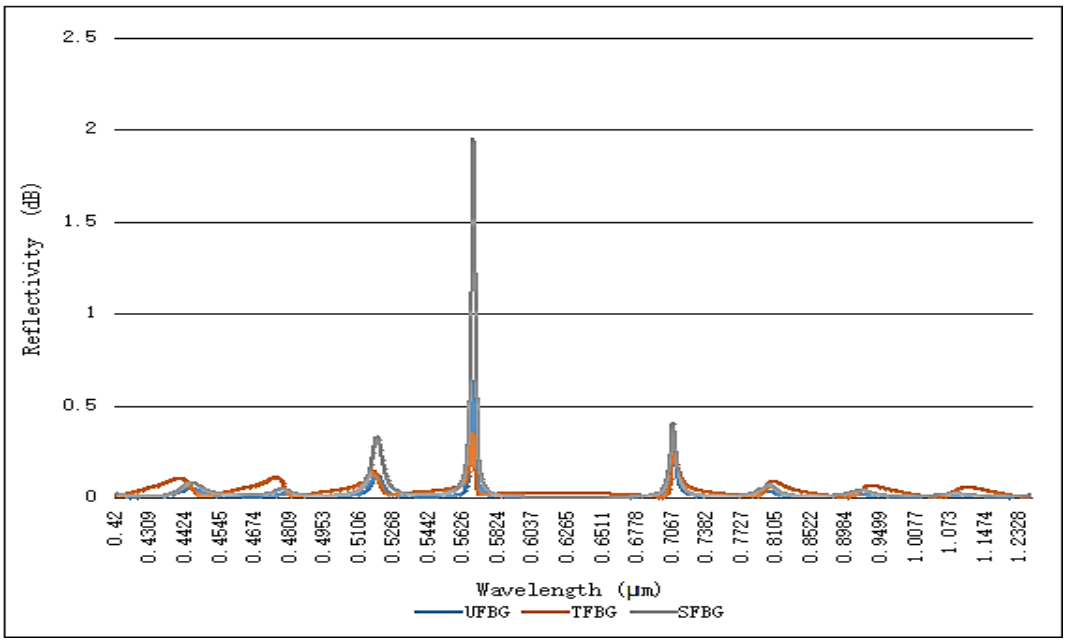

Figure 5.7: Reflectivity spectra with respect to wavelength.

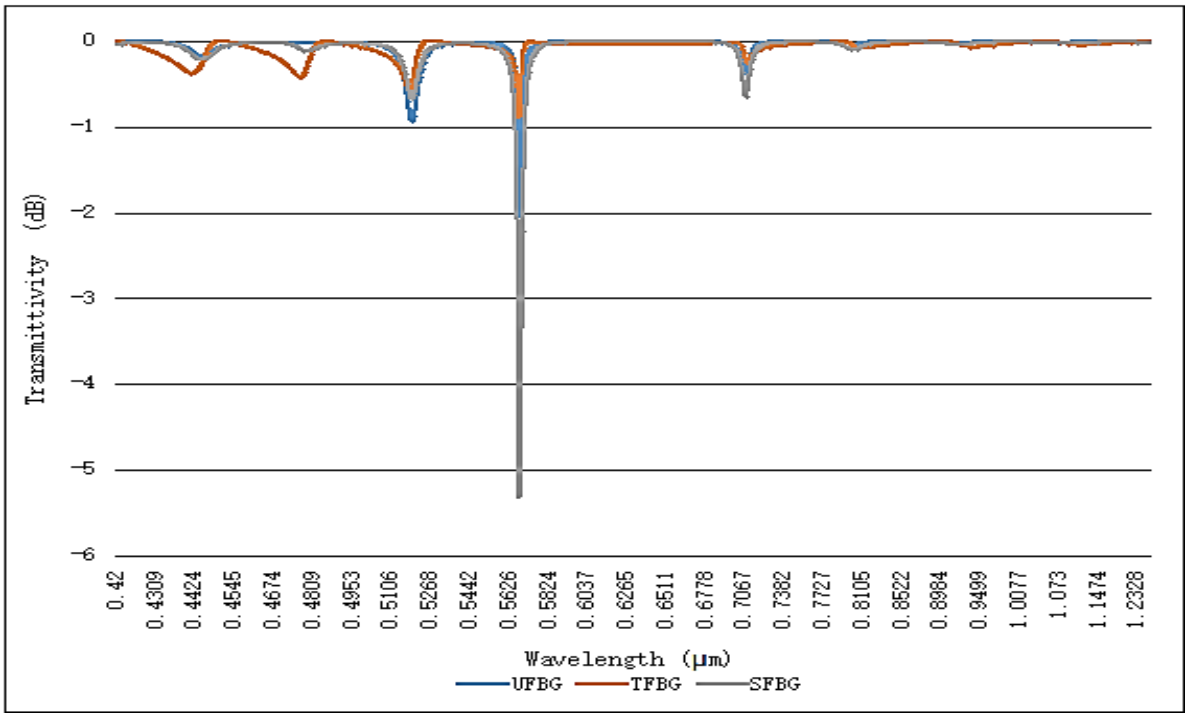

Figure 5.8:Transmittivity spectra of guided light.

From the Fig. 5.7 it can be seen that SFBG shows maximum reflective power (1.94 a.u.) than other gratings i.e. UFBG have 0.6317 a.u. and TFBG have (0.3433 a.u.). For better clarity, transmission spectra's are also taken for proposed grating shapes which is shown in Fig. 5.8. So, from Fig. 5.6-5.8 it is reported that titled grating is better for far field sensing.

5.4 Conclusion

The sensitivity of FBG optical sensor is enhanced with three parameters i.e. grating shapes, grating lengths and refractive index values. It is observed that the uniform grating shape is better than others. After varying the parameters in predefined manner, the sensor performance is enhanced in term of wavelength shift (7 nm). Further, different grating shapes are investigated for far field application and it is concluded that the tilted grating provide maximum amplitude value (0.218 a. u.) than uniform grating (0.0467 a. u.) and superstructure grating (0.0383 a. u.).

Chapter 6

Experiments on FBG Sensors for Health Monitoring of Civil Structures

6.1 Introduction

This Chapter deals with the experimentations on optical sensors for monitoring the health of civil structures. The experiments have been done to monitor the strain, vibration and displacement on different civil structures using FBG based sensor. These experiments have been performed in the Department of Civil Engineering (Structure Lab II), Thapar Institute of Engineering and Technology, Patiala, Punjab, India. In an experimental setup, optical broadband spectrum (module SM-130 of Micron Optic) having 1510-1590nm of wavelength range have been used along with Personal Computer (PC), Alternative Current (AC) supply, ethernet cable and optical sensors. The broadband spectrum module is used to attain the data in terms of wavelength shifting through Ethernet port and using MOI ENIGHT software. Four channels are provided by broadband spectrum module, further, each channel is capable of connecting 16 sensors on single port. As such, the combined capacity of broadband spectrum is equal to 64 sensors. After connection of all the equipment's, the informative data can be analysing from PC with the help of ENLIGHT software. Using ENLIGHT software some parameters of broadband spectrum module, strain sensor, signal recording, alerting, data saving and other functions can be controlled according to the user requirements. The front view of ENLIGHT software with acquisition tab is shown in Fig. 6.1. The tab control, acquisition rate and global control are highlighted. Tab control area is divided into many symbols i.e. acquisition, sensors, charts, image archive, save, alerts and settings. Data can be observed in acquisition tab with the help of spectrum view, table view, chart view and FFT view.

In sensors tab, the definition of FBG can be created with respect to selected application using inbuilt library and can add or delete the desired FBG sensor. In this tab, the bandwidth for results and obtain the spectral view of single or multiple FBG sensors can be fixed/ or unfixed. In charts tab, the performance of FBG can be monitor on one screen when it will come under different condition such as strain, temperature, vibration and displacement. In image tab the current measurement of used FBG sensors can be measured i.e. strain in "μm", displacement in "mm", temperature in "^{o}C" and vibration in "G". In tab archive stored data can be checked, in save tab the configuration for sensors can set and fix

the event for alerting can be controlled through setting tab. In the global control section; connections/ disconnection of sensor, run/ stop the system, saving management, screenshot and exit button can be controlled.

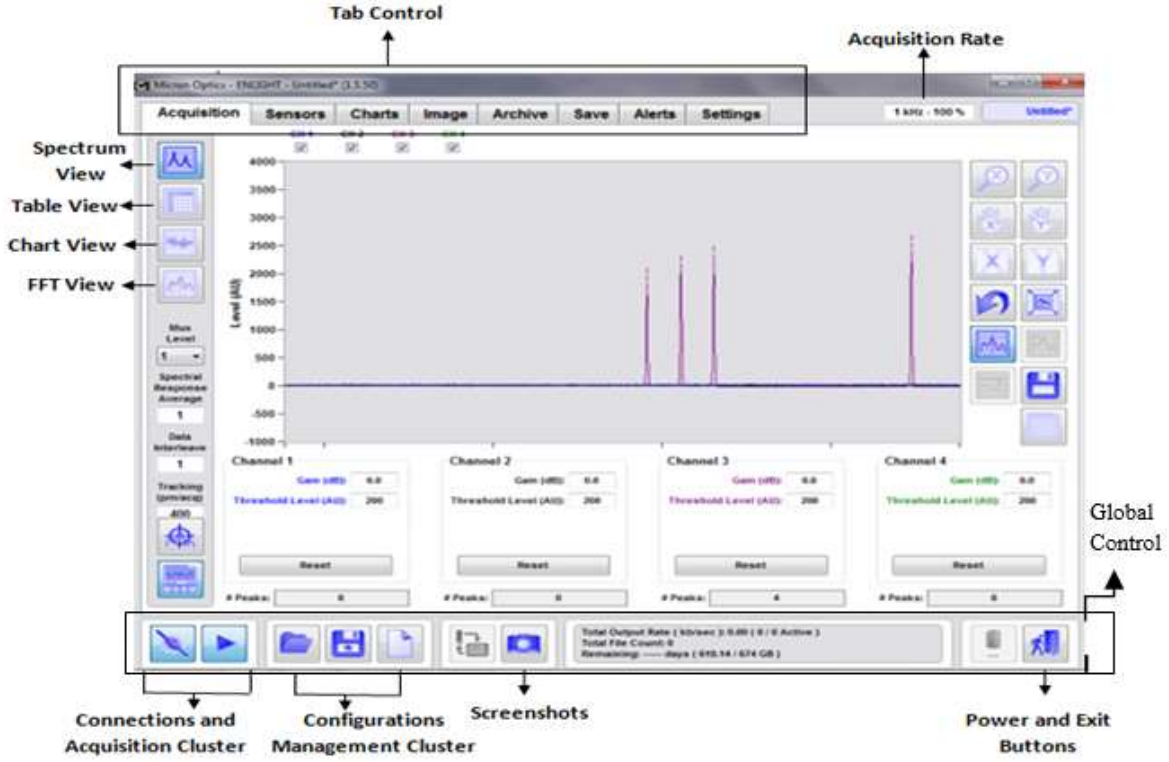

Figure 6.1: View of ENLIGHT software.

6.2 Experiment to Monitor Strain

Deformation are major problem occurs in civil structure which are mostly built under rainy area, underwater structure, land sliding area and it may become major damage if the adequate action will not take on time. The structure can damage

The life of structure is **reduced** with age or with physical and environment effects.

It can be increases proportionally to the structure age. Sometimes, deformation can seek to cause unpredictable damage that can be potentially harmful to humans and costly to repair. Therefore, it is required to detect the deformation at early stage for safety and cost-effective solutions. In this section, we have monitored the strain and Bragg wavelength is shifted due to change in RI and grating pitch when tensile strain is applied. The system setup to measure the strain on a beam using FBG sensor is represented in Fig. 6.2. The FBG sensor is surface mounted on the concrete beam using epoxy kit to monitor the behaviour of sensor at different strain values as shown in Fig. 6.3. We have considered concrete beam with 150 mm x 150 mm dimension with overall length of 750 mm. The light is transmitted by the optical source (at 1550nm) to the OS3200 sensor and continued monitoring of the

wavelength shift will be done by PC which receives the informative data from optical source via ENLIGHT sensing software.

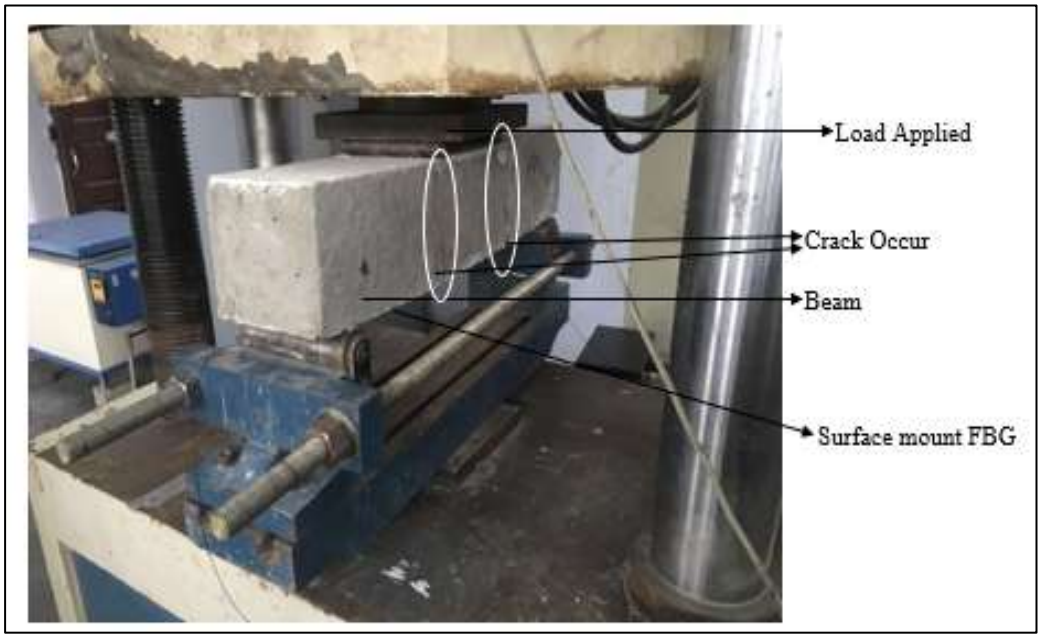

Figure 6.2: Experimental setup for strain monitoring.

Figure 6.3: Surface mounted FBG on beam.

The strain is calculated through the broadband spectrum with the help of following equation:

$$\varepsilon = \left(\frac{\Delta\lambda}{\lambda_o}\right) 1 \times 10^6 / \left(F_G - \varepsilon_{TO}\right) \quad (6.\ 1)$$

$$\varepsilon_{TO} = \Delta T \left[\frac{C_1}{F_G} + CTE_s - C_2\right] \quad (6.\ 2)$$

Where ε_{TO} is thermal output and other parameters of sensor is shown in Table 6.1.

Table 6. 1: Various parameter of Strain sensor (OS3200)

Variable	Variable Name	Value
F_G	Gage Factor	0.796
C_1	Gage Constant 1	6.156µm/m-ºC
C_2	Gage Constant 2	0.70µm/m-ºC
ΔT	Temperature Change	Measured
CTE_S	CTE of Test Specimen	User Defined
$\Delta\lambda$	Wavelength Shift	Interrogated
λ_0	Resonance Wavelength	Initial wavelength

Figure 6.4: Image of load and testing machine.

The load is applied on the sensor by loading machine i.e. “computer servo control material testing machine”, and strain value is calculated through the broadband spectrum using the equation 6.1 and equation 6.2. Figure 6.4 shows the setup of testing machine before installation of beam and sensor.

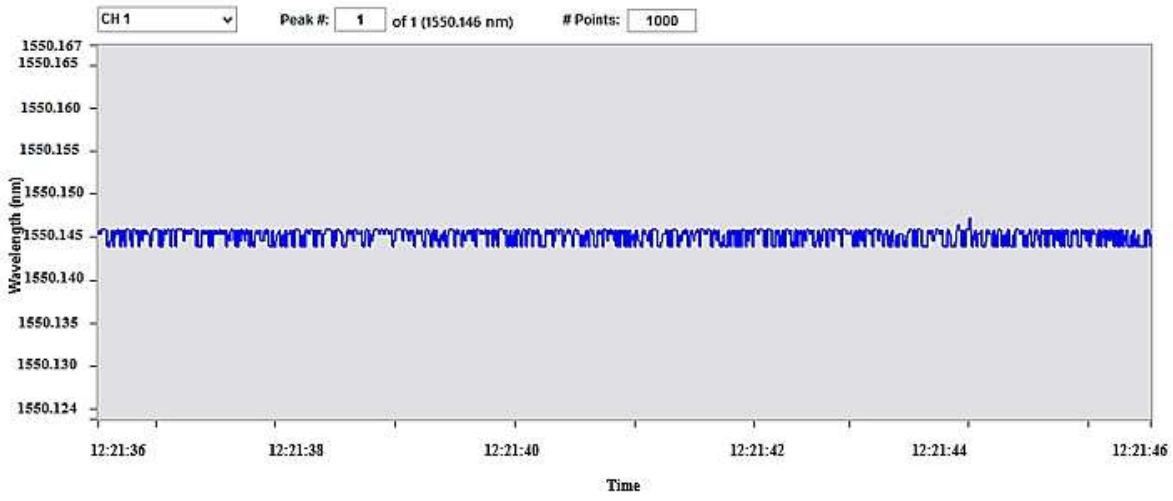

(a)

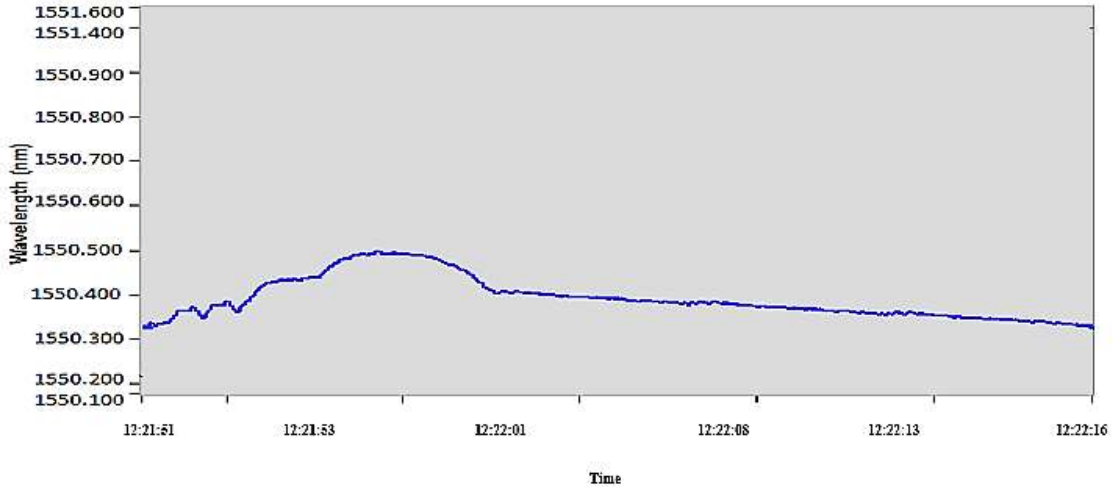

(b)

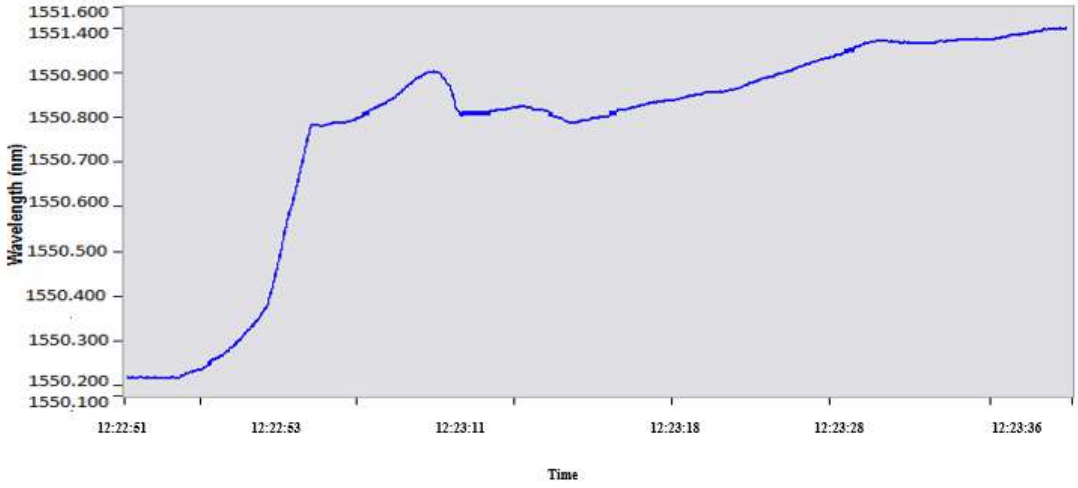

(c)

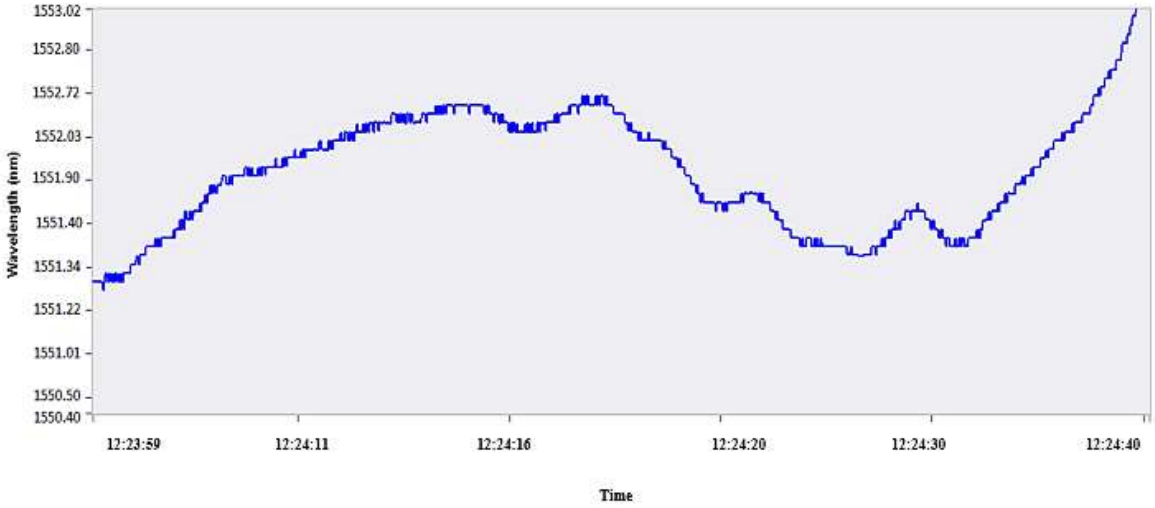

(d)

Figure 6.5: Spectrum of FBG sensor at different strain (a) no strain applied (b) Strain increased to 700 με (c) Strain increased to 1600 με (d) Strain increased to 3000 με

Further, optical spectrum in time domain is taken at reference wavelength (1550nm) with respect to different strain values shown in Fig. 6.5(a) to Fig. 6.5 (d). From the spectrums it can be seen that the light variation shows different peaks as the sensor comes under different strain values and shifts towards the higher wavelength.

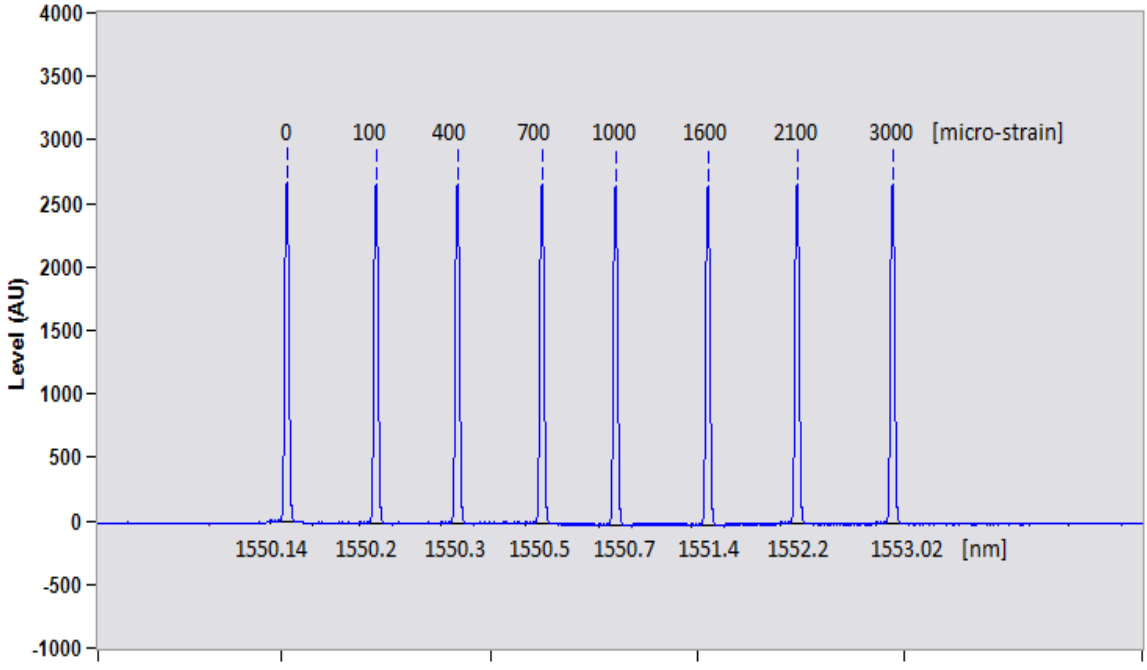

Figure 6.6: Amplitude view of wavelength at different strain.

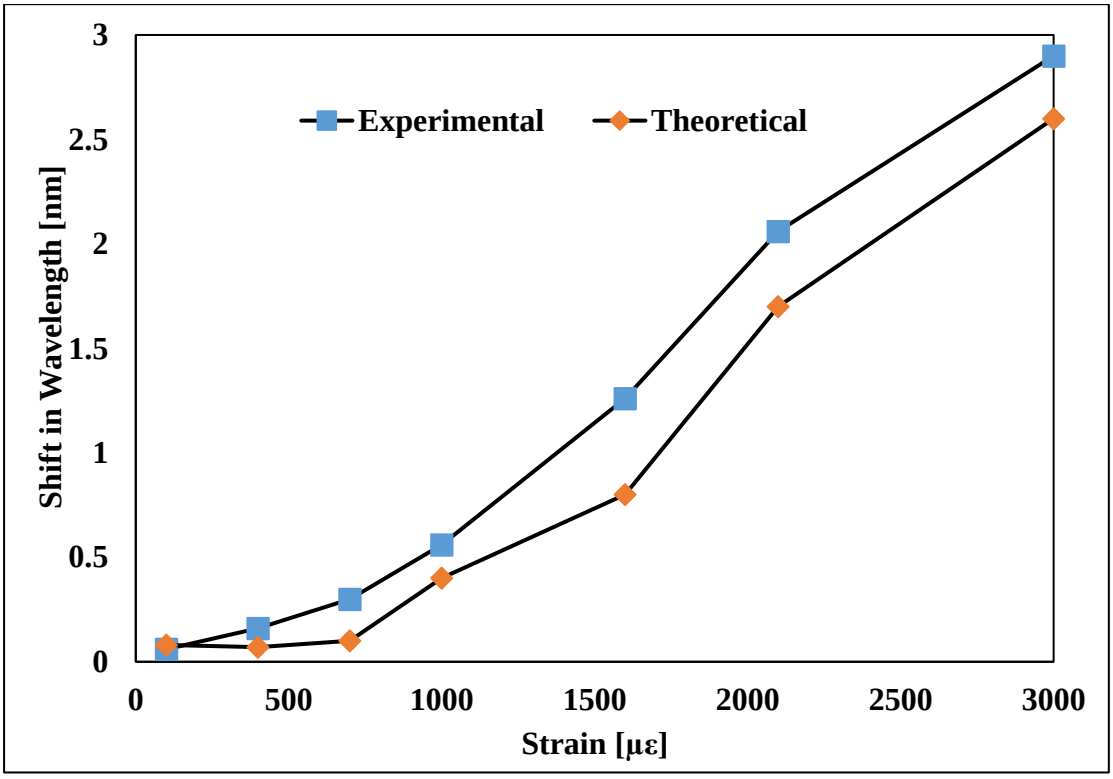

Figure 6.7: Wavelength change with respect to strain values.

Figure 6.6 depicts the amplitude view of strain sensor, where peak of wavelength starts shifting forward as load is increases. The experimental results are compared with theoretical results (which are taken during investigation of FBG sensor with different Grating shape in chapter 5) see in Fig. 6.7. In this experiment, wavelength shifts of 0.06nm, 0.16nm, 0.30nm, 0.56nm, 1.26nm, 2.06nm and 2.9 nm have been observed and wavelength shifts of 0.08nm, 0.07nm, 0.1nm, 0.4nm, 0.8nm, 1.7nm, 2.6nm have been observed theoretically against strain values of 100με, 400με, 700με, 1000με, 1600με, 2100με and 3000με, respectively which is shown in Fig. 6.7. From the results, it is concluded that the theoretical and experimental results concur with each other. It means proposed sensor is good applicant for sensing application with high speed.

6.3 Experiment to Monitor the Strain on Steel Beam

In this system, again we have used OS3200 FBG sensor to monitor the strain value but at different structure as shown in Fig. 6.8. In this system, we have used surface mount FBG sensor on small model of steel beam.

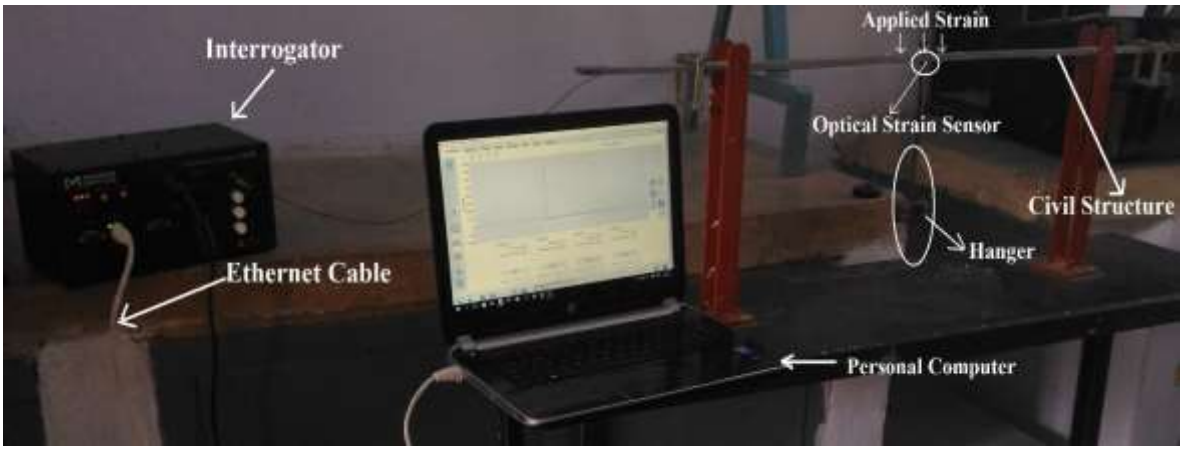

Figure 6.8: Setup for strain monitoring using OS3200.

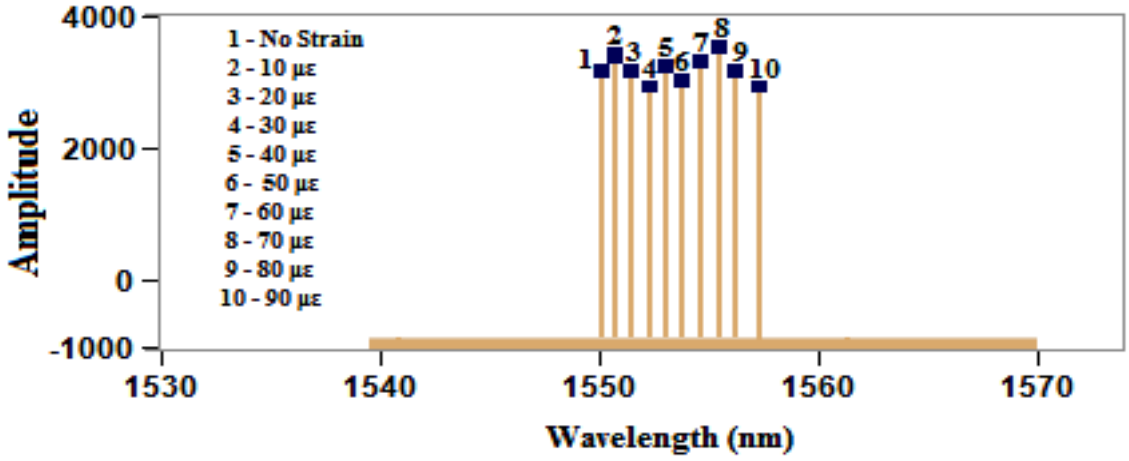

Figure 6.9: Amplitude graph with respect to wavelength at different strain.

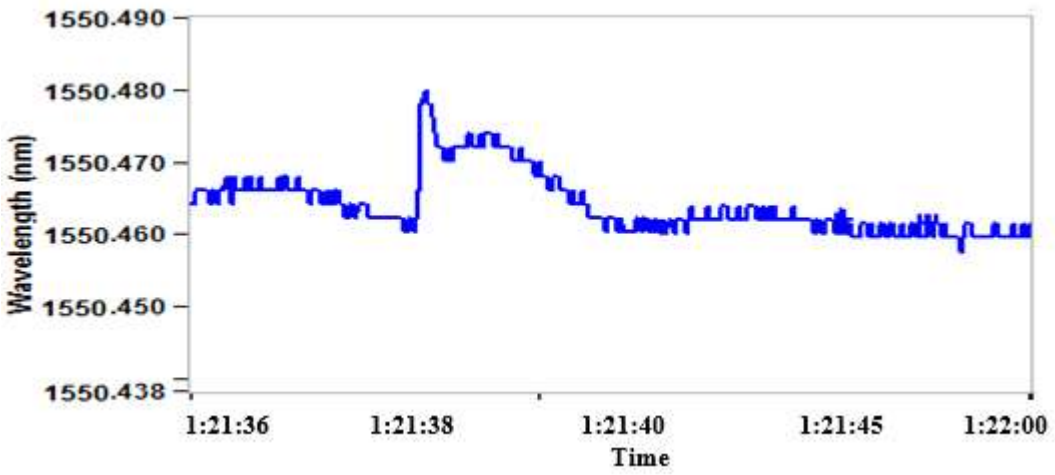

(a)

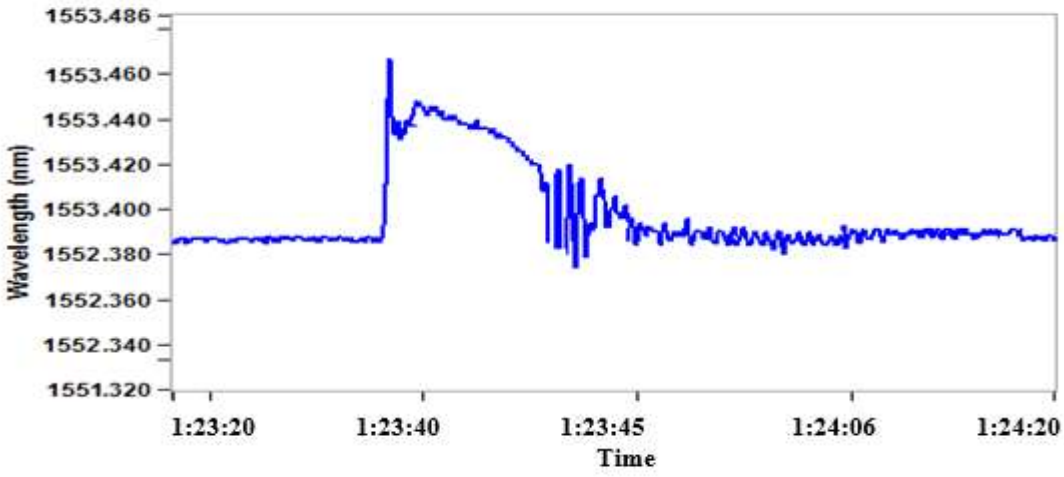

(b)

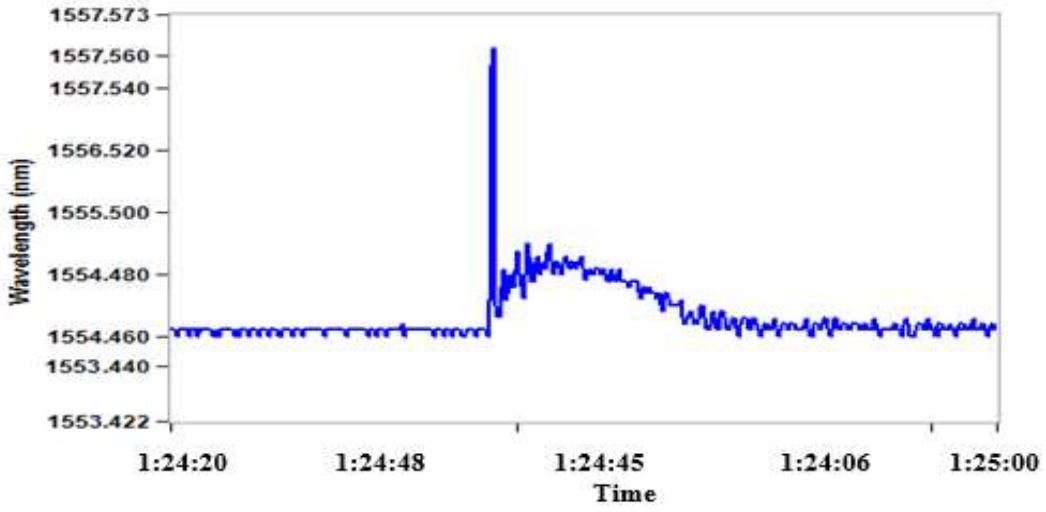

(c)

Figure 6.10: Spectral view of light for different Strain value (a) at strain 10 με (b) at strain 50 με (c) at strain 90 με

As we increase the load on the beam with the help of hanger, we observe the shift in wavelength. Although, load is applied on the structure but the end results are obtained in the terms of strain and this strain is calculated through broadband spectrum using equations 6.1 and 6.2. Figure 6.9 shows the wavelength shift at different strain values as a function of amplitude. The x axis shows change in Bragg wavelength and y axis shows the amplitude of reflected light for different applied strain. It is observed that, as the strain changes on the bridge, the spectral peaks (which are represented to wavelength change) is shifted towards the higher wavelength. Light spectrum view during applied strain is shown in Fig. 6.10 (a) – (c) and it can be seen that, as the strain is varied from 10 με to 90 με then the wavelength changes from 1550.48 nm to 1557.57 nm. The sharp rise is detected in the graph with respect to change in strain.

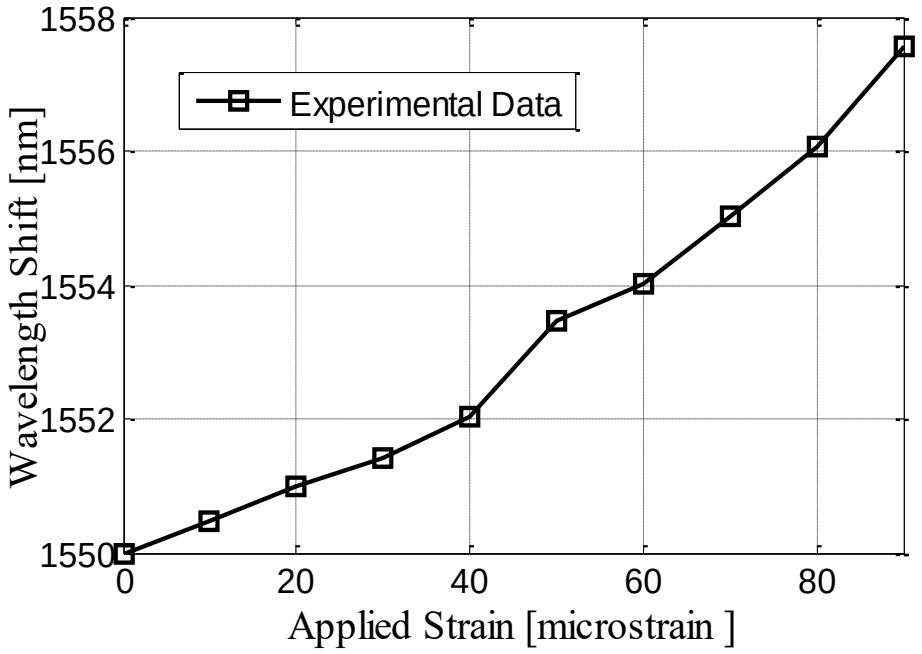

Figure 6.11: Wavelength change with respect to different strain levels.

From the results it is concluded that wavelength shift and strain are directly proportional to each other which is shown in Fig. 6.11. From the experiments we have observed maximum 7 nm wavelength shift.

6.4 Experiment to Monitor the Vibration and Displacement

In this section, vibration and displacement monitoring is performed using the optical sensors. FBG based vibration (OS7100) and displacement sensor (OS5100) is used for this experiment which is manufactured by Micron Optic. Ltd. The deflection during experiment is monitored by an broadband spectrum by the formula:

$$D(mm)=m(\lambda_2-\lambda_1)+b \quad (6.3)$$

Where m is gage factor, and λ_2, λ_1 are wavelengths tuned at 1533 nm and 1539.57nm, respectively.

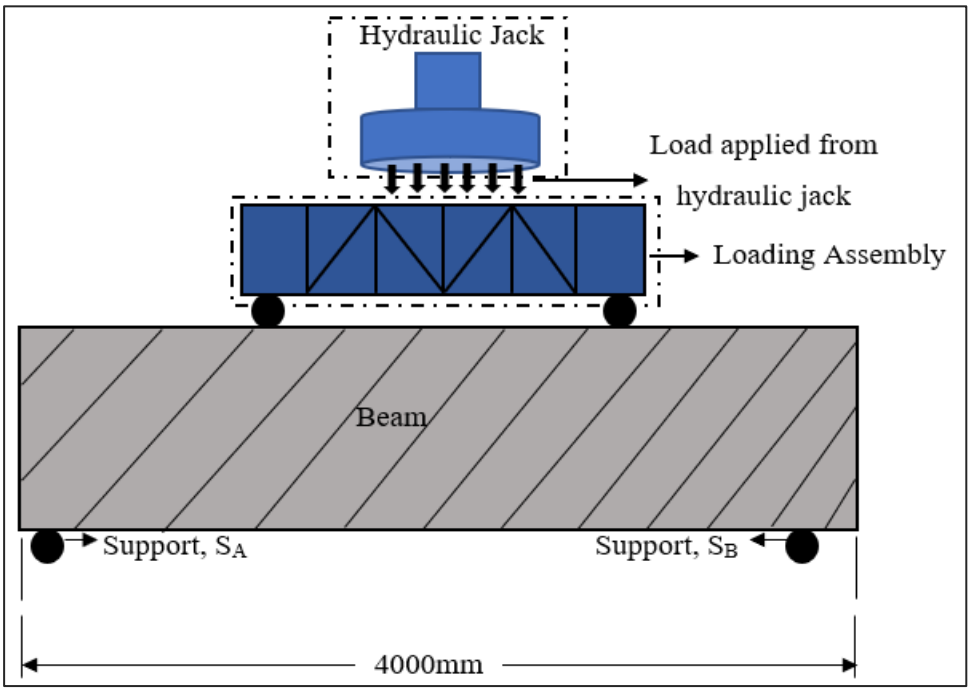

Figure 6.12: Setup for four-point load test.

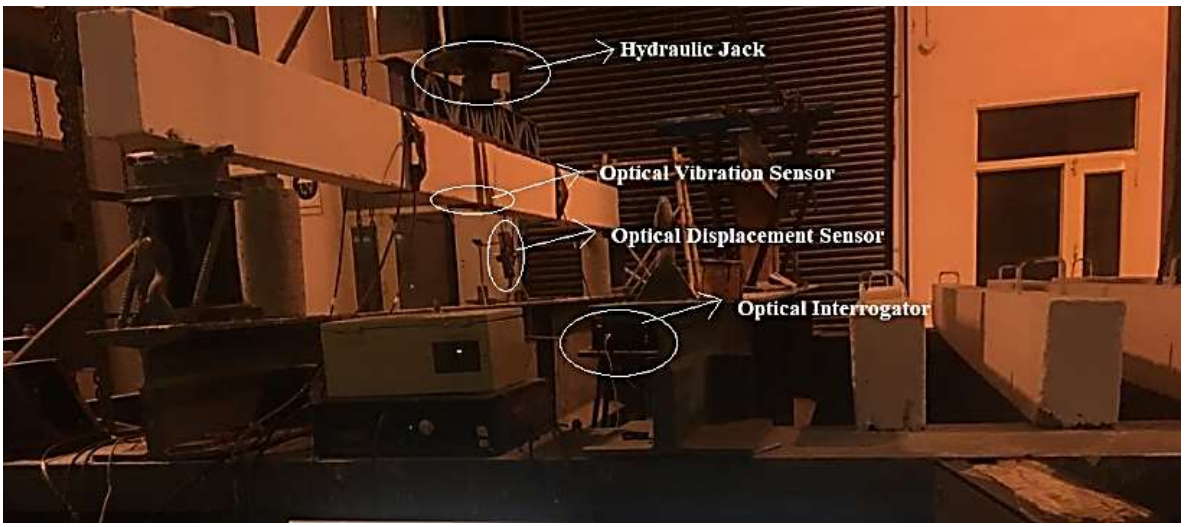

Figure 6.13: Experimental setup for SHM beam using optical sensor.

In this experiment, we have used a concrete beam having overall length of 4100mm, width of 125mm and depth of 225mm. Figure 6.12 shows the four loading points to monitor the health of beam in different conditions. We have applied the load on the beam with the help of hydraulic jack and loading assembly. The experimental setup for beam monitoring using

optical sensor is shown in Fig. 6.13. We have used surface mounted sensors and they mounted on the beam using epoxy kit which is provided by micron optic company. In this experiment, we have monitored these deformations through broadband spectrum, ethernet cable and personal computer. Using ENLIGHT software we have obtained the changes in spectrum view of light at different loading values. Figure 6.14 represents initial wavelength of displacement sensor and it is taken before the experiment starts. As we increase the load on beam by hydraulic jack the variation in wavelength shift for displacement sensor is observed which is shown in Fig. 6.15 to Fig. 6.19.

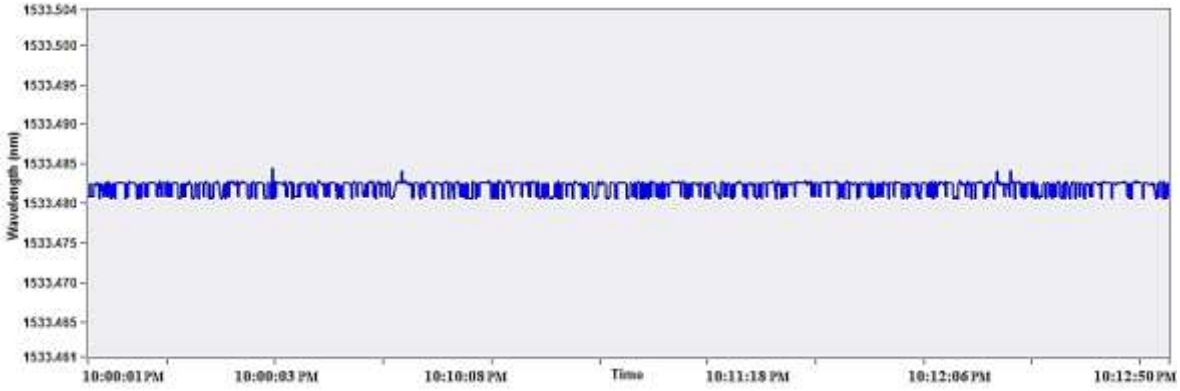

Figure 6.14: Spectrum view of Initial wavelength for displacement sensor.

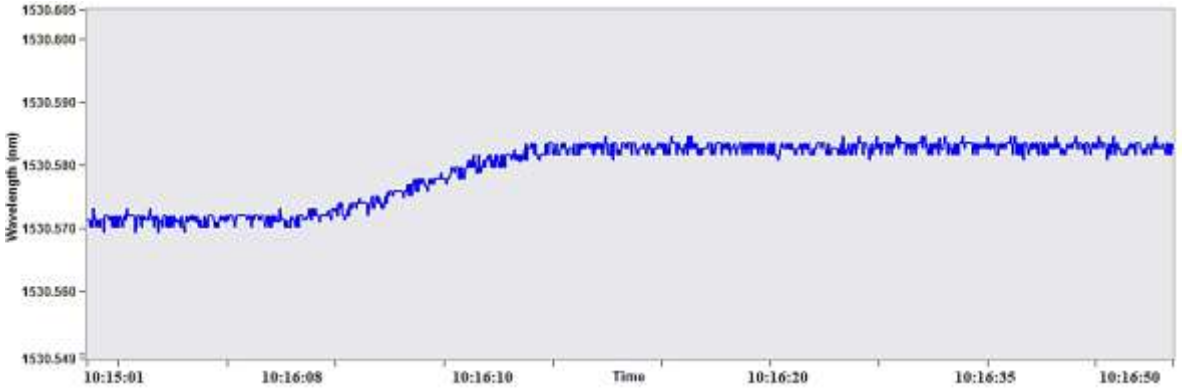

Figure 6.15: Change in spectrum of displacement sensor when load is increase to 5kN.

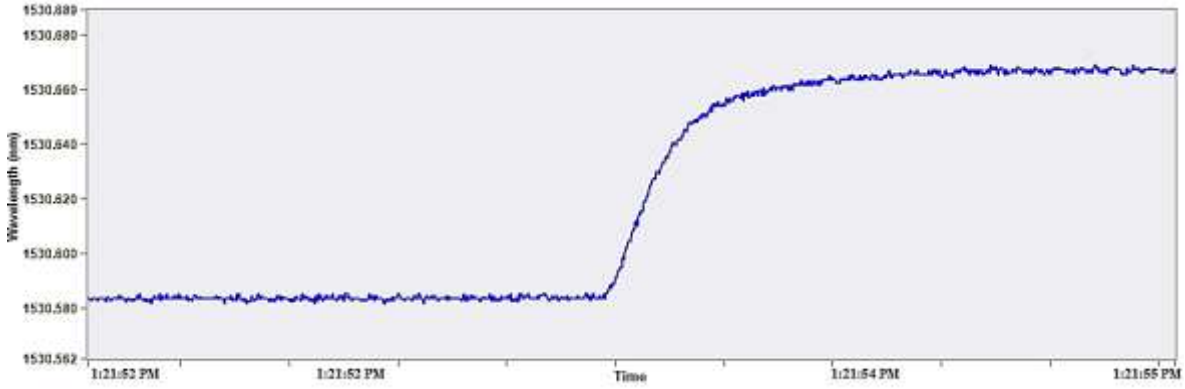

Figure 6.16: Change in spectrum of displacement sensor when load is increase to 10kN.

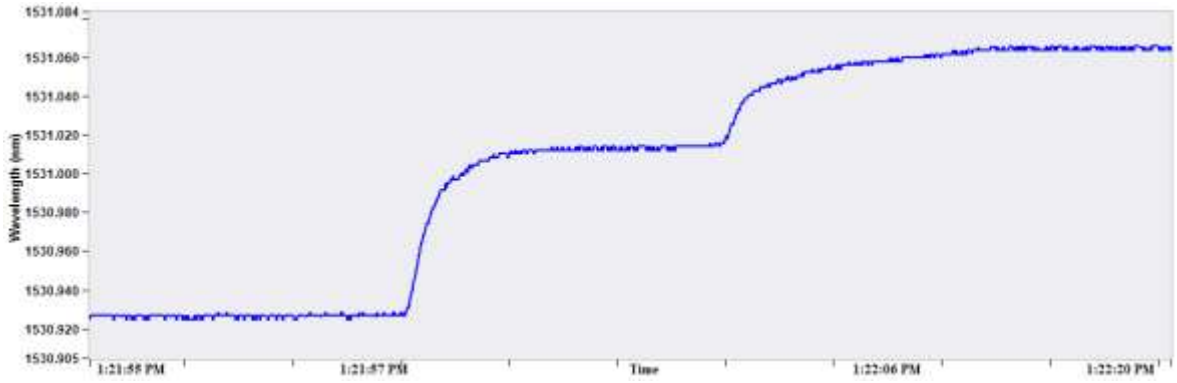

Figure 6.17: Change in spectrum of displacement sensor when load is increase to 15kN.

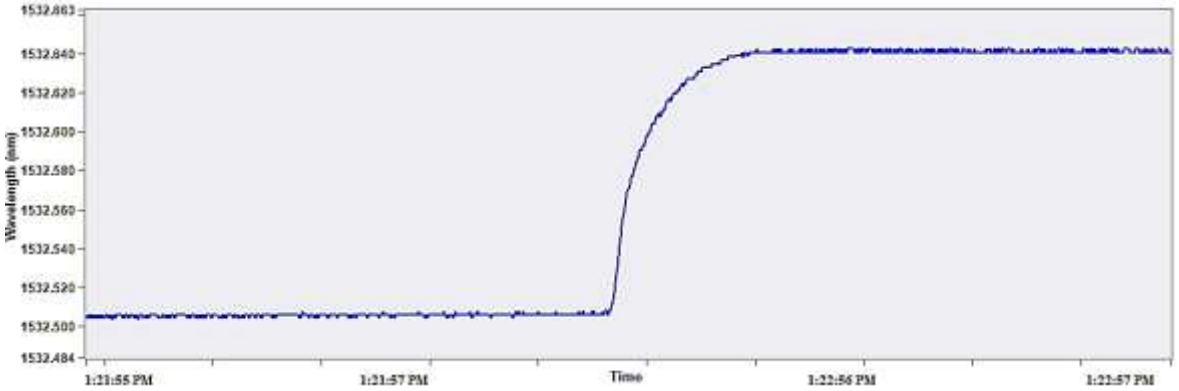

Figure 6.18: Change in spectrum of displacement sensor when load is increase to 20kN.

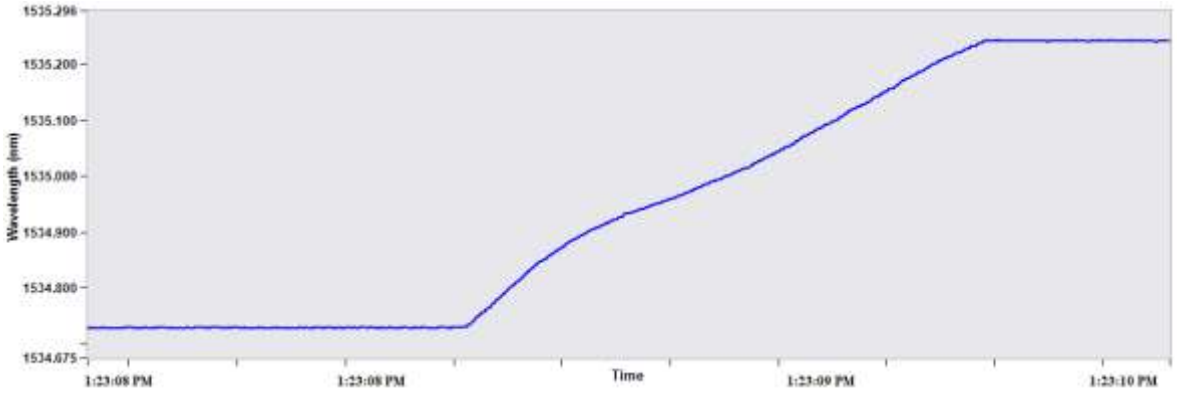

Figure 6.19: Change in spectrum of displacement sensor when load is increase to 30kN.

From these spectra it is observed that as we increase the load on beam the wavelength shows continuous shifting to higher side of the wavelength. During the experiment vibration is also monitored using OS7100 optical sensor. Figure 6.20 shows the reference wavelength of vibration sensors when there is no vibration is applied on the beam. Figure 6.20 to 6.25 shows spectra for wavelength change which is obtained through broadband spectrum device. From the spectrum it can be seen that as we increase the load value on the beam, an optical sensor senses the vibration and displacement through wavelength shifting.

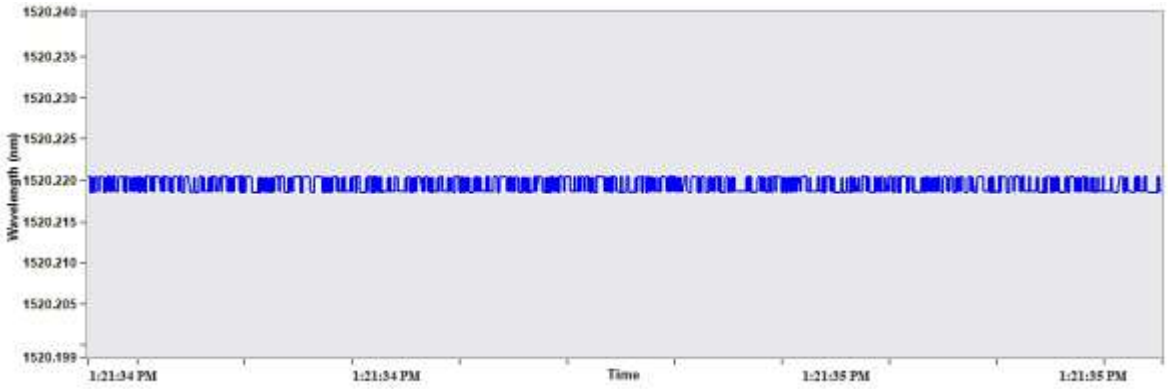

Figure 6.20: Spectrum view of Initial wavelength for vibration sensor.

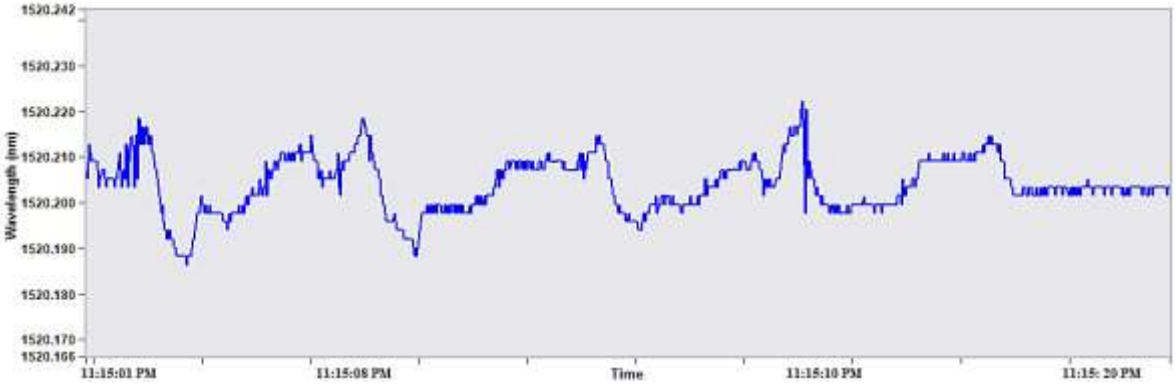

Figure 6.21: Change in spectrum of vibration sensor after the load 5kN.

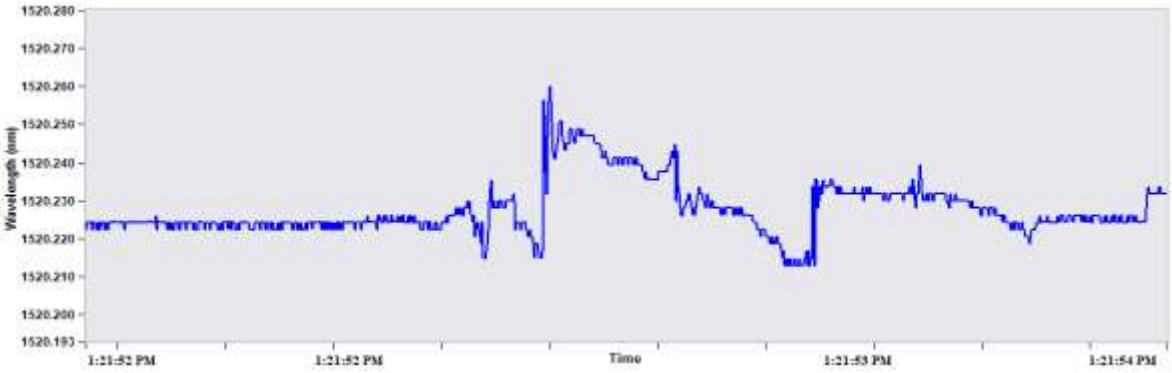

Figure 6.22: Change in spectrum of vibration sensor after the load 10kN.

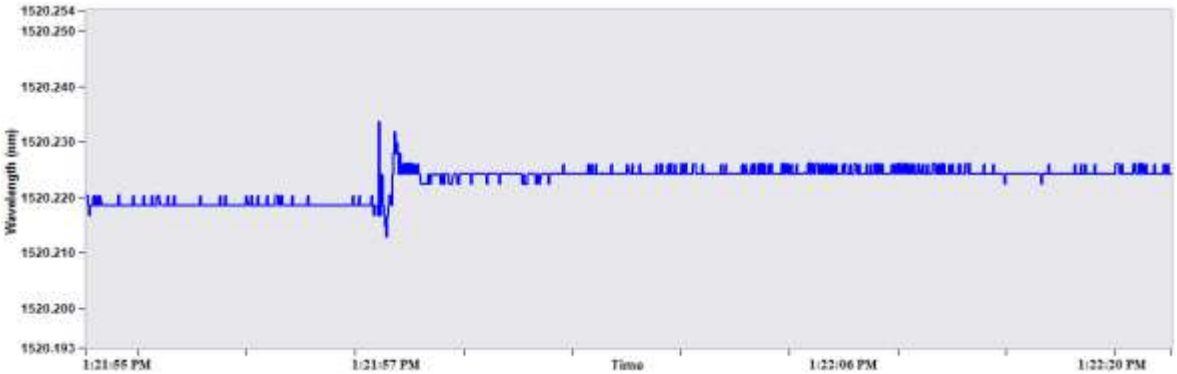

Figure 6.23: Change in spectrum of vibration sensor after the load 15kN.

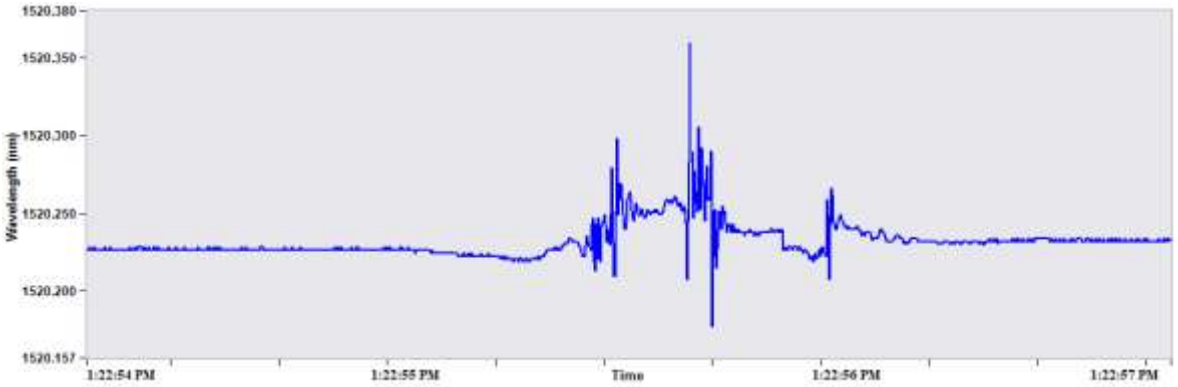

Figure 6.24: Change in spectrum of vibration sensor after the load 20kN.

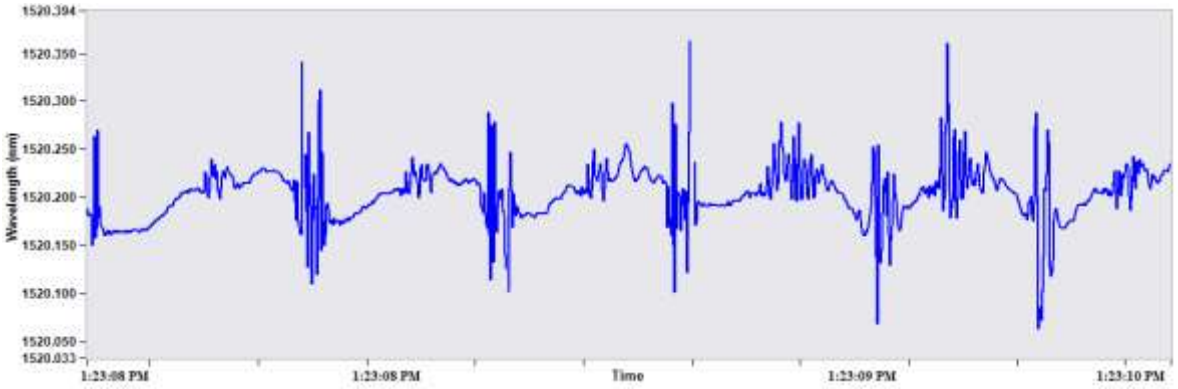

Figure 6.25: Change in spectrum of vibration sensor after the load 30kN.

To analyse the continuous monitoring of vibration and displacement we have presented chart view in Fig. 6.26 to Fig. 6.30. From the charts it is observed that as we increase the load value on the beam, both sensors show the variation in light in terms of distance in millimetre (mm) and vibration in vibration amplitude (G) respectively.

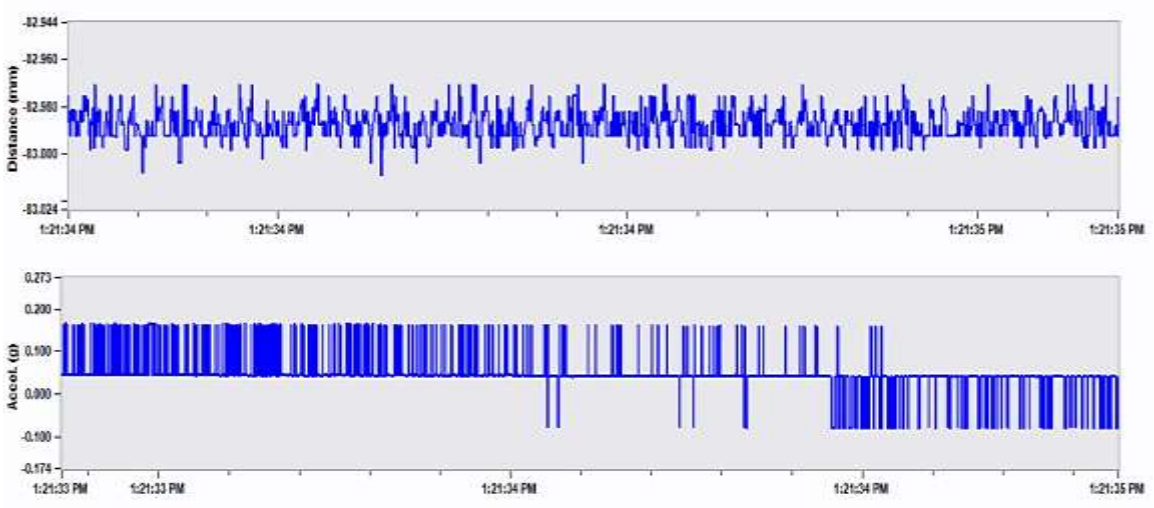

Figure 6.26: Continuous monitoring chart for vibration and displacement sensor when there is no load applied.

Figure 6.26 shows the chart view when there is no load applied and it is observed that the light travels at constant wavelength and it starts showing the variation when the load level is increased.

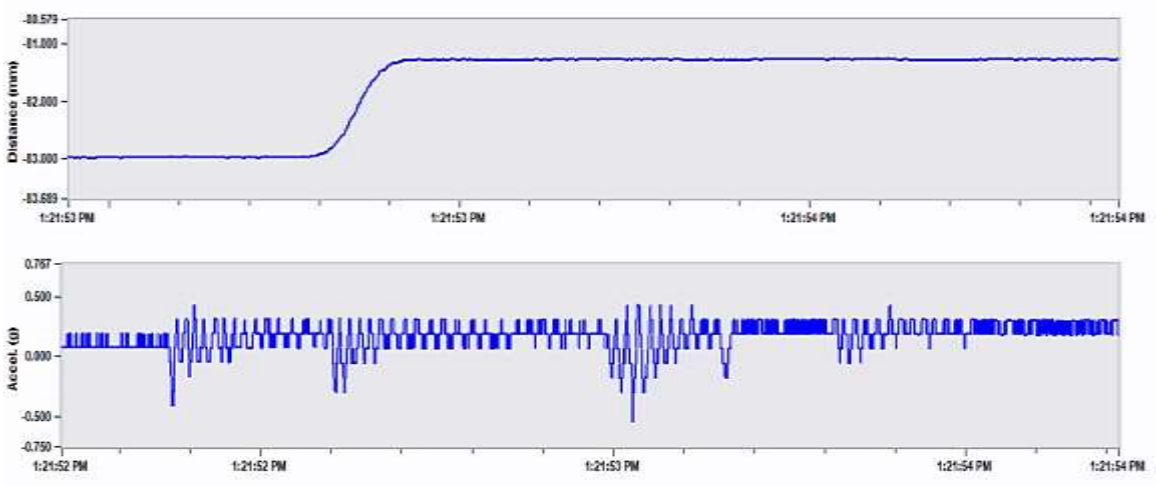

Figure 6.27: Continuous monitoring chart for vibration and displacement sensor when there is 10kN load.

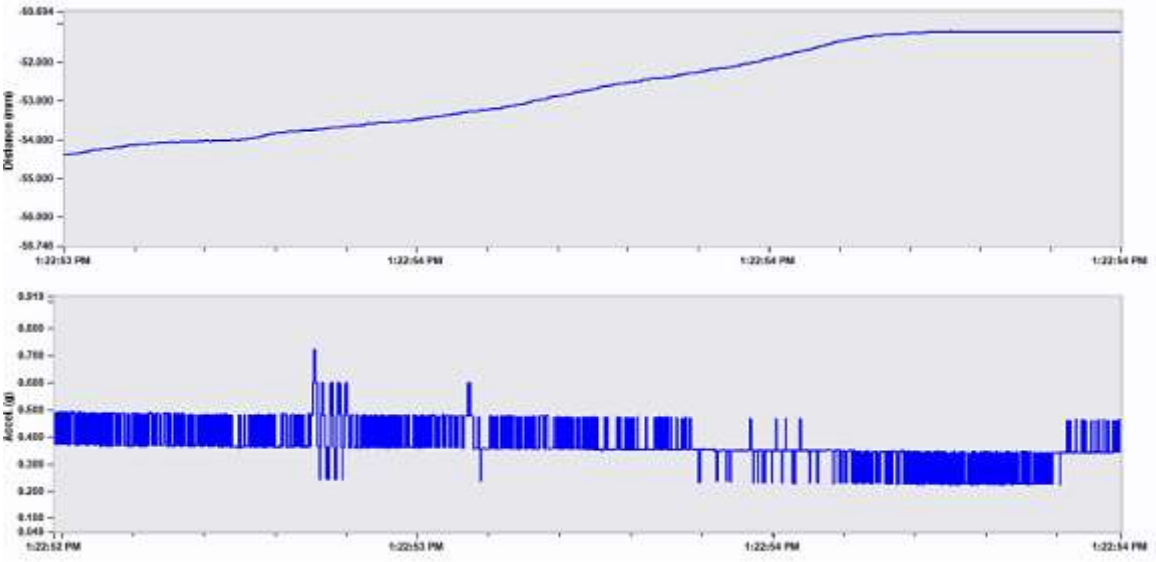

Figure 6.28: Continuous monitoring chart for vibration and displacement sensor when there is 15kN load.

In Fig. 6.27 we have observed that as the value of load is increased to 10kN the light variation shows the deflection from with maximum deflection -81 mm and vibration shows the maximum change 0.5G. From Fig. 6.28 it can be seen that when load is increased by 15kN deflection occurs with value of -51.3 mm and vibration is observed with the value of 0.7G. In Fig. 6.29 deflection is achieved with value of -48 mm and vibration is achieved with the value of 0.6 G when 20 kN load is applied. Similarly, in Fig. 6.30 it is observed that, during

the experiment when the load is increased from 20kN to 30kN then the sensor shows the deflection and vibration with value of -33mm and 0.4G, respectively.

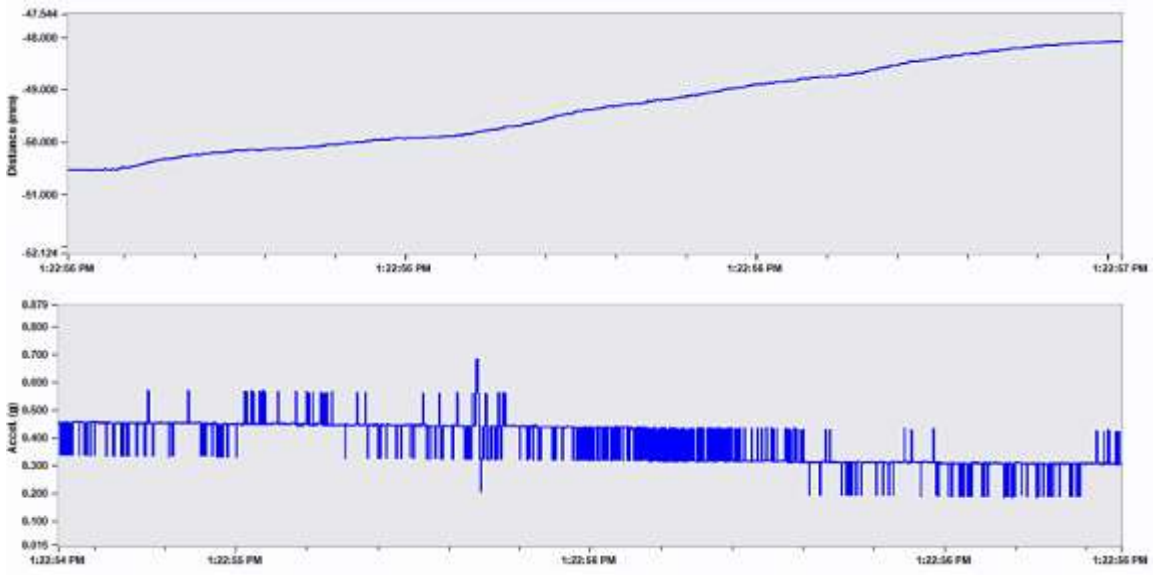

Figure 6.29: Continuous monitoring chart for vibration and displacement sensor when there is 20kN load.

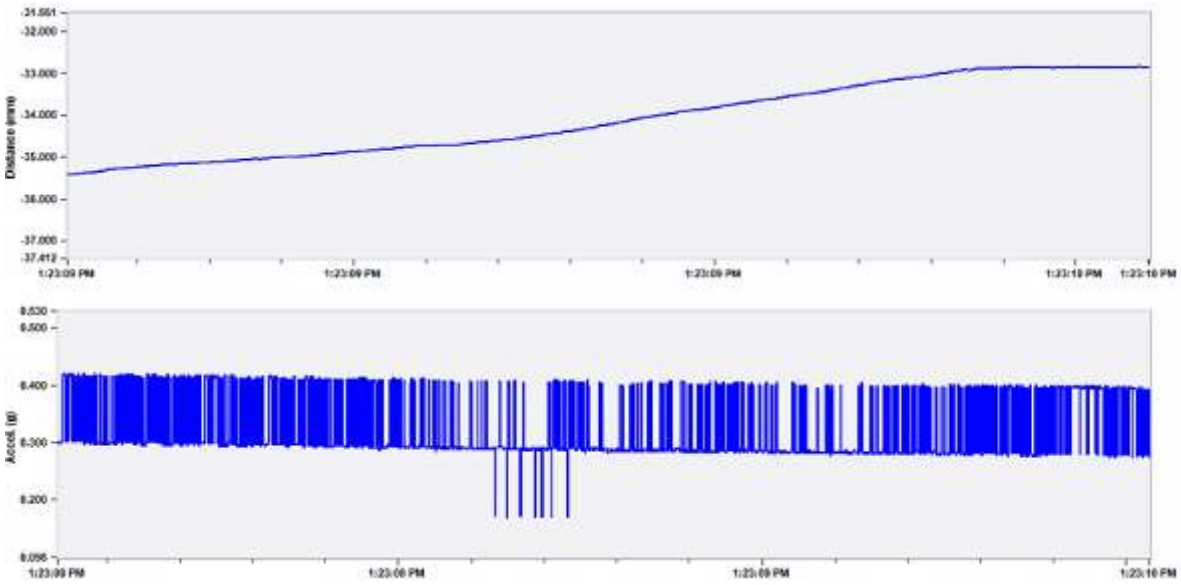

Figure 6.30: Continuous monitoring chart for vibration and displacement sensor when there is 30kN load.

From the results it is observed that maximum deflection value is -32.500mm and vibration amplitude values of 0.7G are obtained at load values of 50kN. The deflection charts show the results in negative value, the reason for this is that during the experiment we have selected 1539.5758 nm as first wavelength (λ_1). From the graphs it is shows that as we increase the load, an operating wavelength shows the shift to higher wavelength side. It is observed that

using proposed sensor we have achieved maximum wavelength shift of 5.2nm and 0.14nm for displacement and vibration sensor, respectively.

6.5 Conclusion

In this chapter, various experiments have been performed in order to support the previous investigations mentioned in chapter 3 to 5. We have used optical sensors to monitor the deformations due to displacement, strain and vibration. The concrete beams and steel beam are used for the experiments to check its health at different load and strain values. Monitoring of vibration and displacement under different level of loads is also performed using optical sensors. From the results it has been observed that when load is increased on the beam, the wavelength is changed from the reference wavelength and shows red shift.

Chapter 7

Conclusions, Recommendations and Future Scope

7.1 Conclusion

This thesis is focused on the investigations of various current problems in sensing applications such as sensitivity of sensor, multiparameter sensing, continuous SHM, high speed monitoring etc. of civil structures using optical sensors. The major outcomes obtained from the study are summarized as follows:

FBG based RI sensor is proposed to measure the chemical concentration levels of calcium hydroxide and calcium analogue of brucite. These chemicals are necessary to be monitored in concrete structure because they create a problem (portlandite) in civil structures in terms of spalling and corrosion. In this work, two types of sensors are proposed, one is uncoated sensor and another is coated sensor. We have used ITO layer to enhance the sensitivity of the sensor. The sensitivity of sensors has been monitored with these chemicals at different concentration levels. After the simulation, the results shows that as we increase the volume of considered chemicals, the values of light power, OSNR and RI arises proportionally. The shift in wavelength is also demonstrated at different concentration of chemicals using proposed sensors and maximum wavelength shift of 8 nm and 6 nm using uncoated sensor and 12 nm and 10 nm using coated sensor is obtained for $Ca(OH)_2$ and $Mg(OH)_2$, respectively. After these investigations, the proposed sensor is recommended for civil applications to measure the portlandite, spalling and corrosion in concrete structures.

Further, experiment is done for strain monitoring using FBG sensor and we have achieved maximum 7 nm wavelength shift. From the experiment it is observed that the sensitivity of sensor needs to be improved. In this work, we have increased sensitivity of proposed sensor by optimized the optical sensor using GA. We have optimized the three parameters of FBG (i.e. Poisson ratio, P_{11} and P_{12}). The sensitivity of the sensor has been analysed for various possible combinations for different values of taken parameters. These combinations keep on repeating itself until we get the desired results. When the procedure of optimization is completed we get ~38 nm wavelength shift which is obtained with the combination of Poisson's ratio, P_{11} and P_{12} having values of 1.94, 1.994 and 1.8103, respectively. This system is cost effective solution to increase the sensitivity because we have only optimized the factors of the sensor and no physical change or any other modification has been done.

To monitor the effects of physical measurands i.e. vibration, temperature and strain on the sensor at same time, we have proposed the HOS technique. In this technique we have used the uniform super structured gratings in RR sensor to monitor these physical measurands simultaneously. The sensitivity of proposed sensor is increased using optimization with different diameters of ring resonator and with different grating materials in terms of wavelength shifting. Various results such as transmittance power, quality factor, overlap integral and change in wavelengths have been taken to observe the sensor performance. The proposed sensor gives desired result using 4.7μm diameter of ring resonator with SiO_2 grating material and observed 7 nm wavelength shift. From the results, it is reported that HOS give better results when it is compared with conventional RR sensor.

The proposed sensor is further modified with different grating shapes i.e. UFBG, TFBG, and SFBG for analysing the performance of sensor. We have also done the investigations on different grating length (30000 μm, 40000 μm and 5000 μm) and different refractive index of grating (1, 1.33 and 1.46). From the results we observed the enhanced performance with UFBG having RI value 1.46 at 50000 μm length of grating. Proposed configurations are also investigated for far field applications.

Further, different grating shapes are investigated for far field applications and it has been seen that tilted grating provide maximum amplitude value (0.218 a.u.) than uniform grating (0.0467 a.u.) and superstructure grating (0.0383 a.u.). Using mode overlap integral, the values of CE is calculated for proposed grating shapes and it has been observed that 5.622%, 0.012% and 0.466% is achieved for titled, uniform and superstructure grating shapes, respectively.

Continuous monitoring of different structures is also performed using optical sensors. The non-metallic optical strain gage, optical displacement gage and vibration sensor is used to monitor the deformation in the structure when different load and vibration is applied on it. These sensors are FBG based and from the Bragg wavelength shift we detect the values of strain, deflection and vibration. Further all the information regarding changes in reflected light is gather from broadband spectrum and send it to personal computer. From the personal computer all the charts, spectrum and time related plots are observed. We have used two types of beams and steel beam to performed the experiments in the lab of Civil Engineering Department at Thapar Institute of Engineering and Technology, Patiala.

In first experiment, we have considered concrete beam with 150 mm x 150 mm dimensions with overall length 750 mm to monitor the strain at different load level. From the experiment it is observed that as we increase the load level on the beam the sensor shows

the variation in strain value and from the variation it is obtained that strain and load values are proportional to each other. We have observed maximum wavelength shift of 2.9 nm at 3000με strain value.

In another experiment we have monitor the model of steel beam under different strain value. We have increased the load on the bridge with the help of hanger. From the experiment it is reported that maximum 7 nm wavelength is shift at 80 με strain value. The strain value is observed through broadband spectrum using calculation strain equation. Further the health of concrete beam having overall length 4100 mm, width 125 mm and depth 225 mm is monitor under different load and vibration levels. From the experiment we again monitor the behaviour of sensor under different loading level on the beam. And from the experiment it is reported that maximum 0.14 nm wavelength is shift for vibration and 5.2 nm wavelength is shift at 30 kN load value. From the results it is also concluded that as the value of load is increased on the structure wavelength start showing the shift to right side due to induced strain and vibration. It is also concluded that the optical sensor has an ability to sense the deformation continuously under different natural or physical hazards. In brief, we have proposed several optical sensors which are further optimized to enhance the sensitivity. For validation of the simulation results we also performed many experiments and found that the results concur with the simulation results.

7.2 Recommendations

The buildings are the major part of any country, but various undesired effects such as earthquake, rainfall, manmade hazards, algal bloom and climate change on rainfall patterns can harm these structures and further human being. It is required to monitor the structure/ buildings for these hazards at early stages so that suitable remedy action can be taken accordingly. In a tropical country like India, where approximately 80% of the annual rainfall takes place in the two monsoon months, rusting, cracking related problems are more alarming, especially in bridges etc. India also has a very long coastline where marine weather prevails. Typically, a structure requires major restoration work within fifteen years of its construction. Consequently, it has become urgent to have a reliable method for accurately measuring the rate of corrosion, strain, vibrations, temperature in existing as well as new structures in better way.

Currently, fiber optic sensors are the best alternative to monitor the health of civil structure along with its high speed, large sensitivity, easy installation, exact measurement etc. So, it is important to investigate the performance of optical sensors to monitor the health of civil structures. In this work, the FBG sensor shows the good results to monitor chemical

concentration level and it can be recommended for civil applications for portlandite monitoring in coastal areas.

Optical sensors i.e. FBG sensors do not require electricity. As such, they are prone to meddling by any other signals. Also, they are naturally protected so they can be used for instrumenting dangerous circumstances. For monitoring and controlling deformation in structures, this study can be beneficial for exploring FBG as optical sensor. The FBG sensors are presented in this thesis work i.e. refractive index sensor, strain sensor, temperature sensor and vibration sensor. In chemical industries, where bulk of chemical solutions are used every day, fiber based refractive index sensing can be very beneficial in performing fast and accurate monitoring of corrosion and spalling. FBG based current sensor presented here is distinct from the existing sensors due to its latest and easy arrangement, its cheap price and capability to perform under extreme conditions. As such, these sensors have a huge opportunity in the electrical field.

Apart from the real time sensing we have observed that there is a requirement of real time communication also, so that the managing officer can observe the readings even sitting in his office or at far places. For the same, the proposed sensors can be make IoT enabled to solve both the real time sensing and communication purpose.

7.3 Scope for Future Work

Tremendous efforts are still going on for the development as well as the improvement of various fiber optic sensor system for diverse applications like manufacturing (through the measurement of temperature, pressure, humidity, strain, displacement, fluid flow, fluid level, etc.), aerospace, defence, undersea surveillance, medical, gas and oil industry, power plant and power distribution system, smart structure and many more. The requirement of active and passive optical sensors is growing day by day. For meeting the needs of swiftly growing application driven market, the major emphasis should be focussed on the development of quick response and large bandwidth based optical sensor system with multi analyte sensing ability and their integration with state of the art optoelectronic systems for data recording and analysis. The other practical challenges of the real-world applications of these fiber optic sensor systems may include the need of ultrafast (i.e. Nano to femtosecond level) sensitivity and multiplexing capabilities (through the possibility of distributed measurement) in real time monitoring of various measurands.

In this work investigations have been observed in the field of FBG as a sensor. Further work can be investigating in other components such as LPG, FFPIS and plastic optical fiber.

In this work Different types of methods have been proposed to increase the sensitivity of FBG sensor using different parameters, dimension, optimization algorithm and coating technique and it can be enhanced further using different other techniques. This work is investigated on small civil structure it can be used for large scale structure using optical network topologies.

The structure can be repaired with the help of Microbial technique. Microbial concrete has emerged as a new technique in recent years which can be used for various purposes, amongst which remediation of cracks in concrete is the primary one. It can be used as an alternative to surface treatment and water purifier. Apart from its other wonderful properties, due to its major property of crack remediation or self-healing, it is also known as self-healing concrete. This technology of using microbes for calcium carbonate deposition or microbial concrete, called as Microbially induced calcium-carbonate precipitation (MICCP), can be used for solving various durability issues of construction materials. Due to natural capability to precipitate calcite continuously bacterial concrete is also called a 'SMART BIO MATERIAL'. Several different microbial groups contribute in the precipitation of mineral carbonates in various natural environments.

In this work the investigation is carried out for civil application to monitor the strain, portlandite, vibration and displacement. Further work can be carried out in other application like underwater application, chemical monitoring application, corrosion monitoring etc.

References

[1] R. J. Essiambre, R. W. Tkach, and R. Ryf, "Fiber Nonlinearity and Capacity: Single-Mode and Multimode Fibers," in *Optical Fiber Telecommunications VIB: Systems and Networks*, 6th ed., USA: Elsevier, 2013, pp. 1–37.

[2] E. Udvary and T. Berceli, "Semiconductor optical amplifier for detection function in radio over fiber systems," *J. Light. Technol.*, vol. 26, no. 15, pp. 2563–2570, 2008.

[3] A. K. Garg, "Traffic prediction based burst assembly mechanism for OBS," *Opt. - Int. J. Light Electron Opt.*, vol. 124, no. 15, pp. 2017–2019, 2013.

[4] A. Kotb, "Performance of All-Optical XNOR Gate Based on Two-Photon," *Adv. Opt. Tecnol.*, vol. 2014, pp. 1–6, 2014.

[5] G. P. Agrawal, *Fiber-Optic Communication Systems*, 3rd ed. New york: Jhon willey & sons, 2010.

[6] P. Garg, R. K. Mallik, and H. M. Gupta, "Performance analysis of space-time coding with imperfect channel estimation," *IEEE Trans. Wirel. Commun.*, vol. 4, no. 1, pp. 257–265, 2005.

[7] V. Singh, Y. N. Singh, and N. K. Verma, "Tradeoff between energy consumption and lifetime in two tiered wireless sensor networks," in *2016 IEEE International Conference on Prognostics and Health Management (ICPHM)*, Ottawa, ON, Canada, Jun. 20-22, 2016, pp. 1–4, paper 16230004.

[8] M. Singh and A. Kaur, "A Review on Injury Severity in Traffic System using Various Data Mining Techniques," *Int. J. Sci. Res.*, vol. 5, no. 1, pp. 1530–1535, 2014.

[9] S. S. Kessler, S. M. Spearing, and C. Soutis, "Damage detection in composite materials using Lamb wave methods," *Smart Mater. Struct.*, vol. 11, no. 2, pp. 1–19, 2002.

[10] B. Wincheski, F. Yu, J. Simpon, P. Williams, and K. Rackow, "Development of SDT sensor based eddy current probe for detection of deep fatigue cracks in multi-layer structure," *NDT E Int.*, vol. 43, no. 8, pp. 718–725, 2010.

[11] K. M. Holford, R. Pullin, S. L. Evans, M. J. Eaton, J. Hensman, and K. Worden, "Acoustic emission for monitoring aircraft structures," *Proc. Inst. Mech. Eng. Part G*

J. Aerosp. Eng., vol. 223, no. 5, pp. 525–532, 2009.

[12] C. K. Y. Leung, K. T. Wan, and L. Chen, "A Novel Optical Fiber Sensor for Steel Corrosion in Concrete Structures," *Sensors*, vol. 8, no. 3, pp. 1960–1976, 2008.

[13] K. T. Wan and C. K. Y. Leung, "Durability tests of a fiber optic corrosion sensor," *Sensors*, vol. 12, no. 3, pp. 3656–68, 2012.

[14] S. Dong, Y. Liao, Q. Tian, Y. Luo, Z. Qiu, and S. Song, "Optical and electrochemical measurements for optical fibre corrosion sensing techniques," *Corros. Sci.*, vol. 48, no. 7, pp. 1746–1756, 2006.

[15] K. Amer;, "2 Tb/s all-optical gates based on two-photon absorption in quantum dot semiconductor optical amplifiers," *Opt. Laser Technol.*, vol. 112, pp. 422–451, 2019.

[16] J. Haus, *optical sensors basics and application*. Germany: Wiley- VCH, 2010.

[17] Y. Ou, C. Cheng, Z. Chen, Z. Yang, H. Lv, and L. Qian, "Continuous-Wave Fiber Cavity Ringdown Pressure," *Sensors*, vol. 18, no. 4, pp. 1–10, 2018.

[18] K. M. Raina, *Optical Fiber Communication System*. 3rd ed. New Delhi: Satya Prakashan, 2011.

[19] L. Sun, H. N. Li, L. Ren, and Q. Jin, "Dynamic response measurement of offshore platform model by FBG sensors," *Sensors Actuators, A Phys.*, vol. 136, no. 2, pp. 572–579, 2007.

[20] S. Wei, Z. Zhang, S. Li, and H. Li, "Strain features and condition assessment of orthotropic steel deck cable-supported bridges subjected to vehicle loads by using dense FBG strain sensors," *Smart Mater. Struct.*, vol. 26, no. 10, 2017.

[21] J. Li and H. Hao, "Health monitoring of joint conditions in steel truss bridges with relative displacement sensors," *Meas. J. Int. Meas. Confed.*, vol. 88, pp. 360–371, 2016.

[22] S. K. S. Kim, J. K. J. Kwon, S. K. S. Kim, and B. L. B. Lee, "Multiplexed strain sensor using fiber grating-tuned fiber laser with a semiconductor optical amplifier," *IEEE Photonics Technol. Lett.*, vol. 13, no. 4, pp. 350–351, 2001.

[23] M. R. A. Hassan, M. H. A. Bakar, K. Dambul, and F. R. M. Adikan, "Optical-based sensors for monitoring corrosion of reinforcement rebar via an etched Cladding Bragg

grating," *Sensors*, vol. 12, no. 11, pp. 15820–15826, 2012.

[24] L. Han, L. Wang, N. Fang, H. Cui, and Z. Huang, "FBG moisture sensor system using SOA-based fiber laser with temperature compensation," in *2011 IEEE international conference on Asia Communications and Photonics Conference and Exhibition (ACP)*, Shanghai, China, Nov. 13-16, 2011, pp. 1–7, paper 12784648.

[25] G. Kister, D. Winter, R. A. Badcock, Y. M. Gebremichael, W. J. O. Boyle, B. T. Meggitt, K. T. V. Grattan, and G. F. Fernando., "Structural health monitoring of a composite bridge using Bragg grating sensors. Part 1: Evaluation of adhesives and protection systems for the optical sensors," *Eng. Struct.*, vol. 29, no. 3, pp. 440–448, 2007.

[26] H. Sekine, S. E. Fujimoto, T. Okabe, N. Takeda, and T. Yokobori, "Structural health monitoring of cracked aircraft panels repaired with bonded patches using fiber bragg grating sensors," *Appl. Compos. Mater.*, vol. 13, no. 2, pp. 87–98, 2006.

[27] J. M. Corres, F. J. Arregui, and I. R. Matías, "Sensitivity optimization of tapered optical fiber humidity sensors by means of tuning the thickness of nanostructured sensitive coatings," *Sensors Actuators, B Chem.*, vol. 122, no. 2, pp. 442–449, 2007.

[28] T. H. Chan, L. Yu, H. Y. Tam, Y.Q. Ni, S. Y. Liu, W.H. Chung and L. K. Cheng, "Fiber Bragg grating sensors for structural health monitoring of Tsing Ma bridge: Background and experimental observation," *Eng. Struct.*, vol. 28, no. 5, pp. 648–659, 2006.

[29] U.J. Dreyer, F. Mezzadri, G. Dutra, T. da Silva, C. A. Bavastri, E.V. da Silva, C. Martelli, and J.C.C da Silva,"Quasi-Distributed Optical Fiber Transducer for Simultaneous Temperature and Vibration Sensing in High-Power Generators," *IEEE Sens. J.*, vol. 18, no. 4, pp. 1547–1554, 2018.

[30] M. R. Islam, M. Bagherifaez, M. M. Ali, H. K. Chai, K.-S. Lim, and H. Ahmad, "Tilted Fiber Bragg Grating Sensors for Reinforcement Corrosion Measurement in Marine Concrete Structure," *IEEE Trans. Instrum. Meas.*, vol. 64, no. 12, pp. 3510–3516, Dec. 2015.

[31] P. Jia, G. Fang, T. Liang, Y. Hong, Q. Tan, X. Chen, W. Liu, C. Xue, J. Liu, W. Zhang, W. and J. Xiong, "Temperature-compensated fiber-optic Fabry–Perot interferometric gas refractive-index sensor based on hollow silica tube for high-temperature

application," *Sensors Actuators, B Chem.*, vol. 244, no. 7, pp. 226–232, 2017.

[32] W. Liang, Y. Huang, Y. Xu, R. K. Lee, and A. Yariv, "Highly sensitive fiber Bragg grating refractive index sensors," *Appl. Phys. Lett.*, vol. 86, no. 15, pp. 1–3, 2005.

[33] S. Lee, S. S. Saini, and M. Jeong, "Simultaneous Measurement of Refractive Index , Temperature , and Strain Using Etched-Core Fiber Bragg Grating Sensors," *IEEE Photonics Technol. Lett.*, vol. 22, no. 19, pp. 1431–1433, 2010.

[34] S. Ashkenazi, C. Y. Chao, L. J. Guo, and M. ODonnell, "Ultrasound detection using polymer microring optical resonator," *Appl. Phys. Lett.*, vol. 85, no. 22, pp. 5418–5420, Nov. 2004.

[35] A. Yalcin, K.C. Popat, J.C. Aldridge, T.A. Desai, J. Hryniewicz, N. Chbouki, B.E., Little, O. King, V. Van, S. Chu, and D. Gill, "Optical sensing of biomolecules using microring resonators," *IEEE J. Sel. Top. Quantum Electron.*, vol. 12, no. 1, pp. 148–155, Jan. 2006.

[36] B. Y. Guo, W. C. Tang, Y. C. Manie, M. A. Bitew, H. K. Lu, and P. C. Peng, "Long-distance sensing fiber sensor system using broadband source and Raman amplifier," in *2017 IEEE International Conference on Consumer Electronics (ICCE-TW)*, Taipei, Taiwan, Jun. 12-14, 2017, pp. 413–414, paper 17062539.

[37] Z. Zhou, W. Liu, Y. Huang, H. Wang, and H. Jianping, "Optical fiber Bragg grating sensor assembly for 3D strain monitoring and its case study in highway pavement," *Mech. Syst. Signal Process.*, vol. 28, pp. 36–49, 2012.

[38] J. Bai, D. Zhao, and X. Zhang, "Structural health monitoring of smart civil structures based on fiber Bragg grating sensing technology," in *2011 IEEE 2nd International Conference on Artificial Intelligence, Management Science and Electronic Commerce (AIMSEC)*, Dengleng, China, Aug. 8-10, 2011, pp. 635–638, paper 12259169.

[39] H. F. Lima *et al.*, "Structural health monitoring of the church of santa casa da misericordia of Aveiro using FBG sensors," *IEEE Sens. J.*, vol. 8, no. 7, pp. 1236–1242, 2008.

[40] P.Capoluongo, C.Ambrosino, S. Campopiano, A. Cutlolo, M. Giordano, I. Bovio, L. Lecce, A.Cusano, "Modal analysis and damage detection by Fiber Bragg grating sensors," *Sensors Actuators, A Phys.*, vol. 133, no. 2, pp. 415–424, 2007.

[41] A. Paolozzi and P. Gabarri, “Dynamic analysis with fibre optic sensors for Structural Health Monitoring,” in *Multifunctional Structures / Integration of Sensors and Antennas*, Italy, Oct. 1, 2006, no. 9, p. 9.1--9.24, paper ADA479893.

[42] S. Takeda, Y. Aoki, T. Ishikawa, N. Takeda, and H. Kikukawa, “Structural health monitoring of composite wing structure during durability test,” *Compos. Struct.*, vol. 79, no. 1, pp. 133–139, 2007.

[43] Y. Zhao, H. Huang, and Q. Wang, “Interrogation technique using a novel spectra bandwidth measurement method with a blazed FBG and a fiber-optic array for an FBG displacement sensor,” *Sensors Actuators, A Phys.*, vol. 165, no. 2, pp. 185–188, 2011.

[44] M. F. S. Ferreira, G. Barabach, D. Kowal, P. Mergo, W. Urbanczyk, and O. Frazao, “Fabry-Perot cavity based on polymer FBG as refractive index sensor,” *Opt. Commun.*, vol. 394, pp. 37–40, 2017.

[45] J. a. Chavez, G. G. Sanchez, D. E. Herrera, J. H. Rodriguez, and T. Schreiber, “Temperature sensing characteristics of tapered Yb-doped fiber amplifiers,” *Opt. - Int. J. Light Electron Opt.*, vol. 124, no. 22, pp. 5818–5821, 2013.

[46] J. Zhu, J. Wang, P. Gan, Z. Hu, and Y. Hu, “Design and Analysis of a Novel Dual FBG Accelerometer Based on Lantern Shape Metallic Shells,” *IEEE Sens. J.*, vol. 17, no. 16, pp. 5130–5135, 2017.

[47] J. M. Kim, C. M. Kim, S. Y. Choi, and B. Y. Lee, “Enhanced strain measurement range of an FBG sensor embedded in seven-wire steel strands,” *Sensors*, vol. 17, no. 7, pp. 1654–1657, 2017.

[48] W. Jingjing, L.Wei, R. Li, Q. Liu, L. Yu, T. Li, and Y. Tan, “An FBG-based 2-D vibration sensor with adjustable sensitivity,” *IEEE Sens. J.*, vol. 17, no. 15, pp. 4716–4724, 2017.

[49] O. Almubaied, H. K. Chai, M. R. Islam, K. S. Lim, and C. G. Tan, “Monitoring Corrosion Process of Reinforced Concrete Structure Using FBG Strain Sensor,” *IEEE Trans. Instrum. Meas.*, vol. 66, no. 8, pp. 2148–2155, 2017.

[50] Q. Zhang, N. Liu, T. Fink, H. Li, W. Peng, and M. Han, “Fiber-optic pressure sensor based on π-phase-shifted fiber Bragg grating on side-hole fiber,” *IEEE Photonics Technol. Lett.*, vol. 24, no. 17, pp. 1519–1522, 2012.

[51] Y. Huang, Y. Li, H. Zhu, G. Tong, B. Fang, L. Li, Y. Shen, Q. Zheng, Q. Liang, M. Yan, F. Wang, Y. Qin, J. Ding, X. Wang, "Tunable superstructure fiber Bragg grating with chirp-distribution modulation based on the effect of external stress," *Opt. Lett.*, vol. 37, no. 18, pp. 3918-20, 2012.

[52] M. Ramakrishnan, G. Rajan, Y. Semenova, and G. Farrell, "Hybrid fiber optic sensor system for measuring the strain, temperature, and thermal strain of composite materials," *IEEE Sens. J.*, vol. 14, no. 8, pp. 2571–2578, 2014.

[53] J. Jung, H. Nam, J. H. Lee, N. Park, and B. Lee, "Simultaneous measurement of strain and temperature using a single fiber Bragg grating with erbium-doped fiber amplifier ," in *Conference Proceedings. LEOS'98. 11th Annual Meeting. IEEE Lasers and Electro-Optics Society 1998 Annual Meeting (Cat. No.98CH36243),* Orlando, FL, USA, Dec. 1-4, 1998, pp. 0–1, page 6370062.

[54] D. Luo, J. Ma, Z. Ibrahim, and Z. Ismail, "Etched FBG coated with polyimide for simultaneous detection the salinity and temperature," *Opt. Commun.*, vol. 392, pp. 218–222, 2017.

[55] H. Kang, H. Bang, C. Hong, and C. Kim, "Simultaneous measurement of strain , temperature and vibration frequency using a fibre optic sensor," *Meas. Sci. Tech.* vol. 13, no. 8, pp. 1191–1196, 2002.

[56] M. Enckell, B. Glisic, F. Myrvoll, and B. Bergstrand, "Evaluation of a large-scale bridge strain, temperature and crack monitoring with distributed fibre optic sensors," *J. Civ. Struct. Heal. Monit.*, vol. 1, no. 1–2, pp. 37–46, Jun. 2011.

[57] C. Massaroni, M. Caponero, R. Amato, D. Lo Presti, and E. Schena, "Fiber Bragg Grating Measuring System for Simultaneous Monitoring of Temperature and Humidity in Mechanical Ventilation," *Sensors*, vol. 17, no. 4, p. 749, 2017.

[58] K. S. Kim, "Dynamic Strain Measurement with Fiber Bragg Grating Sensor System for Smart Structure," *Key Eng. Mater.*, vol. 270–273, pp. 2114–2119, Aug. 2004.

[59] H. Xu, X. Dong, Z. Yang, K. Ni, P. Shum, C. Lu, and H.Y. Tam, "Simple FBG sensor head design for strain-temperature discrimination," in *2009 IEEE 14th OptoElectronics and Communications Conference,* Vienna, Austria, Jul. 13-17, 2009, pp. 1–2, paper 10846042.

[60] H. C. Cheng, J. F. Huang, and Y. L. Lo, “Simultaneous strain and temperature distribution sensing using two fiber Bragg grating pairs and a genetic algorithm,” *Opt. Fiber Technol.*, vol. 12, no. 4, pp. 340–349, Oct. 2006.

[61] S. O. Park, B. W. Jang, Y. G. Lee, C. G. Kim, and C. Y. Park, “Simultaneous measurement of strain and temperature using a reverse index fiber Bragg grating sensor,” *Meas. Sci. Technol.*, vol. 21, no. 3, pp. 0357031-8, 2010.

[62] S. Wu, G. Yan, C. Wang, Z. Lian, X. Chen, and S. He, “FBG Incorporated Side-Open Fabry-Perot Cavity for Simultaneous Gas Pressure and Temperature Measurements,” *J. Light. Technol.*, vol. 34, no. 16, pp. 3761–3767, 2016.

[63] H. V. Thakur, S. M. Nalawade, Y. Saxena, and K. T. V Grattan, “All-fiber embedded PM-PCF vibration sensor for Structural Health Monitoring of composite,” *Sensors Actuators, A Phys.*, vol. 167, no. 2, pp. 204–212, 2011.

[64] P. Antunes, H. Varum, and P. Andre, “Optical FBG sensors for static structural health monitoring,” *Procedia Eng.*, vol. 14, pp. 1564–1571, 2011.

[65] C. Triana, M. V. Duran, and D. P. Abelian, “Fiber Bragg grating strain sensor validation in metallic structures,” in *2013 IEEE 4th International **Conference** on Photonics (ICP)*, Melaka, Malaysia, Oct. 28-30, 2013, pp. 203–205, paper 13990448.

[66] K. Bremer, M. Wollweber, F. Weigand, M. Rahlves, M., Kuhne, R. Helbig, and B. Roth, “Fibre Optic Sensors for the Structural Health Monitoring of Building Structures,” *Procedia Technol.*, vol. 26, pp. 524–529, 2016.

[67] S. wei Lu and H. qin Xie, “Strengthen and real-time monitoring of RC beam using ‘intelligent’ CFRP with embedded FBG sensors,” *Constr. Build. Mater.*, vol. 21, no. 9, pp. 1839–1845, 2007.

[68] N. Roveri, A. Carcaterra, and A. Sestieri, “Real-time monitoring of railway infrastructures using fibre Bragg grating sensors,” *Mech. Syst. Signal Process.*, vol. 60–61, pp. 14–28, 2015.

[69] Z. Zheng, X. Sun, and Y. Lei, “Monitoring corrosion of reinforcement in concrete structures via fiber Bragg grating sensors,” *Front. Mech. Eng. China*, vol. 4, no. 3, pp. 316–319, 2009.

[70] K. Lau, L. Yuan, L. Zhou, J. Wu, and C. Woo, “Strain monitoring in FRP laminates

and concrete beams using FBG sensors," *Compos. Struct.*, vol. 51, no. 1, pp. 9–20, 2001.

[71] Y. Dai, Y. Liu, J. Leng, G. Deng, and A. Asundi, "A novel time-division multiplexing fiber Bragg grating sensor interrogator for structural health monitoring," *Opt. Lasers Eng.*, vol. 47, no. 10, pp. 1028–1033, 2009.

[72] W. Shen, R. Yan, L. Xu, G. Tang, and X. Chen, "Application study on FBG sensor applied to hull structural health monitoring," *Opt. - Int. J. Light Electron Opt.*, vol. 126, no. 17, pp. 1499–1504, 2015.

[73] K. Bremer, F. Weigand, Y. Zheng, L. S. M. Alwis, M. Kuhne, R. Helbig, and B. Roth., "Fibre optic strain sensor for carbon concrete composites," in *2017 European Conference on Lasers and Electro-Optics and European Quantum Electronics Conference*, Munich Germany, Jun. 25-29, 2017, p. 345, paper CH_P_11.

[74] F. Dingyi, X. Qiao, H. Yang, Q. Rong, R. Wang, Y. Du, M. Hu, and Z. Feng, "A Fiber Bragg Grating Accelerometer Based on a Hybridization of Cantilever Beam," *IEEE Sens. J.*, vol. 15, no. 3, pp. 1532–1537, 2014.

[75] F. Ding, L. Wang, N. Fang, and Z. Huang, "Experimental study on humidity sensing using a FBG sensor with polyimide coating," in *2010 Asia Communications and Photonics Conference and Exhibition, ACP 2010*, Shangai, China, Dec. 8-12, 2010, pp. 280–281.

[76] H. Miquel, D. Barrera, R. Amat, G. V Kurlyandskaya, and S. Sales, "Magnetic actuator based on giant magnetostrictive material Terfenol-D with strain and temperature monitoring using FBG optical sensor," *Meas. J. Int. Meas. Confed.*, vol. 80, pp. 201–206, 2016.

[77] A. F. Obaton, G. Laffont, C. Wang, A. Allard, and P. Ferdinand, "Tilted Fibre Bragg Gratings and Phase Sensitive-Optical Low Coherence Interferometry for refractometry and liquid level sensing," *Sensors Actuators A Phys.*, vol. 189, pp. 451–458, Jan. 2013.

[78] G. Kaur, R. S. Kaler, and N. Kwatra, "Experiment on Highly Sensitive Fiber Bragg Grating Optical Sensor to Monitor Strain and Corrosion in Civil Structures," *J. Opt. Technol.*, vol. 85, no. 1, pp. 1–7, 2018.

[79] G. Kaur and R. S. Kaler, “Nanohybrid optical sensor for simultaneous measurements of strain, temperature, and vibration for civil application,” *Micro Nano Lett.*, vol. 13, no. 1, pp. 1–3, 2018.

[80] G. Uva, F. Porco, A. Fiore, and G. Porco, “Structural monitoring using fiber optic sensors of a pre-stressed concrete viaduct during construction phases,” *Case Stud. Nondestruct. Test. Eval.*, vol. 2, no. 1, pp. 27–37, 2014.

[81] O. Regnault, V. Lagneau, and H. Schneider, “Experimental measurement of portlandite carbonation kinetics with supercritical CO2,” *Chem. Geol.*, vol. 265, no. 1–2, pp. 113–121, 2009.

[82] H. Song and velu saraswathy, “Corrosion Monitoring of Reinforced Concrete Structures - A Review,” *Int. J. Electrochem. Sci.*, vol. 2, no. 1, pp. 1–28, 2007.

[83] R. Gupta and R. S. Kaler, “Performance comparison of pre-, boost-, and inline-multimode erbium-doped fiber amplifier configurations to boost mode-division multiplexed multimode fiber link,” *Opt. Eng.*, vol. 55, no. 5, pp. 056102-6, 2016.

[84] S. Singh and K. Singh, “Design of an integrated multi-arm power splitter using photonic crystal waveguide,” *Optik*, vol. 145, pp. 495–502, Sep. 2017.

[85] S. Singh, H. Kaur, and K. Singh, “Far field detection of different elements using photonic crystals,” *J. Nanoelectron. Optoelectron.*, vol. 12, no. 4, pp. 400–403, 2017.

[86] D. John and B. Culshaw, *Optical Fiber Sensors: Principles and components*. michigan, USA: Artech House, 1988.

[87] X. Bao and L. Chen, “Recent progress in Brillouin scattering based fiber sensors.,” *Sensors (Basel).*, vol. 11, no. 4, pp. 4152–87, Apr. 2011.

[88] X. Bao and L. Chen, “Recent progress in distributed fiber optic sensors.,” *Sensors (Basel).*, vol. 12, no. 7, pp. 8601–39, Jun. 2012.

[89] K. O. Hill and G. Meltz, “Fiber Bragg grating technology fundamentals and overview,” *J. Light. Technol.*, vol. 15, no. 8, pp. 1263–1276, 1997.

[90] S. Udoh, J. Njuguma, and R. Prabhu, “Modelling and Simulation of Fiber Bragg Grating Characterization for Oil and Gas Sensing Applications,” in *2014 1st International Conference on Systems Informatics, Modelling and Simulation*, DC, USA, April. 29-May.1, 2014, pp. 255–260.

[91] Z. He and J. Du, “FBG sensor for strain measurement with enhanced sensitivity by using degenerated FWM in highly nonlinear fibre,” *Electron. Lett.*, vol. 49, no. 22, pp. 1399–1401, 2013.

[92] G. Meltz, W. W. Morey, and W. H. Glenn, “Formation of Bragg gratings in optical fibers by a transverse holographic method,” *Opt. Lett.*, vol. 14, no. 15, p. 823, Aug. 1989.

[93] M. Ramakrishnan, G. Rajan, Y. Semenova, and G. Farrell, “Hybrid fiber optic sensor system for measuring the strain, temperature, and thermal strain of composite materials,” *IEEE Sens. J.*, vol. 14, no. 8, pp. 2571–2578, 2014.

[94] Y. Liu, F. Che, Z. Jia, H. Fu, H. Wang, and M. Shao, “Investigation on the characteristics of micro/nanofiber Bragg grating for refractive index sensing,” *Wuli Xuebao/Acta Phys. Sin.*, vol. 62, no. 10, pp. 1128–1133, 2013.

[95] A. Ksendzov and Y. Lin, “Integrated optics ring-resonator sensors for protein detection,” *Opt. Lett.*, vol. 30, no. 24, p. 3344, Dec. 2005.

[96] I. M. White, N. M. Hanumegowda, and X. Fan, “Subfemtomole detection of small molecules with microsphere sensors,” *Opt. Lett.*, vol. 30, no. 23, p. 3189, Dec. 2005.

[97] M. Noto, F. Vollmer, D. Keng, I. Teraoka, and S. Arnold, “Nanolayer characterization through wavelength multiplexing a microsphere resonator,” *Opt. Lett.*, vol. 30, no. 5, pp. 510–512, 2005.

[98] M. Sumetsky, Y. Dulashko, J. M. Fini, A. Hale, and D. J. DiGiovanni, “The microfiber loop resonator: theory, experiment, and application,” *J. Light. Technol.*, vol. 24, no. 1, pp. 242–250, Jan. 2006.

[99] D. Ying, M. S. Demokan, X. Zhang, and W. Jin, “Sensitivity analysis of a fiber ring resonator based on an air-core photonic-bandgap fiber,” *Opt. Fiber Technol.*, vol. 16, no. 4, pp. 217–221, Aug. 2010.